CAMBER, PRESTRESS LOSS, AND DETERMINATION OF DISTRIBUTION FACTORS IN PRETENSIONED CONCRETE GIRDER BRIDGES

By

CHRISTOPHER FILIP

Bachelor of Science in Civil Engineering

Oklahoma State University

Stillwater, Oklahoma

2020

Submitted to the Faculty of the
Graduate College of the
Oklahoma State University
in partial fulfillment of
the requirements for
the Degree of
MASTER OF SCIENCE
December, 2022

CAMBER, PRESTRESS LOSS, AND

DETERMINATION OF DISTRIBUTION FACTORS IN

PRETENSIONED CONCRETE GIRDER BRIDGES

Thesis Approved:

Dr. Bruce Russell

Thesis Adviser

Dr. Mohamed Soliman

Dr. Robert Emerson

ACKNOWLEDGEMENTS

I would like to thank Dr. Bruce Russell for the opportunity to pursue my degree and progress my knowledge. He played a massive role in helping me further my technical skills. I would also like to thank Alla Acheli for his hard work and never-ending dedication. It was an honor to work with you both, and I wish you both the best. I would also like to thank Oklahoma Transportation for funding our research projects. Thank you Dr. Soliman and Dr. Emerson for serving on my defense committee.

Name: CHRISTOPHER FILIP

Date of Degree: December, 2022

Title of Study: CAMBER, PRESTRESS LOSS, AND DETERMINATION OF DISTRIBUTION FACTORS IN PRETENSIONED GIRDER BRIDGES

Major Field: CIVIL ENGINEERING

Abstract: This research investigates prestress losses and camber of Prestressed Concrete bridge beams (PC Beams), and the performance and load testing of the SH 4 Bridge over the North Canadian River in Canadian County, OK. The bridge consists of 15 spans; each span is nominally 100 ft. in length. Each span was also designed and built with unique reinforcement details. An instrument-based structural monitoring program was implemented to measure strains and temperatures within hardened concrete. Materials testing was also performed. Camber measurements were taken at several intervals during the fabrication of the PC Beams and during the construction of the SH 4 Bridge and continuing through service. Several prestress loss analysis methods were performed and compared to gathered strain data. The purpose was to compare how different strand layouts and the inclusion of mild steel reinforcement in the bottom flanges of the girders affected long-term cambers and prestress losses. Static load testing was also performed on this bridge to determine the live load distribution factors of the girders. The research investigated whether distribution factor methods (DF's) are accurate, and whether overestimating DF's for external girders leads to unnecessary levels of prestressing reinforcement. Excess reinforcement can result in increasing camber and increasing prestress losses, and adversely affect cracking in end regions and the constructability of the bridge. Results from the research were compared to analytical methods prescribed in AASHTO codes. A finite element model was also made to recreate the load test and determine the effectiveness of the parapets and diaphragms in distributing live load.

TABLE OF CONTENTS

Chapter Page

I INTRODUCTION 1

1.1 OVERVIEW 1

II REVIEW OF LITERATURE 6

2.1 CAMBER AND PRESTRESS LOSS 6

2.1.1 Jayaseelan and Russell (2019) 7

2.1.2 Kelly et al. (1987) 7

2.1.3 Storm et al. (2013) 8

2.1.4 Almohammedi et al., (2021) 9

2.1.5 Hale & Russell, (2006) 10

2.1.6 Tadros et al., (1985) 12

2.1.7 Baran et al., (2005) 13

2.2 DISTRIBUTION FACTORS AND STATIC LOAD TESTING 16

2.2.1 Dong et al. (2020) 16

2.2.2 Barr et al. (2001) 17

2.2.3 Lin & Vanhorn (1968) 18

2.2.4 Conner & Huo (2006) 18

III CAMBER AND PRESTRESS LOSS 20

3.1 INTRODUCTION 20

3.2 PROJECT BACKGROUND 20

3.2.1 Material Properties 25

3.3 ESTIMATING PRESTRESS LOSSES 28

3.3.1 METHODOLOGY 28

3.4 MEASUREMENT OF PRESTRESS LOSSES 35

3.4.1 METHODOLOGY 35

Chapter .Page
3.4.2 RESULTS 41
3.4.3 DISCUSSION 47
3.5 COMPARISON OF ESTIMATED AND MEASURED LOSSES 50
3.5.1 Prestress Loss Models 50
3.5.2 Predicted VS Measured Losses 51
3.6 ESTIMATING CAMBER 57
3.6.1 METHODOLOGY 57
3.6.2 RESULTS 57
3.6.3 DISCUSSION 59
3.7 MEASUREMENT OF CAMBER 60
3.7.1 METHODOLOGY 60
3.7.2 RESULTS 61
3.7.3 DISCUSSION 65
3.8 COMPARISON OF ESTIMATED CAMBER TO MEASURED CAMBER 67
3.9 CONCLUSIONS 70
3.9.1 Prestress Loss Conclusions 70
3.9.2 Camber Conclusions 71
3.9.3 Recommendations 72
IV DETERMINATION OF DISTRIBUTION FACTORS THROUGH STATIC LOAD TESTING 74
4.1 INTRODUCTION 74
4.2 BACKGROUND 75
4.2.1 The Lever Rule 75
4.2.2 The Rigid Method 75
4.2.3 AASHTO Methods 76
4.3 LOAD TEST METHODOLOGY 77
4.3.1 Static Load Testing 81
4.4 STATIC LOAD TESTING RESULTS 86
4.5 FINITE ELEMENT MODELLING 99
4.6 DISCUSSION 103
4.6.1 Comparison of AASHTO Methods and Load Test Results 103

Chapter Page

4.6.2 Comparison of Load Test and FEA Results 109
4.6.3 Effects of Parapets and Diaphragms 115
4.7 CONCLUSIONS 120
4.7.1 Distribution Factor Conclusions 120
4.7.2 Recommendations 121
V SUMMARY AND CONCLUSIONS 122
5.1 SUMMARY 122
5.2 CONCLUSIONS 123
5.2.1 Prestress Loss Conclusions 123
5.2.2 Camber Conclusions 124
5.2.3 Distribution Factor Conclusions 125
5.2.4 Recommendations 127
VI APPENDICIES 134
6.1 APPENDIX A: CONCRETE MATERIAL PROPERTIES 134
6.2 APPENDIX B: CALCULATION OF PRESTRESS LOSSES 139
6.2.1 Appendix B1: AASHTO Approximate Method 139
6.2.2 Appendix B2: AASHTO Refined Method 141
6.2.3 Appendix B3: PCI Design Handbook Methods 148
6.2.4 Appendix B4: Jayaseelan Time-step Method 150
6.3 APPENDIX C: INTERNAL MOMENTS DERIVED FROM MEASURED STRAIN DURING LOAD TESTING AND IN FEA 158

LIST OF TABLES

Table Page

Table 1: Prestressing strand and mild reinforcement variations by span. 24
Table 2: Significant dates PC beam fabrication, handling, transportation and erection, and SH 4 Bridge construction. 26
Table 3: Early and 28-day compressive strengths. 27
Table 4: Approximate loss estimates for time-dependent losses according to the AASHTO 2020 LRFD Design Specifications. 29
Table 5: Refined estimates of time-dependent prestress losses at midspan calculated using transformed section properties according to the 2020 AASHTO LRFD Bridge Design Specifications. 30
Table 6: Approximate loss estimates using gross section properties according to PCI Design Handbook 6th Edition. 31
Table 7: Approximate loss estimates using transformed section properties according to PCI Design Handbook 6th Edition 32
Table 8: Prestress losses at midspan calculated with the Jayaseelan Time-step method.. 33
Table 9: Comparison of measured and predicted concrete modulus at detensioning. 56
Table 10: Predicted camber using Jayaseelan Time-step method 57
Table 11: Effects of distributed strand patterns and mild steel on camber using the Jayaseelan Time-Step method. 59
Table 12: Average Camber Measurements of Each Span Over Time 62
Table 13: Effects of distributed strand patterns and mild steel on camber. 66
Table 14: Assumed Truck Axle Weights 78
Table 15: Span 9 Configuration 1 tabulated results. 91
Table 16: Span 9, configuration 1 FEA results. 92
Table 17: Span 9 Configuration 3 tabulated results. 93
Table 18: Span 9, configuration 3 FEA results. 94
Table 19: Span 14 Configuration 1 tabulated results. 95
Table 20: Span 14, configuration 1 FEA results. 96
Table 21: Span 14 Configuration 3 tabulated results. 97
Table 22: Span 14, configuration 3 FEA results. 98
Table 23: Comparison of AASHTO methods for determining distribution factors of exterior and interior girders. 104

Table Page

Table 24: ODOT Specifications for Class AA and Class P mixture proportions. 134
Table 25: Fresh concrete properties, Beam Mark 27, Span 9. 134
Table 26: Hardened concrete properties, Beam Mark 27, Span 9. 135
Table 27: Fresh concrete properties, Beam Mark 42, Span 14. 136
Table 28: Hardened concrete properties, Beam Mark 42, Span 14. 136
Table 29: Fresh properties of concrete deck, Span 9. 137
Table 30: Hardened properties of concrete deck, Span 9. 137
Table 31: Fresh properties of concrete deck, Span 14. 138
Table 32: Hardened properties of concrete deck, Span 14. 138
Table 33: Prestress losses calculated at midspan using Jayaseelan Time-step method at significant events. 155
Table 34: Span 9, Configuration 1 internal moment derived from strain readings. 158
Table 35: Span 9, Configuration 1 internal moment derived from FEA strain measurements. 159
Table 36: Span 9, Configuration 3 internal moment derived from strain readings. 160
Table 37: Span 9, Configuration 3 internal moment derived from FEA strain measurements. 161
Table 38: Table 37: Span 14, Configuration 1 internal moment derived from strain readings. 162
Table 39: Table 37: Span 14, Configuration 1 internal moment derived from FEA strain measurements. 163
Table 40: Span 14, Configuration 3 internal moment derived from strain readings. 164
Table 41: Span 14, Configuration 3 internal moment derived from FEA strain measurements. 165

LIST OF FIGURES

Figure Page
Figure 1: Satellite view of SH 4 bridge over the North Canadian River. 3
Figure 2: Distribution factors are the percent of the applied forces transferred to each of the girders..... 4
Figure 3: Photograph of the SH 4 Bridge over N. Canadian R., Canadian Co., OK. 21
Figure 4: Cross-section of the bridge. 21
Figure 5: Detailing of longitudinal reinforcement layouts. 23
Figure 6: Aerial view of the SH4 bridge over the North Canadian River. 25
Figure 7: Estimated prestress losses using the Jayaseelan Time-step method..... 34
Figure 8: Sensor locations at each length increment of the girders. 36
Figure 9: Sensor locations shown in girder cross-section. 36
Figure 10: North end reinforcement and instrumentation, Beam Mark 27, Span 9..... 37
Figure 11: Dillon Cochran (left), M.S., and Alla Acheli, Ph.D. are pictured installing instrumentation. 37
Figure 12: Vibrating Wire Gauge (blue) is located in the foreground at approximately C.G.S. 38
Figure 13: Instrumentation at midspan, Mark 27, Span 9. Four #7 reinforcing bars are placed in the corners of the bottom flange. 38
Figure 14: Mark 27, Span 9 at finishing station..... 39
Figure 15: Girder Mark 27, Span 9. Recorded temperatures at midspan during the first 72 hours of the PC Beam life. 42
Figure 16: Girder Mark 42, Span 14. Recorded temperatures at midspan during the first 72 hours of the PC Beam life. 42
Figure 17: Measured strains in concrete at midspan during the first 72 hours for Mark 27, Span 9..... 43
Figure 18: Measured strains in concrete at midspan during the first 72 hours for Mark 42 Span 14..... 44
Figure 19: Measured ambient and concrete temperature at midspan for Mark 42, Span 14. 44
Figure 20: Measured strains in Span 9, Mark 27, beginning when the girder was cast (April 2020) and going through mid-October 2021. 45
Figure 21: Measured strains in Span 14, Mark 42 beginning on the date the girder was cast (April 2020) and going through mid-October 2021. 45

Figure Page
Figure 22: Direct measurements of prestress losses from strain gauge data at midspan for Mark 27 Span 9. 48
Figure 23: Direct measurements of prestress losses from strain gauge data at midspan for Mark 42 Span 14. 49
Figure 24: Predicted and measured losses prior to deck casting (110 days) 51
Figure 25: Predicted and measured losses at 500 days. 52
Figure 26: Span 9 measured losses and estimated losses with the Jayaseelan Time-step method 53
Figure 27: Span 14 measured losses and estimated losses with the Jayaseelan Time-step method 54
Figure 28: Predicted Camber from Jayaseelan Time-Step Method 58
Figure 29: Average measured camber by reinforcement layouts. Note that girders were placed approximately 40 days after detensioning. 63
Figure 30: Mark 27, Span 9 measured camber from strain and on site. 63
Figure 31: Mark 42, Span 14 measured camber from strain and on site. 64
Figure 32: Predicted and measured camber for Case A. 67
Figure 33: Predicted and measured camber for Case B. 67
Figure 34: Predicted and measured camber for Case C. 68
Figure 35: Predicted and measured camber for Case D. 68
Figure 36: Lever rule example from section C4.6.2.2.1-1 of 2020 AASHTO LRFD. 75
Figure 37: Rigid method equation 76
Figure 38: Table provided by AASHTO for determining distribution factors. 77
Figure 39: Assumed axle weights of each truck. 78
Figure 40: Instrumentation location for load testing plan. 79
Figure 41: LVDT and accelerometer locations. 80
Figure 42: Instruments at midspan for SH 4 load test. Viewed are an LVDT and accelerometer. 80
Figure 43: Testing setup for SH 4 load test. 81
Figure 44: Truck configuration 1 view looking North. 82
Figure 45: Truck configuration 1 plan view. 82
Figure 46: Truck configuration 3 view looking North. 83
Figure 47: Truck configuration 3 plan view. 83
Figure 48: Truck configuration 1 for static load testing. 84
Figure 49: Truck configuration 3 for static load testing. 84
Figure 50: Span 9 Configuration 1 measured Midspan deflections. 87
Figure 51: Span 9 Configuration 3 measured midspan deflections. 88
Figure 52: Span 14 Configuration 1 measured midspan deflections. 89
Figure 53: Span 14 Configuration 3 measured midspan deflections. 90
Figure 54: End region reinforcing in FEA model of Span 9. 99

Figure Page

Figure 55: Photograph of the Abaqus model. 100
Figure 56: Abaqus model of Span 9 before the model was run. In view are truck wheel loads set to configuration 3 at midspan..... 101
Figure 57: Span 9 configuration 3 deflection results. The dark red color displays upward deflection caused by camber. The lighter colors display that upward deflection was limited by truck loading. 102
Figure 58: Truck configuration 1 at midspan results. 105
Figure 59: Truck configuration 3 at midspan results 107
Figure 60: Span 9 Western Girders Load Test and FEA Results 109
Figure 61: Span 14 Western Girders Load Test and FEA results. 110
Figure 62: Strain measurements of external West girders from load test and FEA for trucks placed at midspan. 111
Figure 63: Comparison of distribution factors found using relative deflection and curvatures in the External West Girders. 113
Figure 64: Configuration 1 finite element results. 116
Figure 65: Configuration 3 finite element results. 118
Figure 66: Predicted camber with Jayaseelan Time-step method that include a reinforcement "Case 0" that is a modified version of Case A that doesn't include top strands. 156
Figure 67: Prestress losses with Jayaseelan Time-step method that include a reinforcement "Case 0" that is a modified version of Case A that doesn't include top strands. 157

CHAPTER I

1 INTRODUCTION

1.1 OVERVIEW

The use of prestressed concrete bridges has been popular in the United States since the early 1950's. The benefits these types of bridges were highlighted following a steel shortage due to the Korean War, as these types of bridges are able to achieve longer spans while using less concrete and steel reinforcement when compared to standard reinforced concrete bridges. In 1956, AASHTO developed its first four I-beam sections (Brinckerhoff, 2005) [7], setting the groundwork for general practices with this material and promoting the use of precast concrete in these systems. The use of prestressed concrete bridges has only increased in the United States over the last 50 years. With the increased use of prestressed concrete for bridge girders, efficient and effective design of prestressed concrete girders is essential for providing quality infrastructure to the highway system. Currently, about two-thirds of new bridges in the United States are constructed using precast concrete girders (Jayaseelan & Russell, 2019) [15]. High performance concrete (HPC) is the most commonly used material for manufacturing concrete bridge girders. The main benefit of using HPC is that it is easy to place into formwork. It typically has a low water to cement ratio (w/cm) of about 0.25 -

0.4, as opposed to normal concrete with a w/cm of 0.4-0.5 (ACI Committee 363, 2010) [2]. This leads to increased strength from about 4,000 psi to upwards of 10,000 psi (ACI Committee 363, 2010) [2] and reduces permeability of the concrete, improving the long-term durability. The benefits of the increased strength are that it allows longer spans, reduces the amount of concrete needed, and can reduce the number of girders needed in the overall structure (Hassanain & Loov, 1999) [14].

This research examines the effects of differing prestress moment and inclusion of mild steel reinforcement in the bottom flange of bridge girders on camber and prestress loss. Prestressing moment is defined as effective prestressing force multiplied by the eccentricity of prestressing strands. Mild steel reinforcement is defined as rebar placed in the pre-compression zones of the prestressed girders.

The bridge tested for this research is located on SH 4 over the North Canadian River in Yukon, OK. The bridge consists of 15 spans, each approximately 100 ft. in length. Four AASHTO Type IV girders are present in each span. Camber measurements were taken on 60 girders at varying construction stages and while the bridge was in service. Prestress losses were calculated and compared using several standard approximation methods, specifically the AASHTO 2020 LRFD approximate method, AASHTO 2020 LRFD Refined method, PCI Design Handbook method, a modified version of the PCI Design Handbook method, and the Jayaseelan Time-Step Method. The results on prestress loss are compared to losses found using vibrating wire gauges embedded in two girders on this bridge.

Figure 1: Satellite view of SH 4 bridge over the North Canadian River.

Efficiency and accuracy of design have also been a subject of discussion in design of bridges. More detailed approaches need to be considered to provide effective and cost-efficient designs. One of these items is determining the distribution factor for the girders used in these bridges. Distribution factors are an estimate of the percent of applied load prescribed to each girder in a span. In the case of concrete girder bridges, the governing distribution factor of a single girder in a span controls the design for all girders in the span. The two most common methods for approximating distribution factors are the lever rule and the rigid method. The lever rule is required for calculating distribution factors of exterior girders. Interior girder distribution factors are calculated based on design criteria for this method. Alternatively, the rigid method can be used to find interior girder distribution factors when rigid end diaphragms are used in design. Although they are

valuable tools, they are considered conservative and typically overestimate the distribution factor of the external girder, which will govern the design of the girders in each span. This leads to more prestressing reinforcement being used, which can increase cost, cause more significant camber, and increase prestress loss. Using more prestressing strands can damage the bridge's constructability, cost, the efficiency of the design, and influence durability issues in the system, such as end region cracking (Kizilarslan et al., 2020) [17].

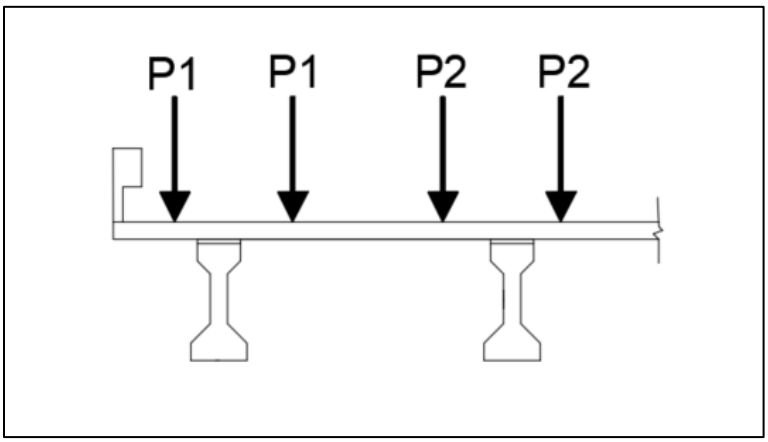

Figure 2: Distribution factors are the percent of the applied forces transferred to each of the girders.

For this project, a long-term structural health monitoring program was paired with a static load test of a bridge. The load test measured the distribution factors using a combination of vibrating wire gauges and LVDTs and results were compared to AASHTO prescribed methods. A 3-dimensional finite element model was also developed to simulate the effects of the static load test. The model results are compared to those found by the instrumentation used in this project.

Results from this research show that mild steel reinforcement can significantly reduce camber and mildly reduce losses. Prestressing strand patterns with reduced eccentricity were shown to significantly reduce camber and mildly reduce losses. Combining both mild steel and strand patterns with reduced eccentricity showed the most reduction in camber and prestress losses, but not significantly more than when these changes were used separately. From this, it is recommended to implement either mild steel or a distributed strand pattern as both provide a cost-effective way of reducing camber and prestress loss.

Static load testing results indicated that current AASHTO methods overpredict distribution factors of both internal and external bridge girders. This is was consistent with finite element modelling results. Investigation into the effects of parapets and diaphragms in distributing live load showed that parapets are effective in distributing load away from exterior girders, while diaphragms do not contribute significantly in distributing live load between girders. From this it is recommended that parapets be implemented into AASHTO methods for determining distribution factors.

CHAPTER II

2 REVIEW OF LITERATURE

2.1 CAMBER AND PRESTRESS LOSS

It is important to make accurate predictions of camber and prestress losses in the design of prestressed concrete girder bridges. Upward deflection, or camber, is caused by eccentric prestress forces, otherwise known as prestress moment. Camber is typically considered a positive benefit of prestressed concrete, as it negates downward deflection from gravity loads. Being able to control it is helpful, as excessive camber can limit serviceability, constructability, and affect ride quality. However, camber can only be controlled if it can be consistently and accurately predicted. The ability to accurately predict prestress loss can also contribute to the need for less prestressing reinforcement and being able to predict the behavior of a prestressed girder more accurately. Both camber and prestress loss are affected by several factors, including creep, shrinkage, elastic modulus of the concrete, tendon profile, superimposed dead loads, and service loads (Almohammedi et al., 2021) [3].

2.1.1 Jayaseelan and Russell (2019)

Jayseelan and Russell (2019) [15] investigated the effects of fully tensioned top strands and including mild steel reinforcement near the center of gravity of prestressing strands. Five designs were analyzed: one being a base case with no top strands and mild steel included, two designs that included either two or four fully tensioned top strands, and two designs that included mild steel reinforcing using either four no. 7 bars or five no. 9 bars. The group developed a prestress loss model known as the Jayaseelan Time-step method that is based off the AASHTO Refined method and breaks down the change in concrete strength and modulus over time using the ACI 209R Eq. (2-1). The group compared the losses found using PCI Design Handbook method, the 2014 AASHTO LRFD Approximate and Refined methods, and the Jayaseelan Time-step method. Cambers were also predicted using computed curvature with the Jayaseelan Time-Step method.

Jayaseelan and Russell found that including four fully tensioned top strands can reduced short-term and long-term camber by 16% and 45%, respectively. The inclusion of top strands also reduced long-term losses by 8%. It was also found that mild steel reinforcing reduced short-term and long-term camber by 12% and 24%, respectively. Mild steel reinforcing near the center of gravity of prestressing steel also reduced long-term losses by 5%. Combining both fully tensioned top strands and mild steel reinforcement reduced short term and long-term cambers by 31% and 72% respectively.

2.1.2 Kelly et al. (1987)

Kelly et al. (1987) [16] investigated the long-term deflection and camber in eight pretensioned AASHTO Type IV girders. Deflection was measured using a reference

piano wire with a constant force retensioning system. Results from these measured deflections was compared to a modified version of the PCI multiplier method. The group discusses that camber and prestress loss is affected by time dependent properties such as concrete modulus, creep, shrinkage and steel relaxation. The effects of the composite deck are also discussed. When a concrete deck is added, the rate at which camber grows is also slowed due to the increase in stiffness of the system and the added dead load causes strands below the center of gravity to regain tensile stresses.

The group measured camber starting at detensioning of the prestressing strands, before and after deck casting, and up to 1 year in service. The group found that cambers range between 2 to 6 in. at erection and from -0.75 and 2 in. while in service. Using AASHTO and PCI methods, the group found that camber was overpredicted by 0.64 in. and 0.15 in. for both before and after deck casting. The difference between the measured and estimated camber was attributed to design strength at deck casting being specified as 6660 psi, but measured concrete strength being 11,000 psi, meaning that concrete modulus is underpredicted in design.

2.1.3 Storm et al. (2013)

Storm et al. (2013) [25] discuss factors in precast, prestressed girder construction that affect camber. The main factors attributing to camber that were investigated are compressive strength, elastic modulus, void deformation in box beams and cored slabs, debonding, and transfer length. Secondary factors are discussed, such as temperature

change of the strands due to sun exposure, cement hydration, and heat curing before the transfer of prestressing force; the girder production schedule; and the curing procedure.

An approximate and a refined camber prediction method were proposed. The approximate method is based on the PCI multiplier method and does not require calculating time-dependent losses. The refined method is based on 2010 AASHTO LRFD Refined losses and utilizes the creep coefficient to predict camber.

Storm et al. (2013) [25] investigated the compressive strength of concrete and found that, on average, measured concrete strength at transfer was 1.24 times that of the specified strength at transfer. On average, the 28-day compressive strength of concrete was measured at 1.45 times that of the specified 28-day strength. The investigation into elastic modulus found that, on average, the measured elastic modulus was 0.85 times that of the predicted modulus.

2.1.4 Almohammedi et al., (2021)

Almohammedi et al. (2021) [3] investigated prestress losses and compared the design values to instrumented prestressed girders. The group instrumented nine prestressed girders from two different precast plants, consisting of AASHTO types II, III, IV, and VI girders. The group also performed materials testing of compressive strength, modulus of elasticity, shrinkage, and creep.

Results from materials testing are as follows. From plant 1, the measured compressive strength at transfer exceeded design values by 73%, 60%, and 27% for AASHTO Type II, III, and VI girders, respectively. From plant 2, the measured compressive strength at transfer exceeded design values by 59% for AASHTO Type IV girders. Average

measured 28-day strength exceeded design strength by 69%. Design modulus of elasticity was found to be significantly underestimated at transfer and 28-days.

The group measured short-term and long-term prestress losses using strain readings from the instrumented girders. Predicted elastic shortening loss was calculated using the 2017 AASHTO LRFD Refined Method with transformed section properties. It was found that elastic shortening loss was underpredicted by up to 10% or overpredicted by up to 26%. The concrete modulus at release was the main contributing factor to accurately predicting elastic shortening loss. Since modulus was underpredicted, elastic shortening was overpredicted. For long-term losses before deck casting, it was found that using design values typically leads to an overestimation of long-term prestress loss. The overprediction of losses is likely due to minimum specified compressive strength being significantly exceeded by the actual compressive strength.

2.1.5 Hale & Russell, (2006)

Hale and Russell (2006) [13] investigated the allowable compressive stress limit at release in precast, pretensioned concrete girders. The work also investigated the effects of prestress loss and compared measured losses to loss prediction methods. The purpose of this work was to investigate the effects from increasing allowable compressive stress at release from $0.60 f'_{ci}$ to $0.70 f'_{ci}$ and to compare measured prestress losses to the following loss prediction models: (1) the 2004 American Association of Highway Transportation Officials load-resistant factor design (AASHTO LRFD) Bridge Design Specifications (Refined method), (2) the PCI Design Handbook method described by Zia

et al. (1979) [30], and (3) the method proposed in the National Cooperative Highway Research Program (NCHRP) Report 496 [26] (detailed method).

Four girders were fabricated for this project. The four concrete girders were geometrically identical and two similar concrete mixtures were used between all four girders. Two girders used a concrete mixture that included an air-entraining admixture. The remaining two girders used a concrete mixture that did not include air-entraining admixture and used an adjusted sand content to compensate for the volumetric difference in the mixture. The strand patterns between all girders were identical, utilizing 10 strands in the concrete. Some girders had strands debonded to meet a specified effective prestress after elastic shortening loss.

Prestressing was released for two of the girders when they reached a target strength of $0.60\,f'_{ci}$. The remaining two girders were released when they reached a target strength of $0.75\,f'_{ci}$. No adverse effects were observed on the girders when the compressive strength limit provided by AASHTO was exceeded. Strains were measured and recorded using detachable mechanical strain (DEMEC) gauge targets attached to the concrete's surface at midspan near the bottom and top flange. The change in strain was found for both the top and bottom of the girders and was considered linear along the beam's depth. The change in stress could be measured by multiplying the elastic modulus of prestressing strands at the center of gravity of the prestressing strands.

Comparing the measured prestress loss to the three loss prediction methods found that the 2004 AASHTO LRFD Refined method and PCI Design Handbook method overestimated prestress loss, while the NCHRP Report 496 was found to be more accurate and slightly

underestimated prestress loss. The AASHTO refined equations, on average, overestimated prestress loss by 18%. The PCI Design Handbook method, on average, overestimated prestress loss by 13%. The NCHRP Report 496 method, on average, underestimated prestress loss by 6%.

The group concluded that prestress loss was not significantly impacted by the air entrainment of the concrete. The AASHTO Refined method was the least accurate method for predicting prestress loss. The NCHRP Report 496 detailed method was the most accurate method. At release stress of $0.82 f'_{ci}$, all loss prediction methods predicted losses within 10% of the measured losses and prestress loss was found to increase with higher release stresses.

2.1.6 Tadros et al., (1985)

Tadros et al. (1985) [28] detailed steps to calculate the deflection of prestressed concrete members. Instantaneous deflection of both uncracked and cracked concrete deflection is discussed. A proposal for time-dependent calculations of long-term camber is covered that considers shrinkage and creep of the concrete, as well prestress loss. Empirical formulas were developed using previous research to predict time-dependent deflections and curvature accurately. The proposed formulae also account for non-prestressing reinforcement in the concrete cross-section. The accuracy of the proposed method was compared to the PCI Design Handbook method for calculating the deflection of prestressed concrete beams.

The proposed deflection method from Tadros et al. (1985) [28] specifies the calculation of accurate prestress loss, then determining the instantaneous deflection of the uncracked

concrete section using gross section properties, then using proposed multipliers to determine final deflection. If a member is calculated to crack under service loads, then empirically derived cracked section properties are to be considered as well as tension stiffening effects. Multipliers were empirically derived for use in calculating immediate and long-term deflections. Naaman (1982) [21] proposed a formula for the moment of inertia of a cracked concrete section that was suggested to use this method. This equation is mentioned explicitly due to it accounting for non-prestressing steel. The proposed method was compared to measured values of a prestressed concrete girder used in this research and closely matched that of the measured values.

The effects of non-prestressing reinforcement on camber are discussed as well. Including mild steel in the bottom flange reduces camber and can increase time-dependent downward deflection. The increased stiffness caused by the inclusion of non-prestressing steel restrains creep and shrinkage of the surrounding concrete in the bottom fiber relative to the top fiber, causing an increase in prestress loss.

2.1.7 Baran et al., (2005)

Baran et al. (2005) [5] performed experiments to determine effective prestress in pretensioned concrete girders. The group cast eleven 20 ft long Type 28M beams; three did not experience pre-release cracks, and the remaining eight incorporated a single pre-release crack at varying depths and widths. Grade 270, 0.6 diameter, low-relaxation strands were used. The strands were partially prestressed to 0.54 f_{pu} instead of the standard 0.75 f_{pu}. Throughout the experiments, effective prestress was measured using vibrating wire gauges, LVDTs, surface strain gauges, and resistance strain gauges.

Experimental results on prestress loss were compared to prediction methods, specifically the AASHTO LRFD Refined method and the PCI Committee method.

The first method for testing effective prestress utilized vibrating wire gauges embedded in the concrete beams and measured strain throughout testing, starting at concrete casting. After the concrete set, change in strain was measured and used to find change in effective prestress due to elastic shortening. The beams were then flexurally load tested under four-point bending and strain was recorded. Prestress loss from elastic shortening was measured between 5.7 and 7.1 ksi between all samples. Total measured loss at the time of load testing ranged between 20.7 and 26.4 ksi.

The second method for testing effective prestress was to load test the concrete beams. Prestress loss was estimated using mechanics to relate effective prestress to loadings that caused initial crack propagation. Material tests were used to determine the concrete modulus of rupture. Flexural crack initiation was determined through visual observation, crack detection gauges, and strain gauges. After initial crack propagation occurred, the beams were unloaded and reloaded again to determine the crack reopening loads. It is also noted by Baran et al. (2005) [5] that the calculation of prestress loss was more accurately predicted using considering crack reopening loads because prestress loss is not dependent on the concrete modulus of rupture. Long-term losses computed using flexural cracking load were found to be 98.4 ksi on average. Long-term losses computed using flexural crack reopening load were found to be 69.2 ksi on average. The inaccuracy of these results was attributed modulus of rupture not being accurately predicted and inadequacies in determining the load at which cracking occurred.

The third method for testing effective prestress was to cut strands attached with strain gauges. Two beams were selected following the load tests. Two strands were exposed over about 20 in. at about 50 in. away from each side of the beams. Resistance strain gauges were attached to the strands and the strands were flame cut. The resulting total losses were found to be 34.5 ksi and 34.8 ksi in the two beams.

Their research concluded that the resulting prestress loss measured by the vibrating wire gauges in the experiment agreed well with the losses calculated using AASHTO LRFD Refined and PCI Committee methods. The group also found that using crack propagation loads and crack reopening loads with mechanics of materials in the second experiment could not accurately measure prestress loss. This was attributed to inadequacies in determining when flexural cracking occurred during the load tests and uncertainties in finding modulus of rupture. The strand cutting test performed in the third experiment was determined to be an effective way of determining effective prestress.

2.2 DISTRIBUTION FACTORS AND STATIC LOAD TESTING

Load testing is a standard way to determine the behavior of a bridge. This can be paired with visual inspection, structural health monitoring, non-destructive testing, and finite element-based structural modeling to assess bridge performance, strength, and serviceability. One significant observation that can be determined through load testing is the distribution factor of the bridge girders. Typically, the distribution factor (DF) for girders has always been determined through conservative approaches. This usually leads to overestimating loading on external girders, which leads to unnecessary reinforcement being used in the girders. More reinforcement, specifically prestressing steel, leads to higher costs on the bridge girders, can increase camber and prestress losses, and can negatively affect the durability of the bridge.

2.2.1 Dong et al. (2020)

Dong et al. (2020) [11] conducted load tests on multi-span, prestressed concrete bridges with several spans of the same geometry and material properties. One of the main goals was to measure the distribution factors of the bridge and evaluate the load-carrying capacity. The bridge was constructed in 1964 with a total length of 912 m. Each span was 24.5 m long and featured five AASHTO Type II girders spaced at 2.4 m. One span was selected and instrumented using three types of sensors. A total of 15 accelerometers were placed at midspan at ¼ & ¾ span. Five displacement sensors (potentiometers) were installed at the midspan of each girder. Strain gauges were installed at ¼ of the span.

The static load test from this research utilized two trucks. One truck weighed 26,280 lb and the other weighed 69,660 lb. Two identical static load tests were performed with each

static test only utilizing one of the trucks. The truck was centered over the first interior girder and moved at quarter points along the length of the bridge. The truck was then placed on the incoming traffic lane and the test was repeated. Instrumentation measurements were taken throughout the testing. The results from each of the tests were then combined to reflect multi-lane loading. It is worth noting that the multi-lane loading results cause the center girder to have the highest distribution factor. The group developed a finite element model using SAP 2000 (CSI 2019) to recreate the testing. The distribution factor of the center girder from multi-lane loading was found to be 0.59. From FEM, the distribution factor of the center girder was 0.52. AASHTO methods found the distribution factor to be 0.61. The research concluded that the AASHTO prescribed methods' distribution factors provided slightly more conservative results than the experimental and finite element approaches.

2.2.2 Barr et al. (2001)

Barr et al. (2001) [6] performed finite element analysis to determine distribution factors in prestressed concrete girder bridges. The group performed a static load test to validate their results and used the model to investigate the effects of lifts, intermediate diaphragms, end diaphragms, and load types. Load testing was performed on a three-span bridge and utilized a two-axle truck that weighed 35.6 kips. The group measured strain using vibrating wire gauges that were installed at both midspan and 5 ft. from the ends of the span. The strain measurements were used to derive moment inside the girders and distribution factors were derived by comparing to the applied truck moment to the measured moment. Results were compared to AASHTO methods of determining distribution factors. The group found that FEA was able to predict midspan moment

within 6% of the measured moment during load testing. It was also concluded that AASHTO methods were typically conservative by as little as 6% and as high as 28% compared to the finite element results. The FEA results also showed that intermediate diaphragms had little effect on distribution of loads, while end diaphragms and lifts significantly reduced distribution factors in the bridge girders.

2.2.3 Lin & Vanhorn (1968)

Lin & Vanhorn (1968) [18] investigated the effects diaphragms have on load distribution of prestressed concrete girder bridges. The group performed load testing on a bridge and measured strain using strain gauges. Data from the strain gauges was used to derive deflection and internal moments. Measured and predicted distribution factors were compared. The group concluded that diaphragms minorly affected load distribution by up to 3% and suggested that diaphragms do not need to be used in design.

2.2.4 Conner & Huo (2006)

Conner & Huo (2006) [8] developed finite element models to determine the effects of parapets and aspect ratio on live load distribution factors. The group developed finite element models that had different skew angles, overhang lengths, and different width to length (aspect) ratios. It is worth noting that the group kept girder spacing consistent throughout the experiment and added in new girders as width of the model was increased. The group found that distribution factors of the exterior girders increased when overhang of the deck was increased. As overhang increased, the distribution factors of the exterior

girder increased at a higher rate than the model with the parapets included, meaning that the parapet becomes more effective at distributing load as overhang increases. The group found that parapets can greatly reduce distribution factors in exterior by up to 36%, and reduce distribution factors in interior girders by as much as 13%. The group also found that the AASHTO lever rule overpredicted distribution factors of exterior girders on average by 21% due to the method ignoring the effects of parapets in the analysis.

CHAPTER III

3 CAMBER AND PRESTRESS LOSS

3.1 INTRODUCTION

This chapter discusses the background information of the SH4 bridge project, as well as prestress loss calculations and camber measurements. The primary objective of this chapter is to discuss the mild steel reinforcement and distributed prestressing reinforcement and the effects these design changes have on camber and prestress losses.

3.2 PROJECT BACKGROUND

This work is based on a research project on the South Highway 4 Bridge over the North Canadian River in Yukon, Oklahoma. The bridge consists of 15 spans traveling North and Southbound. Each span is approximately 100 ft. long and 42 ft. 2in. wide. All spans were constructed using Type IV prestressed concrete girders and contain four girders per span at 11 ft. 4 in. center to center spacing with an 8 in. concrete deck. A photograph of the structure is shown in Figure 3. The cross-section of the concrete girders with the deck is shown in Figure 4.

Figure 3: Photograph of the SH 4 Bridge over N. Canadian R., Canadian Co., OK.

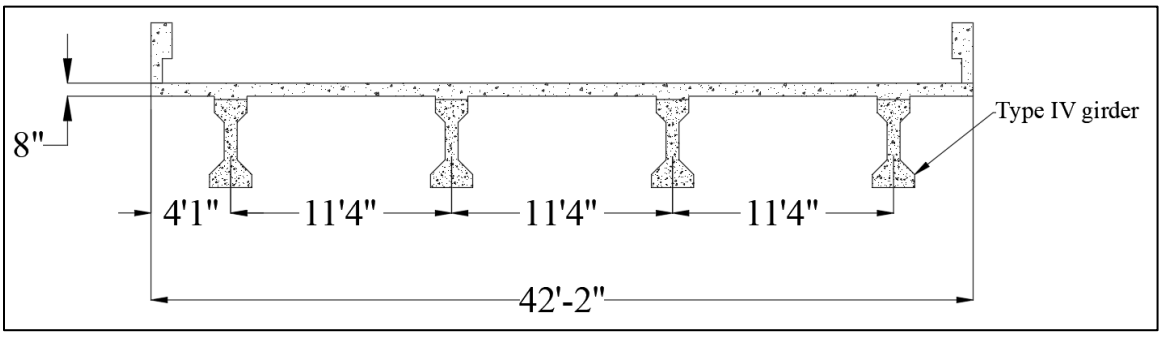

Figure 4: Cross-section of the bridge.

Each span featured variations in vertical and longitudinal reinforcement. Variations in vertical reinforcement variations included

1) Placement of bundled shear reinforcement in end regions (with or without).
2) Placement of an L-bar in the end regions (with or without).
3) Variations in prestressing reinforcement (the number of strands, the strand pattern, number of debonded strands, length of debonding).
4) Inclusion of four #7 bars in the bottom flanges (with or without, and the length of mild steel).

The two primary variables discussed in this research are the use of different strand patterns and whether or not mild steel reinforcement was used in the bottom flange.

Each span featured some variation of the different combinations of the two variables:

- Whether or not a "traditional" strand pattern or "distributed" strand pattern was used.
- Whether or not mild steel reinforcement (4-#7's) was used in the bottom flange at midspan.

Distributed strand patterns were investigated is because prestress moment is significantly reduced when compared to a traditional strand pattern. Prestress moment is defined as prestress force multiplied by the eccentricity of the strands. The distributed strand pattern places more prestressing steel closer to the neutral axis of the girder, therefore reducing eccentricity of the strands and reducing prestress moment. The reduction in prestress moment reduces camber and affects prestress loss.

From this, four longitudinal reinforcement cases are present between all spans in the bridge:

- Case A: Traditional strand pattern with no mild reinforcement in the bottom flange.
- Case B: Traditional strand pattern with mild reinforcement in the bottom flange.
- Case C: Distributed strand pattern with no mild reinforcement in the bottom flange.
- Case D: Distributed strand pattern with mild reinforcement in the bottom flange.

For this work, a traditional strand pattern refers to when prestressing strands are placed as close as possible to the extreme bottom fiber of the concrete girder to maximize the effects of prestress moment. A distributed strand pattern refers to when prestressing strands are placed closer to the center of gravity of the concrete to prevent excessive camber. All strand patterns include fully tensioned top strand, as this has been standard practice in Oklahoma since the late 1990's (Russell, 2018) [23]. Details of all reinforcement layouts are shown in Figure 5. Vertical and longitudinal reinforcement variations by span are shown in Table 1.

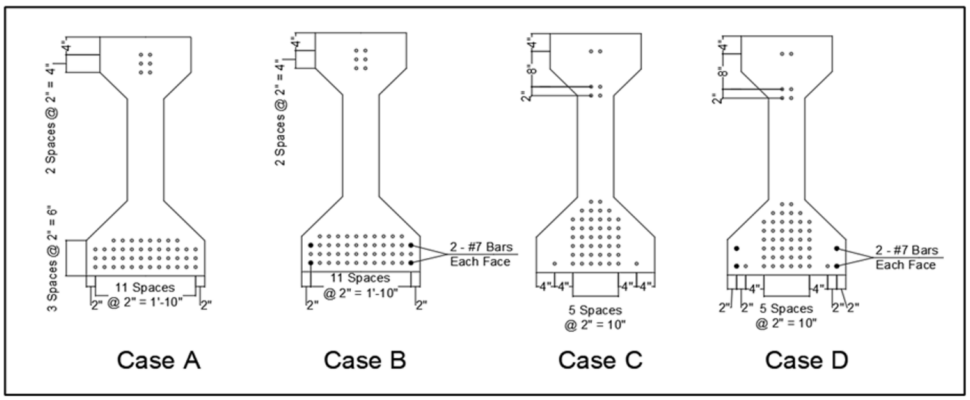

Figure 5: Detailing of longitudinal reinforcement layouts.

Table 1: Prestressing strand and mild reinforcement variations by span.

	Longitudinal Reinforcement Case	No. Strands	Distributed (Y or N)	No. of Debonded Strands	Bundled Verticals (Y or N)	L-Bar	Mild Steel Bottom Flange
Span 1	Case C	50	1	2	1	0	0
Span 2	Case C	50	1	2	1	1	0
Span 3	Case A	50	0	12	1	0	0
Span 4	Case A	50	0	12	0	0	0
Span 5	Case C	50	1	2	0	0	0
Span 6-1	Case D	50	1	2	0	0	(4) #7's
Span 6-2	Case D	50	1	2	1	0	(4) #7's
Span 7-1	Case D	50	1	2	0	0	(4) #7's
Span 7-2	Case D	50	1	2	1	0	(4) #7's
Span 8-1	Case B	48	0	8	0	0	(4) #7's
Span 8-2	Case B	48	0	8	0	0	(4) #7's
Span 9-1	Case B	48	0	8	0	0	(4) #7's
Span 9-2	Case B	48	0	8	1	0	(4) #7's
Span 10-1	Case A	48	0	8	0	0	0
Span 10-2	Case A	48	0	8	0	0	0
Span 11	Case C	50	1	2	0	0	0
Span 12	Case A	50	0	12	0	0	0
Span 13	Case A	50	0	12	1	0	0
Span 14	Case C	50	1	2	1	1	0
Span 15	Case C	50	1	2	1	0	0

Two external girders were instrumented with embedded thermocouples and vibrating wire gauges (VWGs) to measure changes in temperature and strain, respectively. The two instrumented girders are Mark 27, Span 9 and Mark 42, Span 14. Details of instrumentation are discussed further in of this paper. The Mark 27, Span 9 girder falls under Case B reinforcement layout and contains a traditional strand pattern that includes four #7 mild steel reinforcing bars in the bottom flange. The Mark 42, Span 14 girder

falls under Case C and contains a distributed strand pattern with no mild steel included in the bottom flange.

Figure 6: Aerial view of the SH4 bridge over the North Canadian River.

3.2.1 Material Properties

Two different concrete mixtures were employed. For the prestressed girders, the concrete mix design conformed to the Class P specifications in the Oklahoma Department of Transportation Standard Specifications for Highway Construction. The concrete mixture design for the concrete deck conforms to the Class AA specifications in the Oklahoma Department of Transportation Standard Specifications for Highway Construction. The design specifications for both classes are displayed in Table 24 in Appendix A. The concrete deck cast dates are displayed in Table 2.

Table 2: Significant dates PC beam fabrication, handling, transportation and erection, and SH 4 Bridge construction.

	Beam Mark 27, Span 9	Beam Mark 42, Span 14
Girder Casting	April 23, 2020	April 28, 2020
Detensioning	April 24,2020	April 29, 2020
Placement of girders	May 26, 2020	June 1, 2020
Deck Placement	August 14, 2020	August 18, 2020

The girders were cast at Coreslab Structures in Oklahoma City, Oklahoma. Span 9 girders were cast in the same prestressing bed on April 23, 2020. The four PC Beams for Span 9 are reinforced as shown in Case B and contains a "traditional" prestressing pattern; all four PC Beams contain longitudinal mild reinforcement midspan. Span 14 girders were cast in the same prestressing bed on April 28, 2020. The four PC Beams for Span 14 are reinforced as shown in Case C and contains a "distributed" prestressing pattern. Span 14 PC beams do not contain longitudinal mild reinforcement. Fresh concrete samples were taken during the fabrication of the Span 9 and Span 14 girders, and fresh and hardened concrete testing was performed. Slump testing was performed in accordance with ASTM C143. Unit weight was measured following ASTM C138. Air content was measured following ASTM C231. For each girder, 32 cylinders were made for hardened concrete materials testing. Compressive strength was measured according to ASTM C39, the elastic modulus was measured following ASTM C469, and splitting cylinder tensile strength was measured according to ASTM C496. Early and 28-day compressive strengths are reported in Table 3. The results of all concrete testing are present in Appendix A.

Table 3: Early and 28-day compressive strengths.

Average Compressive Strength (ASTM C39) (psi)		
Day	**3**	**28**
Span 9, Mark 27	8,760	10,810
Span 14, Mark 42	8,970	10,490
Span 9 Deck	4,750	6,340
Span 14 Deck	4,000	5,210

3.3 ESTIMATING PRESTRESS LOSSES

3.3.1 METHODOLOGY

Prestress losses were estimated by several common methods. Estimates of prestress losses are compared to losses derived from strain measurements made on the PC Beams through the Structural Monitoring system. The following methods were used to compute/estimate the prestress losses and compare them with the measured data:

- AASHTO 2020 LRFD [4] Specification, Approximate method.
- AASHTO 2020 LRFD [4] Specification, Refined method.
- PCI Design Handbook [20] method.
- Modified Version of the PCI Design Handbook method (using transformed cross section properties).
- Jayaseelan Time-Step Method (2018) [15].

The procedures of each of these methods is shown in Appendix B.

3.3.1.1 AASHTO 2020 LRFD Approximate Method

The computation of the prestress losses for this method follows the procedures provided in the LRFD AASHTO 2020 [4] specifications. This method lumps long-term losses from creep and shrinkage of the concrete and relaxation of prestressing strands together. Gross section properties are used, meaning this method does not directly account for the inclusion of mild reinforcing steel. Designers do have the option to use transformed section properties, but it is not commonly practiced as this method provides an approximation. Elastic shortening is calculated separately and added to the total long-

term losses. Results are tabulated in Table 4. This method was calculated using gross-section properties.

Table 4: Approximate loss estimates for time-dependent losses according to the AASHTO 2020 LRFD Design Specifications.

Approximate estimates of time-dependent prestress losses according to the 2020 *AASHTO LRFD Bridge Design Specifications*			
Case	**ES, (ksi)**	**Δf_{pLT} (ksi)**	**Total, ksi**
A	21.9	28.6	50.5
B	20.5	27.8	48.3
C	19.6	28.6	48.2
D	19.6	28.6	48.2
Note: ES = prestress loss due to elastic shortening; Δf_{pLT} = long term losses (CR +SH +RE); 1 ksi = 6.895 MPa.			

3.3.1.2 AASHTO 2020 LRFD Refined Method

This method follows the procedures in the 2020 edition of AASHTO LRFD [4]. In standard practice, gross section properties are used in this procedure, but transformed section properties are permitted to be used. For this research, transformed section properties were used in which steel in the concrete girder and composite deck were transformed. This procedure is time-dependent and requires calculation of the creep coefficient of concrete, $\psi_b(t_f, t_i)$ and shrinkage strain of concrete, ε_{sh}, for both the girder and concrete deck at different time intervals. The creep coefficient, ψ_b is a function of the time at loading, t_i and the time at which the creep coefficient is evaluated, t_f. Prestress losses were calculated before deck casting (110 days) and at 500 days at midspan. Elastic

shortening is calculated separately and added to get total loss at 110 days and 500 days individually. Tabulated results are shown in Table 5.

Table 5: Refined estimates of time-dependent prestress losses at midspan calculated using transformed section properties according to the 2020 AASHTO LRFD Bridge Design Specifications.

Refined estimates of time-dependent prestress losses at midspan calculated using transformed-section properties according to the 2020 AASHTO LRFD Bridge Design Specifications							
Case	**Concrete age, days**	**ES, ksi**	**CR, ksi**	**SH, ksi**	**RE, ksi**	**SH of Deck, ksi**	**Losses at midspan, ksi**
A	110	19.7	15.3	5.9	1.2	0	42.1
	500	19.7	15.3	7.2	2.4	-0.8	43.8
B	110	18.1	14.2	5.9	1.3	0	39.5
	500	18.1	14.1	7.2	2.6	-0.8	41.2
C	110	17.9	14.2	6.0	1.3	0	39.4
	500	17.9	14.4	7.3	2.6	-0.6	41.7
D	110	17.5	13.9	6.0	1.3	0	38.7
	500	17.5	14.1	7.3	2.6	-0.6	41.0
Note: CR = prestress loss due to creep; ES = prestress loss due to elastic shortening; RE = prestress loss due to relaxation; SH = prestress loss due to shrinkage. 1 ksi = 6.895 MPa.							

3.3.1.3 PCI Design Handbook Method

The PCI Design Handbook 6th Edition [20] method offers a descriptive method for estimating prestress losses. The loss method provided by PCI is based on work done by Zia et al. (1979) [28]. Although more complicated methods of estimating losses have since been developed, this method remains a valuable tool for estimating prestress losses

for all types of precast, prestressed concrete structural members. As described by Zia et al. [30], and also in the PCI Handbook [20], this method uses gross section properties to estimate prestress losses. The method using gross properties will not include the effects of mild reinforcement. Results are tabulated in Table 6.

Table 6: Approximate loss estimates using gross section properties according to PCI Design Handbook 6th Edition.

Prestress losses at midspan calculated using gross section properties with the *PCI Design Handbook* method						
Case	**Concrete age, days**	**ES, ksi**	**CR, ksi**	**SH, ksi**	**RE, ksi**	**Losses at midspan, ksi**
A	110	23.3	35.0	5.9	2.4	66.6
	500	23.3	20.7	5.9	3.0	52.9
B	110	21.7	33.0	5.9	2.6	63.2
	500	21.7	19.0	5.9	3.1	49.7
C	110	20.9	31.9	5.9	2.7	61.4
	500	20.9	19.7	5.9	3.1	49.6
D	110	20.9	31.9	5.9	2.7	61.4
	500	23.3	35.0	5.9	2.4	66.6
Note: CR = prestress loss due to creep; ES = prestress loss due to elastic shortening; RE = prestress loss due to relaxation; SH = prestress loss due to shrinkage. 1 ksi = 6.895 MPa.						

3.3.1.4 Modified PCI Design Handbook Method

This section repeats the PCI Design Handbook [20] method but employs transformed section properties in the calculation. Cross-section properties and other parameters are

computed using the same formulae but using transformed cross-section properties instead of gross-section properties. Transformed section properties were calculated with steel in the concrete girder and composite deck transformed. When computing losses with transformed section properties, as opposed to gross section properties, minor changes in creep and shrinkage losses are observed, but elastic shortening loss changes significantly. Results are tabulated in Table 7.

Table 7: Approximate loss estimates using transformed section properties according to PCI Design Handbook 6th Edition

Prestress losses at midspan calculated using transformed section properties with the *PCI Design Handbook* method						
Case	**Concrete age, days**	**ES, ksi**	**CR, ksi**	**SH, ksi**	**RE, ksi**	**Losses at midspan, ksi**
A	110	23.0	34.6	5.9	2.5	66.0
	500	23.0	21.7	5.9	3.0	53.6
B	110	20.9	31.9	5.9	2.7	61.4
	500	20.9	19.7	5.9	3.1	49.6
C	110	20.8	31.9	5.9	2.7	61.3
	500	20.8	20.7	5.9	3.1	50.5
D	110	20.2	31.1	5.9	2.7	59.9
	500	20.2	20.3	5.9	3.1	49.5
Note: CR = prestress loss due to creep; ES = prestress loss due to elastic shortening; RE = prestress loss due to relaxation; SH = prestress loss due to shrinkage. 1 ksi = 6.895 MPa.						

3.3.1.5 Jayaseelan Time-step Method

This section is based on the proposed time-step loss model from Jayaseelan & Russell (2019) [15]. One of the main mechanics of this method is that it breaks down concrete strength and modulus as a function of time, which can be computed on a day-by-day basis. Transformed section properties are used in this method. The strain from creep and shrinkage are considered separately and are computed similarly to that of the AASHTO LRFD [4] Refined method. The initial age of concrete at transfer was taken as 1 day, and the deck cast was taken as 110 days. Final prestress losses were taken at 500 days. Results are tabulated in Table 8. Results calculated on a day by day basis are presented in Figure 7.

Table 8: Prestress losses at midspan calculated with the Jayaseelan Time-step method

Prestress losses at midspan calculated with the Jayaseelan time-step method						
Case	**Concrete age, days**	**ES, ksi**	**CR, ksi**	**SH, ksi**	**RE, ksi**	**Losses at midspan, ksi**
A	110	21.5	12.2	5.4	1.1	40.2
	500	21.5	8.9	6.5	1.6	38.5
B	110	19.7	11.1	5.3	1.2	37.3
	500	19.7	8.2	6.3	1.7	35.9
C	110	19.5	11.1	5.4	1.2	37.2
	500	19.5	8.0	6.5	1.7	35.7
D	110	19.0	10.8	5.3	1.3	36.4
	500	19.0	7.7	6.3	1.7	34.7
Note: CR = prestress loss due to creep; ES = prestress loss due to elastic shortening; RE = prestress loss due to relaxation; SH = prestress loss due to shrinkage. 1 ksi = 6.895 MPa.						

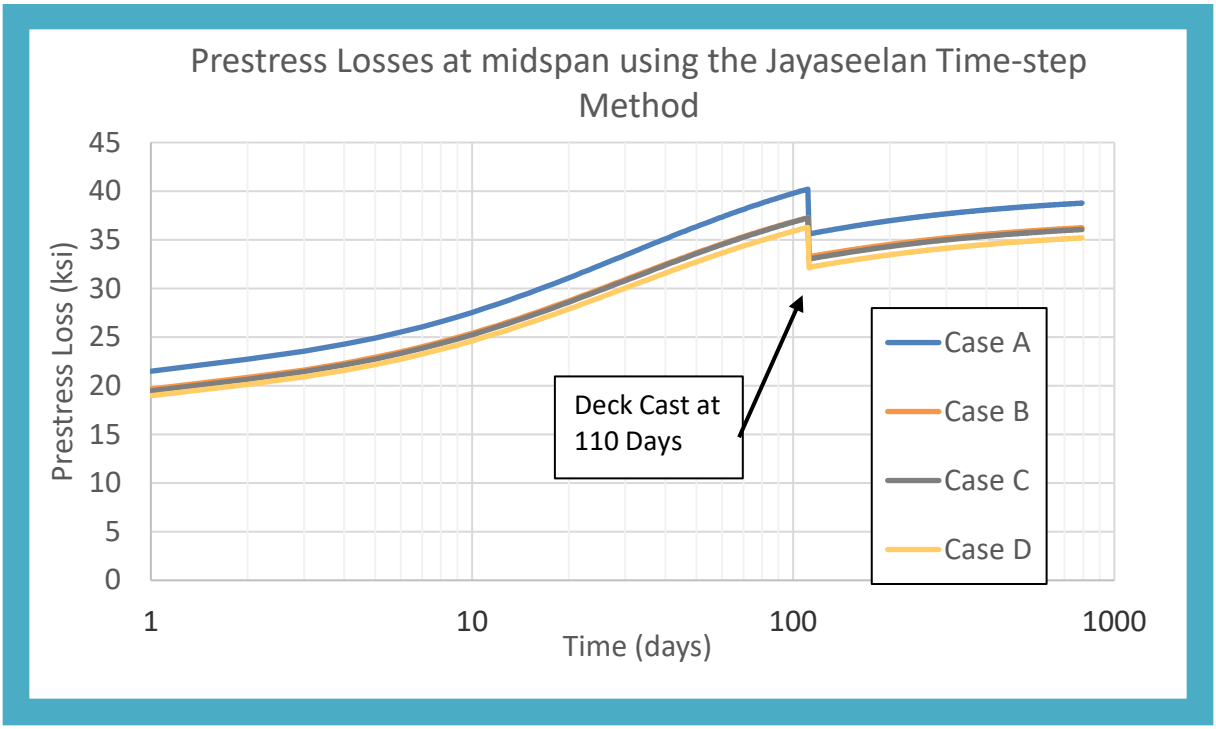

Figure 7: Estimated prestress losses using the Jayaseelan Time-step method

The calculations for the Jayaseelan Time Step Method are shown in Appendix B4. Using this method, it is possible to compute prestress losses and related time-dependent strains at every time interval (daily). However, the method does not require a loss calculation every day. Instead, the "time-step method" can be employed and losses computed only at significant days where there is a change of loading or change of environmental conditions, similar to the AASHTO Refined method. In these calculations, the Jayaseelan Time Step Method was used to compute losses immediately after release at 24 hours, during storage, at erection of the girders on the bridge site, just prior to deck casting, just after deck casting and at 500 days, (approximately 400 days of life in-service). Results of this analysis are also present in Table 33 in Appendix B4.

3.4 MEASUREMENT OF PRESTRESS LOSSES

3.4.1 METHODOLOGY

Beams Mark 27, Span 9 and Mark 42, Span 14 were selected for the structural monitoring program and instrumented for this study. In the bridge plan, both of the beams will be located as external girders, on the West side of each's respective span. Beam Mark 27 is the external West girder for Span 9 and Beam Mark 42 is the external West girder for Span 14. Instrumentation was installed the locations found in Figure 7. Vibrating wire gauges and thermocouples were used to measure strain and temperature data. Instrumentation was placed at:

- 4 in. from the end region of the beams.
- 16.0 in. from the end region of the beams.
- 32.0 in. from the end region of the beams.
- At the midspan of the beams.

Figure 9 displays the location of the installed sensors along the girder's cross-section. Instrumentation and data acquisition systems allowed continuous monitoring of data from the time of fabrication through handling, storage, transportation, erection, and continuing through the construction and service life of the bridge. Measurements are still being recorded to date. Data gathered from this program is used to measure strain in the concrete, which can be used to find prestress losses and camber at midspan.

For this thesis, the only data presented and discussed involve data on strains and temperatures from midspan locations.

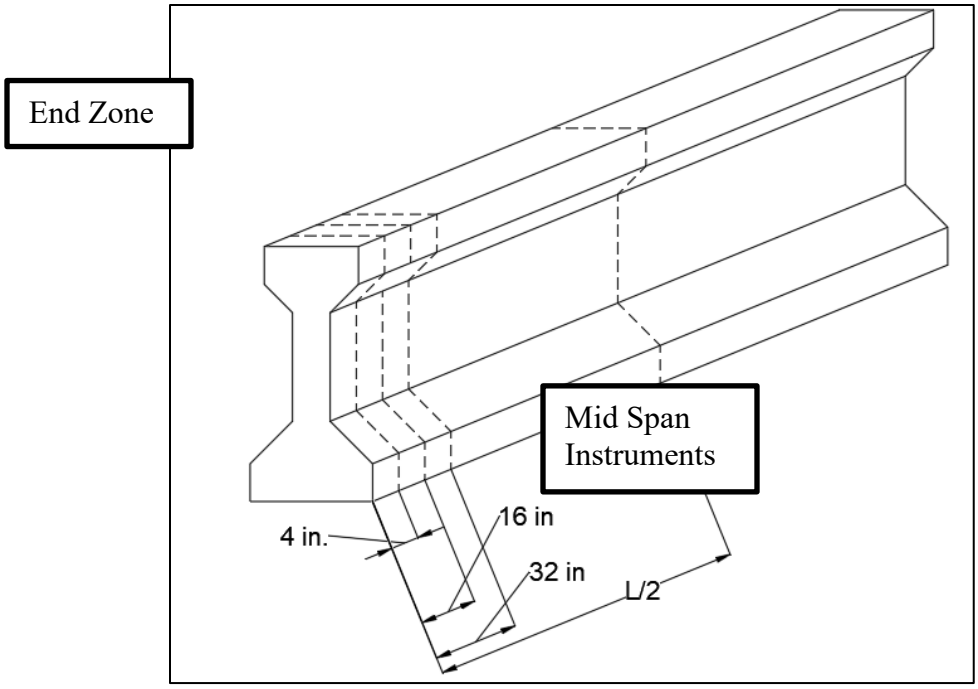

Figure 8: Sensor locations at each length increment of the girders.

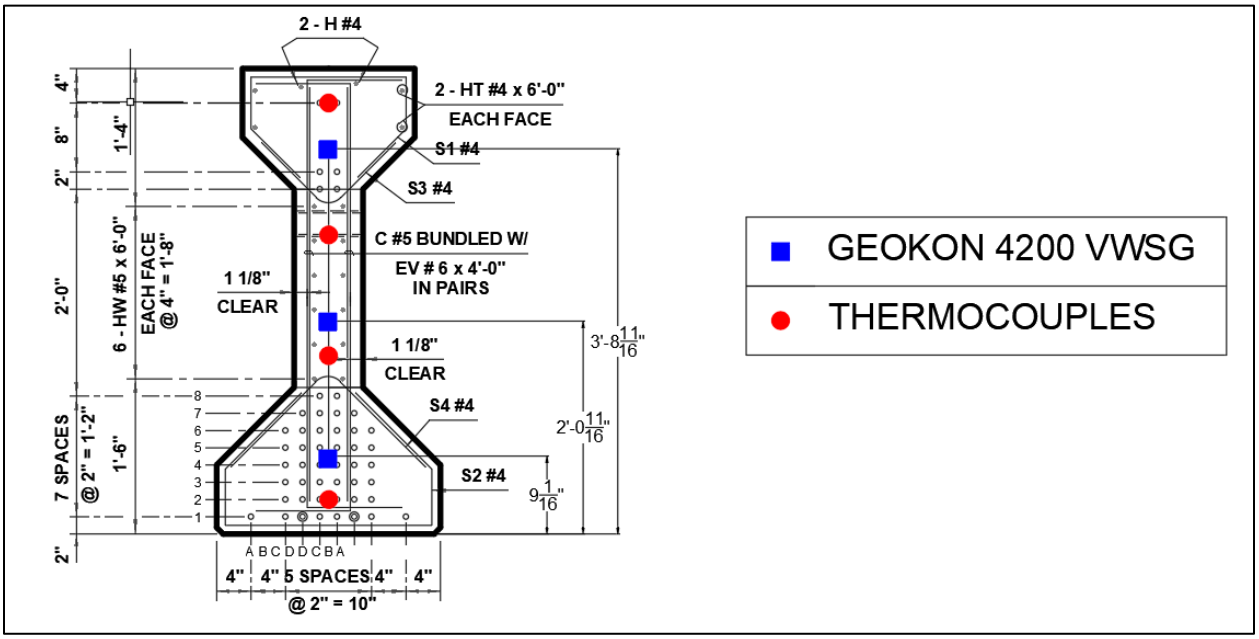

Figure 9: Sensor locations shown in girder cross-section.

Figure 10: North end reinforcement and instrumentation, Beam Mark 27, Span 9.

Figure 11: Dillon Cochran (left), M.S., and Alla Acheli, Ph.D. are pictured installing instrumentation.

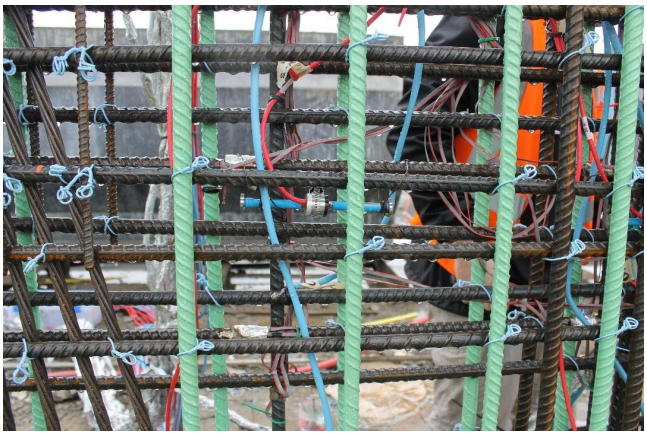

Figure 12: Vibrating Wire Gauge (blue) is located in the foreground at approximately C.G.S.

Figure 13: Instrumentation at midspan, Mark 27, Span 9. Four #7 reinforcing bars are placed in the corners of the bottom flange.

Figure 14: Mark 27, Span 9 at finishing station.

Figure 10 shows a photograph of the sensors before the girder cast at the end region of girder Mark 27 Span 9. Instrumentation was installed on girder Mark 27 Span 9 on April 21 and 22, 2020. The beam was cast on April 23, 2020, and de-tensioned on April 24, 2020. The process was repeated for the Mark 42, Span 14 girder. Instrumentation was installed on April 26 and 27, 2020. The beam was cast on April 28 and detensioned on April 29. The structural monitoring system recorded and stored concrete strain and temperature data throughout the concrete casting, curing, form removal, detensioning, transportation, hauling, deck cast, and service life. Figure 10, Figure 11, Figure 12, and Figure 13 show the work in progress during the instrumentation installation.

The data gathered from the thermocouples provides and insight on how concrete is affected during heat of hydration, as well as maps seasonal changes in temperature. Temperature data is also needed to calibrate measurements from the vibrating wire gauges. Strain readings provide real time data on bridge behavior. The results of the

strain data near the center of gravity of prestressing steel are multiplied by the elastic modulus of the prestressing steel to find effective prestress in the system. Note that the recorded data is the strain in the concrete and not directly measured from the prestressing steel.

3.4.2 RESULTS

3.4.2.1 Measured Concrete Temperatures at Early ages

Both Girders (Mark 27 and Mark 42) were cast in the late morning. The heat from the hydration of cement begins immediately upon water being combined with the cement. As sulfate ions impede the acceleration of hydration of calcium silicates and aluminates, heat is produced from the solution of Ca ions, and heat begins to build as pH increases. Figure 15 and Figure 16 display the entire heating and cooling cycle during concrete hydration along with measured concrete temperatures for Mark 27 and Mark 42, respectively.

Figure 15 starts at concrete casting at 11:30 AM on April 23, 2020. The casting of the PC Beam took approximately 30 minutes. The heat from cement hydration is shown to increase temperature dramatically in the first 24 hours, reaching a maximum concrete temperature of 167 ^{0}F at 5:30 PM, approximately 6.0 hours after casting. Note that the top flange of the PC Beam is approximately 22 ^{0}F hotter than the bottom flange, which reached a maximum temperature of about 145 ^{0}F. The charts show the cooling that corresponds with the hydration reactions slowing down through the natural hydration process. Form removal concluded at 6:30 AM the next day, and the concrete's cooling accelerated afterward. From 24 to 72 hours, it is shown that the concrete temperature mirrors the ambient temperatures as the PC Beam reverts to the baseline ambient temperature.

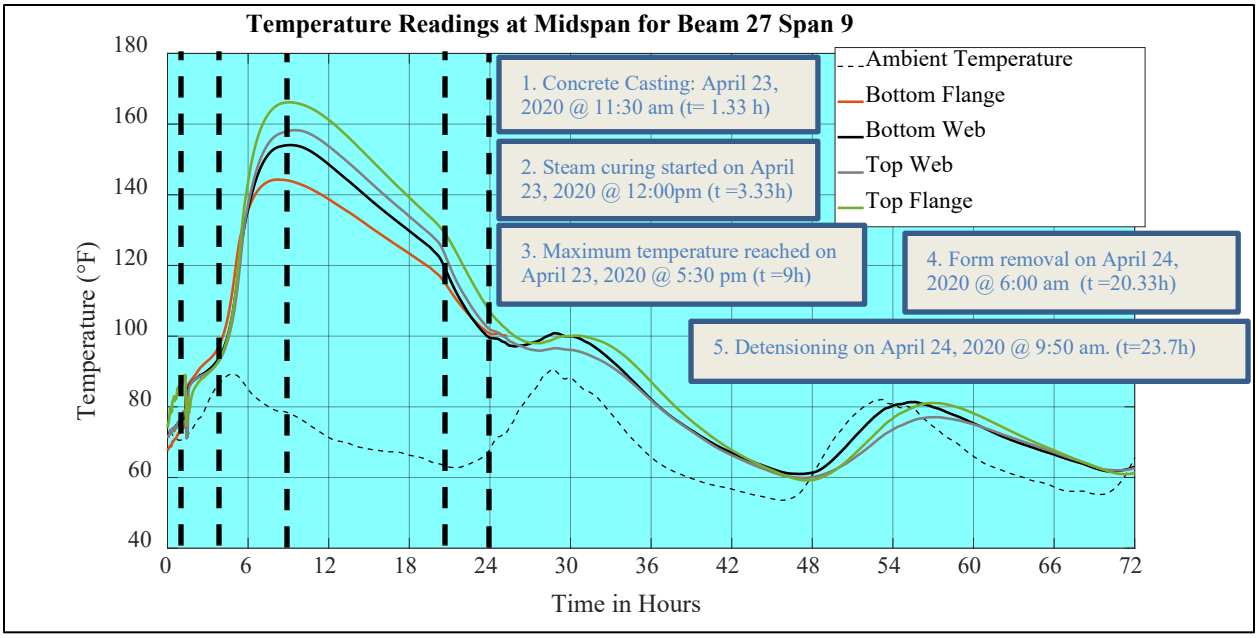

Figure 15: Girder Mark 27, Span 9. Recorded temperatures at midspan during the first 72 hours of the PC Beam life.

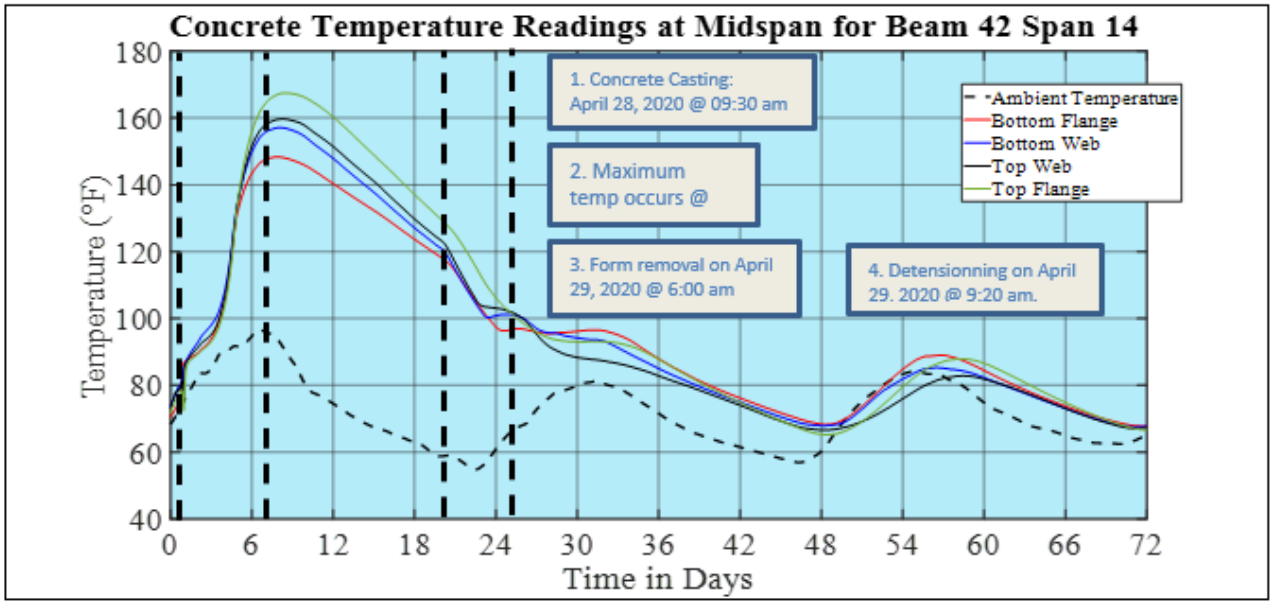

Figure 16: Girder Mark 42, Span 14. Recorded temperatures at midspan during the first 72 hours of the PC Beam life.

3.4.2.1.1 Measured Concrete Strain at Early ages

Figure 17 and Figure 18 chart the concrete strains measured by vibrating wire gauges installed in Beam Mark 27, Span 9 and Beam Mark 42, Span 14 at Midspan during the first 72 hours of the beam's life, respectively. Positive strains (lengthening) occur as concrete temperatures increase. Cooling did not significantly alter the measured strains, indicating that the concrete was restrained by a combination of reinforcement and the formwork. However, significant changes in concrete strains are shown with the detensioning of the prestressing strands. During detensioning, the prestressing forces impose net compressive strains into the concrete. Additionally, because the prestress force is eccentrically located, the compressive strains following detensioning are more prominent in the bottom flange. The figure shows concrete strains at the bottom flange, located at the approximate location of the C.G.S., concrete strains at the centroid of the Type IV girder, or the C.G.C., and strains near the top flange.

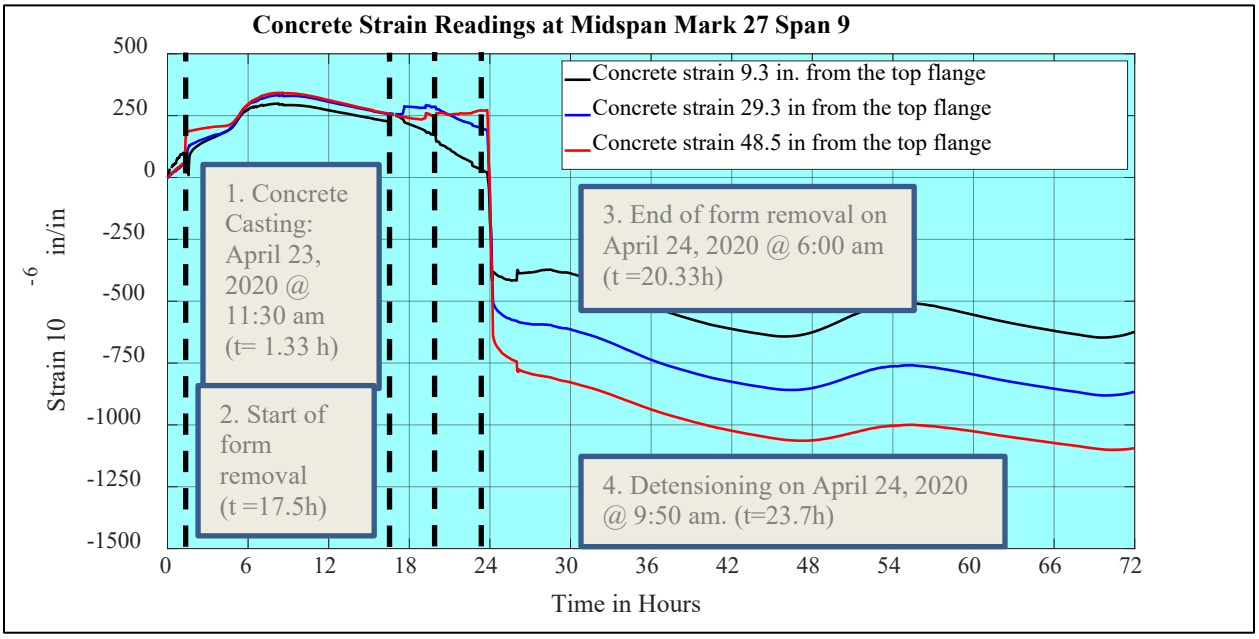

Figure 17: Measured strains in concrete at midspan during the first 72 hours for Mark 27, Span 9.

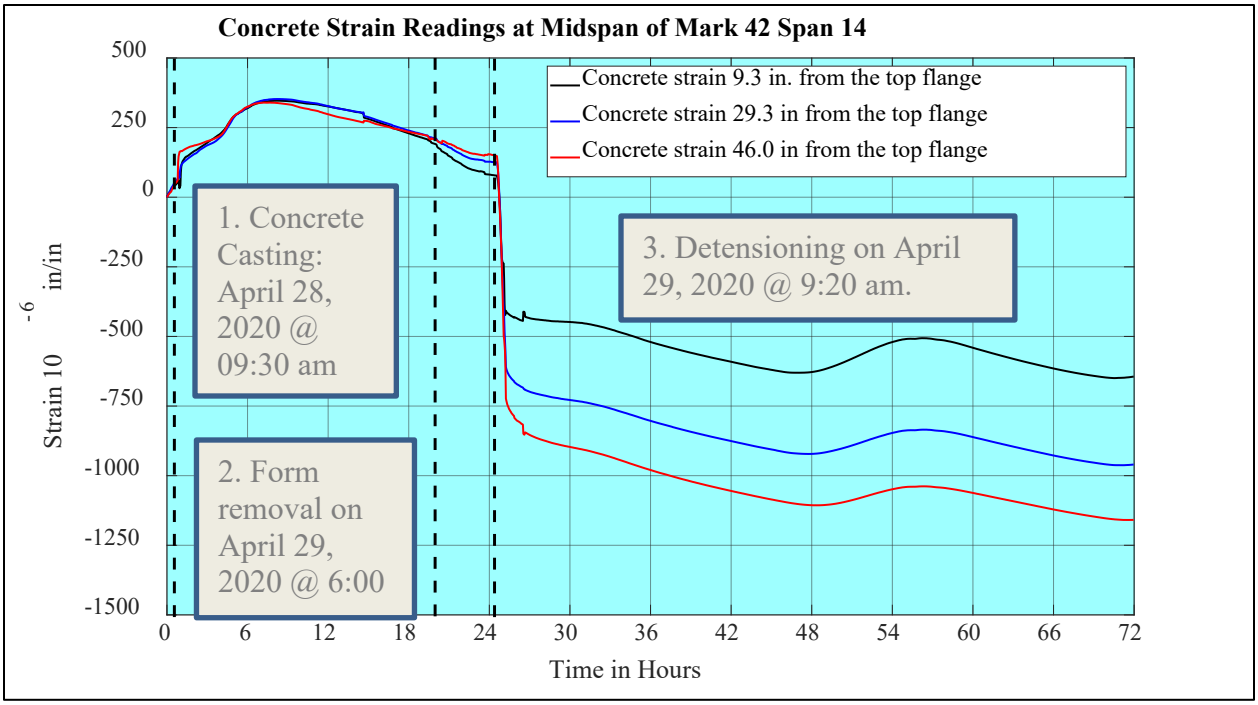

Figure 18: Measured strains in concrete at midspan during the first 72 hours for Mark 42 Span 14.

3.4.2.2 Long Term Measurements

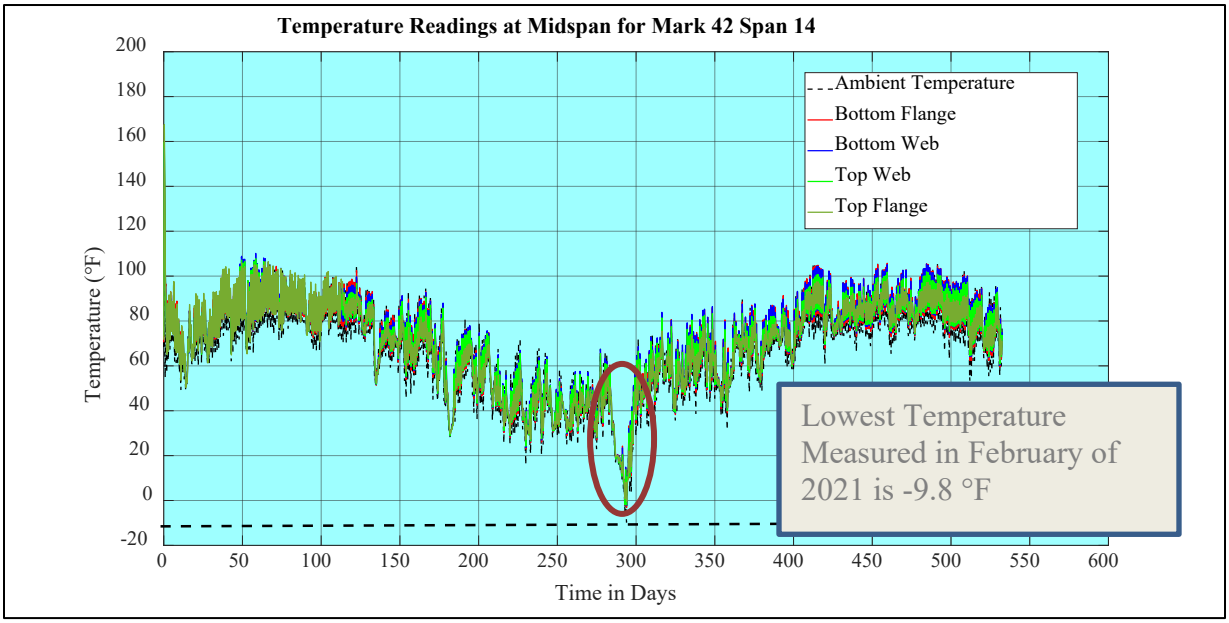

Figure 19: Measured ambient and concrete temperature at midspan for Mark 42, Span 14.

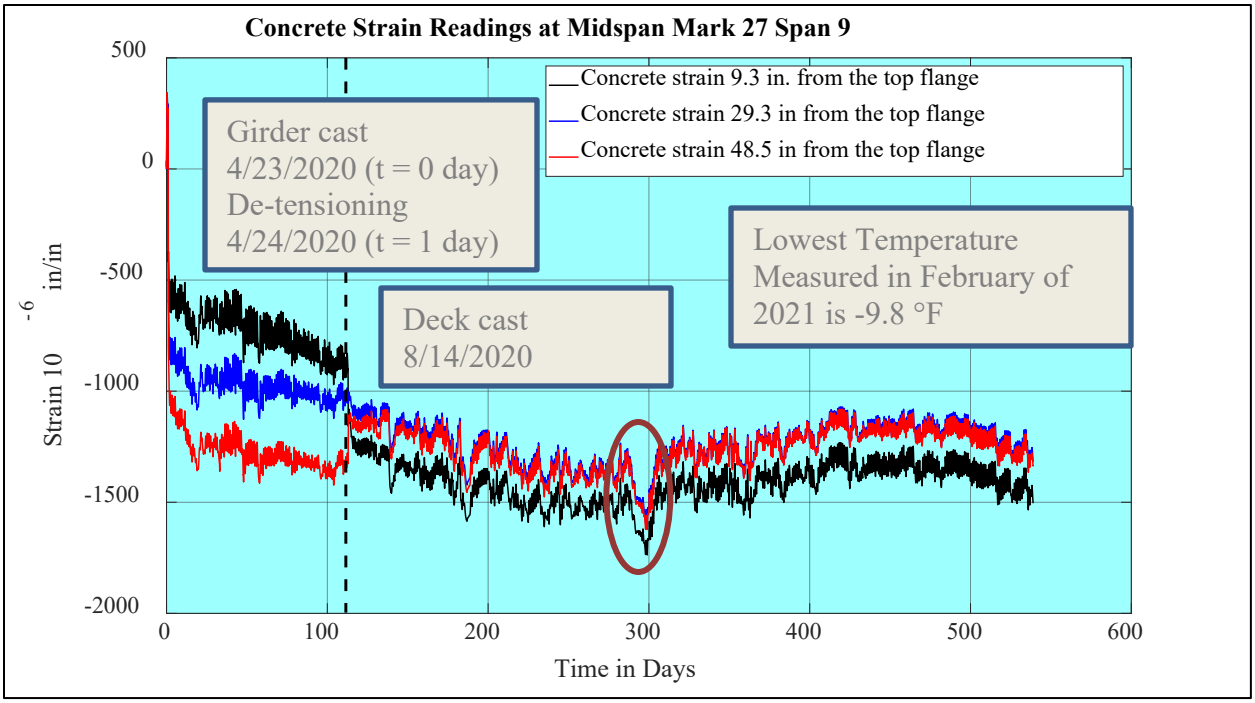

Figure 20: Measured strains in Span 9, Mark 27, beginning when the girder was cast (April 2020) and going through mid-October 2021.

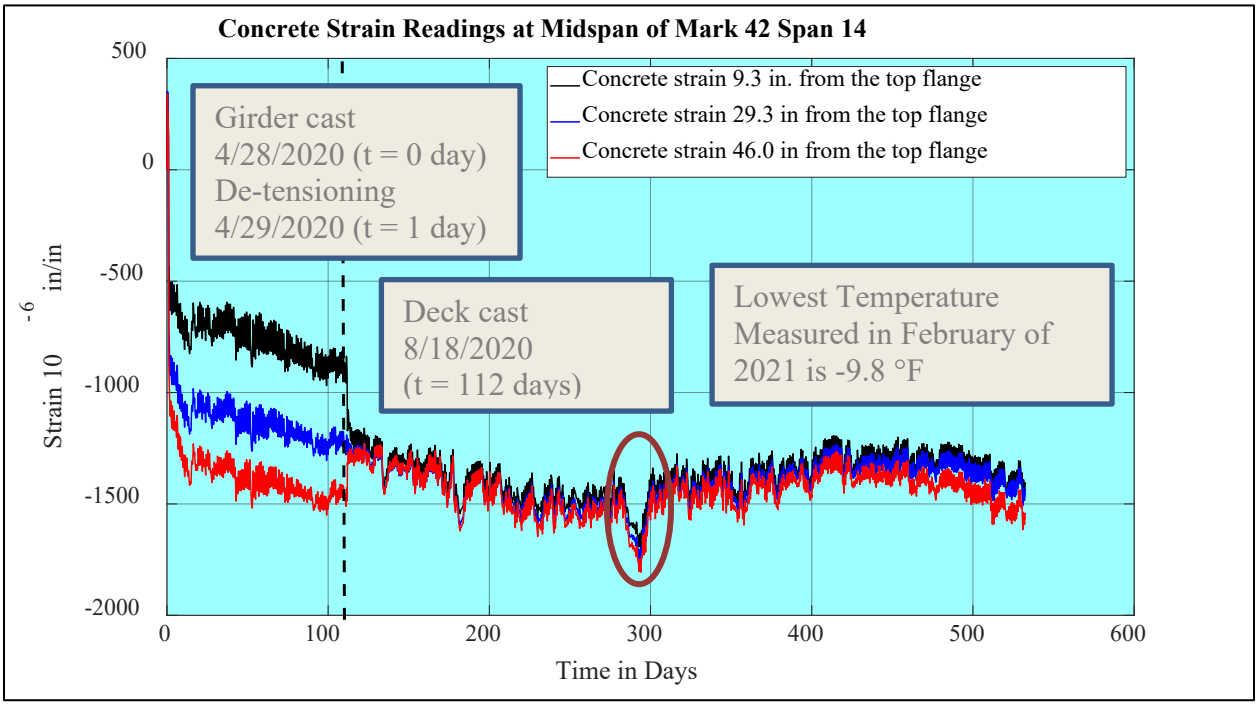

Figure 21: Measured strains in Span 14, Mark 42 beginning on the date the girder was cast (April 2020) and going through mid-October 2021.

Figure 19 shows the concrete temperature and ambient temperature for Span 14, Mark 42, from the girder cast day (April 28, 2020) up to October 14, 2021. Figure 20 shows measured strains at various depths within Span 9, Mark 27 girder for Span Mark 42 girder, respectively. The charts show that during the early life of the bridge girders, before slab casting, the concrete strain near the top fiber has far less compression than the concrete strain near the bottom fiber. Curvature can be derived from the measured strain values and used to measure camber. However, strain was not perfectly linear along the cross-section of the girders and variances between measured strain was enough to not provide consistent results. The data from this analysis are discussed further this thesis. The charts show that the compressive strains increase over time, and the increase in compressive strains at early ages is quite dramatic. This is because early-aged concrete is susceptible to creep and shrinkage, reflected in the increasing strains over time. As the concrete ages, creep and shrinkage decelerate as the magnitude of compressive strains increases.

3.4.3 DISCUSSION

The temperature data of bottom flange shown in Figure 15 and Figure 16 indicates that strain in prestressing steel changes during hydration and curing of the concrete. Strands were tensioned when temperature was approximately 75 ^{0}F and detensioned at approximately 100 ^{0}F for both the Mark 27, Span 9 and Mark 42, Span 14 girders. Multiplying this temperature difference of 25 ^{0}F by the coefficient of thermal expansion of the steel ($\alpha = 6.5*10^{-6}$ in/in/^{0}F) gives a strain of approximately 163 microstrains. Multiplying this to the modulus of elasticity of the steel (28,500 ksi) shows a decrease in prestress of approximately 4.6 ksi. This correlates with the strain readings taken prior to detensioning. Change in strain of the bottom flange between tensioning and detensioning due to temperature changes was approximately 200 and 125 microstrains for Mark 27, Span 9 and Mark 42, Span 14, respectively. Multiplying this by modulus of elasticity of the steel (28,500 ksi) shows a decrease in prestress of 5.7 and 3.6 ksi for Mark 27, Span 9 and Mark 42, Span 14, respectively. These losses are not commonly considered in design, as losses from temperature changes can vary between locations, seasonal changes, and precast manufacturer practices.

The strain gauge data from Figure 20 and Figure 21 is also used to assess the prestress losses indirectly from concrete strain data. The total losses can be computed by multiplying the interpolated strain at the C.G.S. by the modulus of elasticity of the prestressing steel. For this research, the steel's nominal modulus of elasticity was defined as 28500 ksi. Changes in strain from temperature were removed in computation of these measured losses. Figure 22 and Figure 23 show the interpolated prestress losses at midspan for Mark 27, Span 9 and Mark 42, Span 14, respectively.

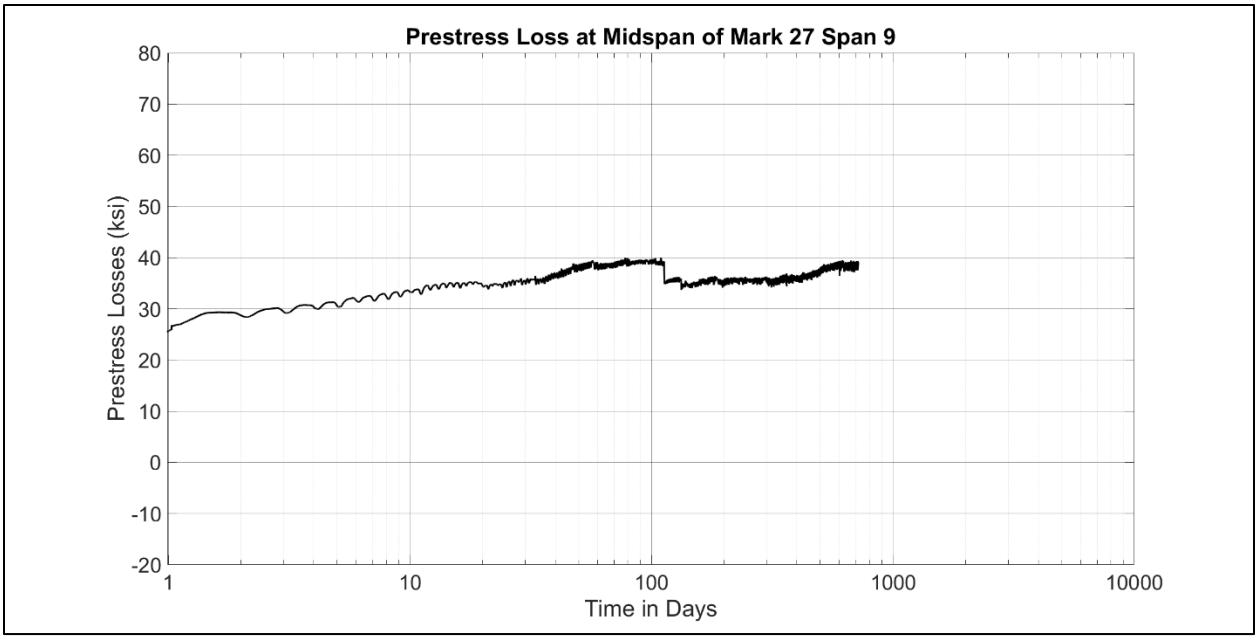

Figure 22: Direct measurements of prestress losses from strain gauge data at midspan for Mark 27 Span 9.

Figure 22 shows the losses at midspan for Mark 27, Span 9. Prestress Loss in Mark 27 Span 9 is measured at approximately 39 ksi before the deck cast. After the deck cast, the additional tension from the slab self-weight decreases the losses to about 34 ksi. Over time the losses increase and reach approximately 38 ksi.

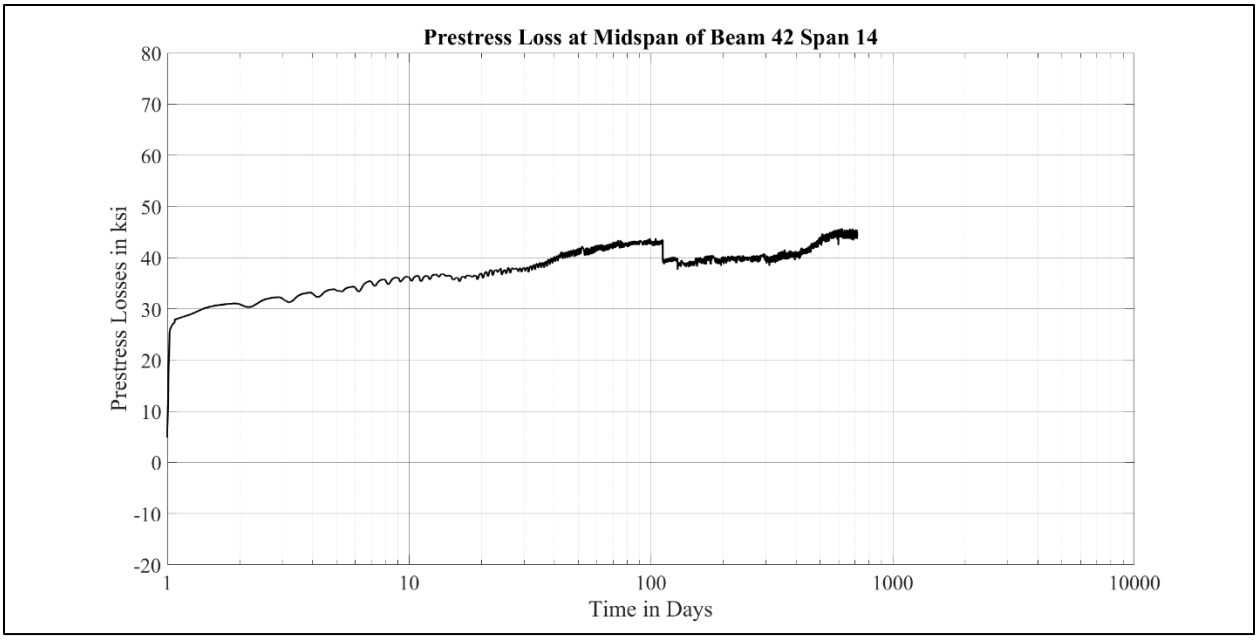

Figure 23: Direct measurements of prestress losses from strain gauge data at midspan for Mark 42 Span 14.

Figure 23 shows the losses at midspan for Mark 42, Span 14. The midspan data indicates that the prestress losses are about 43 ksi just before slab casting and that the additional tension from the slab self-weight decreases the losses to about 39 ksi. Over time, losses increased to approximately 45 ksi.

3.5 COMPARISON OF ESTIMATED AND MEASURED LOSSES

3.5.1 Prestress Loss Models

The total losses for each of the five methods prestress loss models fall between 53.6 ksi and 34.7 ksi at 500 days. The AASHTO LRFD Approximate method shows that Case A has the highest prestress loss of 50.5 ksi. The losses estimated for Case B were 48.3 ksi which is 4.4% smaller than Case A. The losses estimated for cases C & D were 48.2 ksi which is 4.6% smaller than the estimated losses in Case A.

For the AASHTO Refined method, the losses at 500 days for Case A were 43.8 ksi. Case B has experienced losses of 41.2 ksi (6.1% smaller than Case A). Case C experienced slightly higher losses than Case B (41.7 ksi). However, Case C experienced less losses than Case A by 5.0%. Case D has the lowest losses of about 41 ksi, 6.7% smaller than Case A.

The PCI Design handbook method using gross properties methods, the losses at 500 days for Case A were 52.9 ksi. The predicted losses for Case B were 49.7 ksi, which is 5.1% smaller than the predicted losses in case A. The estimated losses for cases C and D are 49.6 ksi which is 6.2% smaller than the predicted losses in Case A.

Using the modified PCI Handbook method with transformed properties, the losses at 500 days for Case A were 53.6 ksi. The predicted losses for Case B were 49.6 ksi, which is 7.5% smaller than the predicted losses in case A. The estimated losses for Case C are 50.5 ksi which is 5.8% smaller than the predicted losses in case A. The estimated losses for Case D are 49.5 ksi which is 7.6% smaller than the predicted losses in Case A.

Using the Jayaseelan time-step method, the long-term losses for Case A were 38.5 ksi. The predicted losses for Case B were 35.9 ksi which is 6.8% smaller than the predicted losses in Case A. The estimated losses for Case C are 35.7 ksi which is 7.3% smaller than the predicted losses in Case A. The estimated losses for Case D are 34.7 ksi which is 9.9% smaller than the predicted losses in Case A.

The results of this analysis show that limiting prestress moment or including mild steel can reduce prestress loss by up to 10%.

3.5.2 Predicted VS Measured Losses

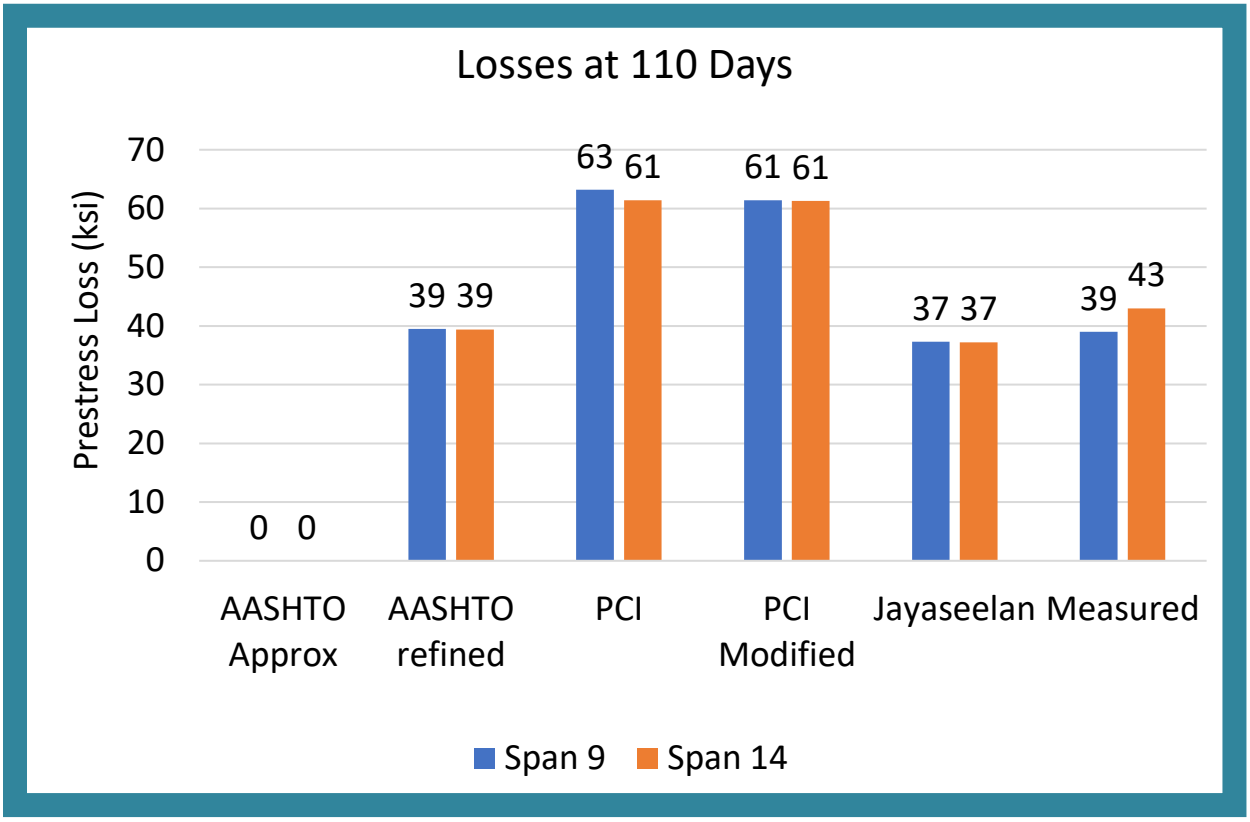

Figure 24: Predicted and measured losses prior to deck casting (110 days)

Figure 24 displays prestress losses measured prior to deck casting at 110 days, immediately prior to when deck casting occurred. Note that the AASHTO Approximate method results were left out of this table, as this method does not compute any losses before deck casting except for elastic shortening. Comparing the measured and predicted results, the AASHTO Refined method overpredicted losses in Span 9 by 1.3% and underpredicted losses in Span 14 by 8.7%. The PCI Design handbook method using gross section properties overpredicted losses in Span 9 by 47% and overpredicted losses in Span 14 by 35%. The modified PCI design handbook method using transformed section properties overpredicted losses in Span 9 by 45% and overpredicted losses in Span 14 by 35%. The Jayaseelan time-step method underpredicted losses in Span 9 by 4.5% and underpredicted losses in Span 14 by 14%.

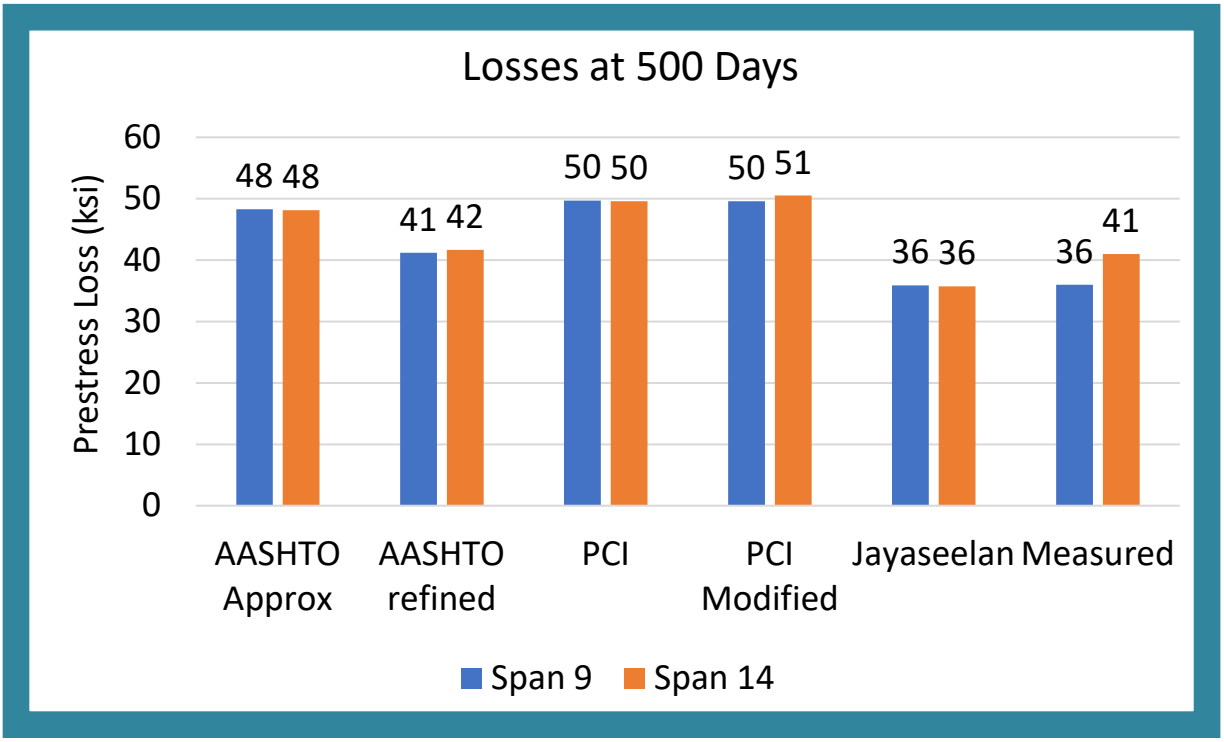

Figure 25: Predicted and measured losses at 500 days.

Figure 25 displays prestress losses measured at 500 days, approximately 390 days after deck casting. Comparing the measured and predicted results, the AASHTO Approximate method overpredicted losses in Span 9 by 29% and overpredicted losses in Span 14 by 16%. The AASHTO Refined method overpredicted losses in Span 9 by 13% and overpredicted losses in Span 14 by 1.6%. The PCI Design handbook method using gross section properties overpredicted losses in Span 9 by 32% and overpredicted losses in Span 14 by 19%. The modified PCI design handbook method using transformed section properties overpredicted losses in Span 9 by 32% and overpredicted losses in Span 14 by 21%. The Jayaseelan time-step underpredicted losses in Span 9 by 0.3% and underpredicted losses in Span 14 by 14%.

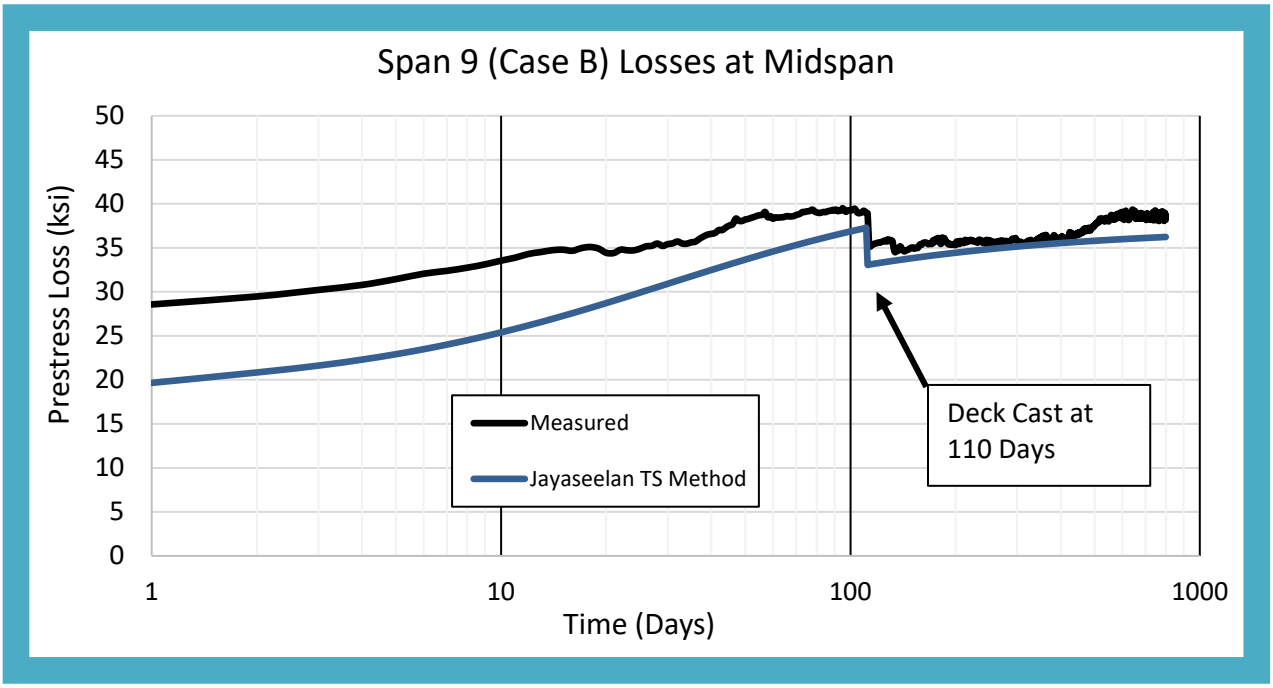

Figure 26: Span 9 measured losses and estimated losses with the Jayaseelan Time-step method.

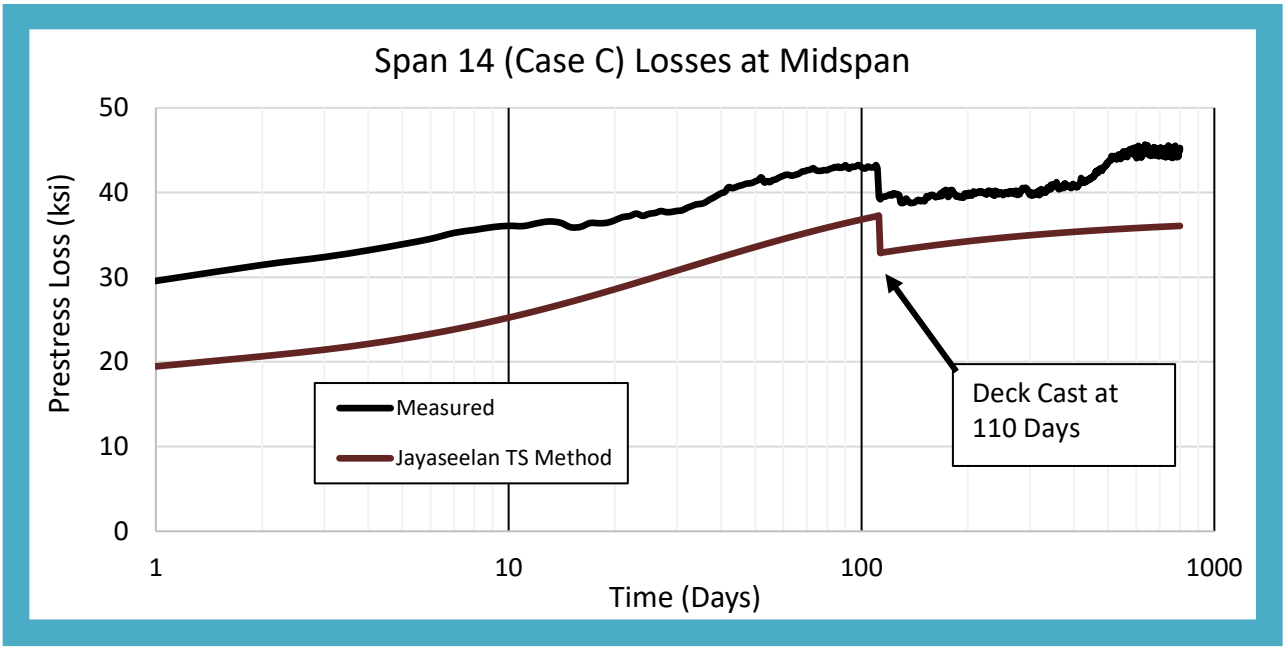

Figure 27: Span 14 measured losses and estimated losses with the Jayaseelan Time-step method.

Figure 26 and Figure 27 show losses measured with VBWs and predicted with the Jayaseelan Time-step method. It is observed that the Jayaseelan Time-step method consistently underpredicted prestress loss in both girders, especially within the first 50 days. This is due to concrete modulus at early ages being significantly overpredicted.

The overprediction of concrete modulus in this method can be observed in early strain readings. Strain data at detensioning gives a direct measurement of elastic shortening loss. This can be found by finding change in strain between the start and end of detensioning. The change in strain measured by the VBWs can be interpolated to the center of gravity of prestressing steel and multiplied by the elastic modulus of the prestressing steel to find elastic shortening loss. The measured elastic shortening loss can then be input into equations for predicting elastic shortening and an estimate of true concrete modulus at detensioning can be calculated algebraically.

Investigation into early age modulus was done on the AASHTO Refined method and the Jayaseelan Time-step method. Both methods use the following equation for computation of elastic shortening loss:

$$ES = \frac{E_p}{E_c} f_{cgp}$$

Where:

ES = Elastic shortening loss.

E_p = Modulus of prestressing steel, taken as 28,500 ksi.

E_c = Modulus of concrete at detensioning.

f_{cgp} = Sum of concrete stresses at the center of gravity of prestressing strands due to prestressing force at transfer and the self-weight of the member, calculated to be approximately 3.2 ksi in all presented cases.

The equation can be rearranged to compute concrete modulus at detensioning:

$$E_c = \frac{E_p}{ES} f_{cgp}$$

Using the measured elastic shortening loss from strain readings in this equation, true concrete modulus at detensioning can be found. Results are tabulated in Table 9. It was found that AASHTO equations overpredicted concrete modulus at transfer by up to 30%. The Jayaseelan Time-step method overpredicted concrete modulus at transfer by up to 21%. The results show that concrete modulus is significantly and consistently

overpredicted at early ages, meaning that elastic shortening loss is underpredicted in design.

Table 9: Comparison of measured and predicted concrete modulus at detensioning.

Comparison of measured and predicted concrete modulus at detensioning.										
	AASHTO Refined					Jayaseelan Time-step Method				
	Estimated		Measured		% diff	Estimated		Measured		% diff
	Ec (ksi)	ES (ksi)	Ec (ksi)	ES (ksi)		Ec (ksi)	ES (ksi)	Ec (ksi)	ES (ksi)	
Span 9	5130	18.1	3796	24.4	30%	4667	19.7	3773	24.40	21%
Span 14	5130	17.9	4301	21.4	18%	4667	19.5	4262	21.40	9.1%
Note: Ec = Concrete modulus at detensioning ES = Elastic Shortening Loss Ep = 28500 ksi f_{cgp} = 3.2 ksi for all cases										

3.6 ESTIMATING CAMBER

3.6.1 METHODOLOGY

Camber was predicted following the Jayaseelan time-step method detailed in Jayaseelan and Russell (2019) [15]. Strains were computed at each increment in the top and bottom fiber of the concrete cross-section. Curvature was derived at both midspan and at the end regions from the computed strains and then camber was derived using moment-area method.

3.6.2 RESULTS

Table 10 displays the tabulated camber results using the Jayaseelan time-step method. Figure 28 provides graphical representation of these results, measured on a day-by-day basis. Cambers were predicted starting at the first date physical measurements taken on June 11, 2020.

Table 10: Predicted camber using Jayaseelan Time-step method

	Date	Days after Detensioning	Predicted Camber (in)			
			Case A	Case B	Case C	Case D
Jayaseelan Time-Step Method	11-Jun-20	40	3.53	3.17	2.95	2.80
	18-Jun-20	47	3.55	3.19	2.96	2.82
	29-Jul-20	88	3.63	3.25	3.03	2.87
	1-Oct-20	152	1.78	1.38	1.13	0.968
	26-Oct-21	542	1.76	1.35	1.09	0.921
	7-Apr-22	705	1.76	1.34	1.09	0.915

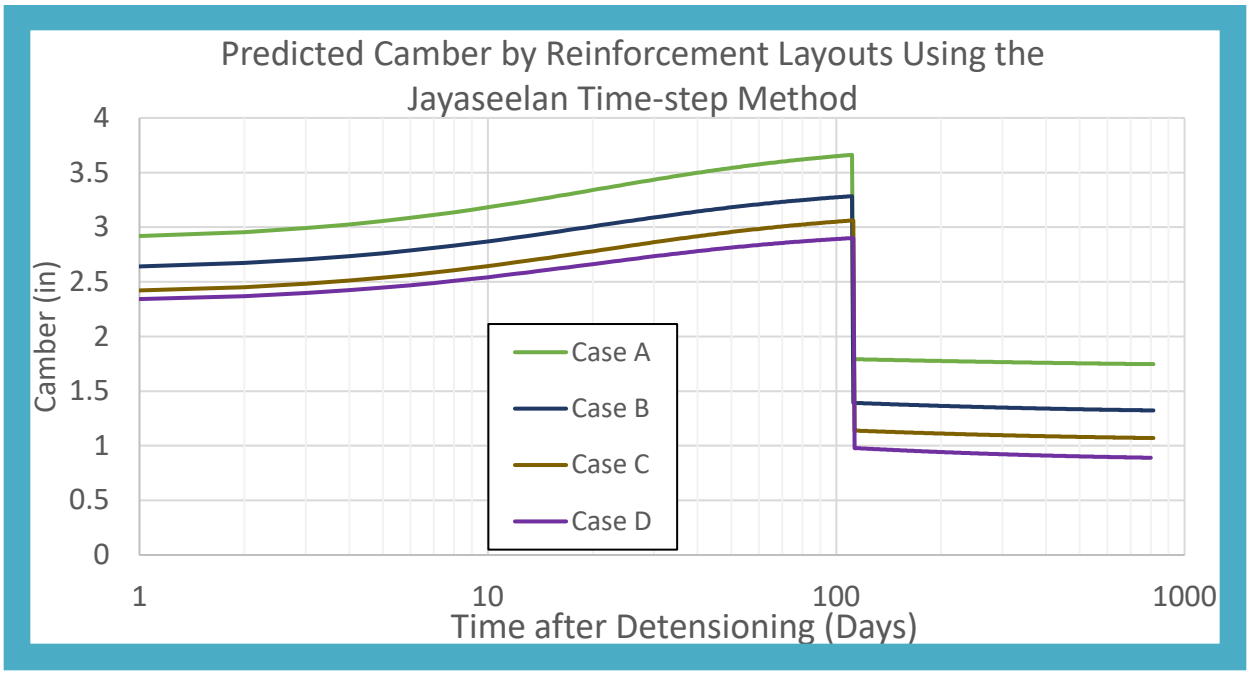

Figure 28: Predicted Camber from Jayaseelan Time-Step Method

3.6.3 DISCUSSION

Table 11: Effects of distributed strand patterns and mild steel on camber using the Jayaseelan Time-Step method.

		Difference in Camber (in) From Case A			Percent Change		
Date	Days After Detensioning	Traditional w/ Mild Steel	Distributed w/o Mild Steel	Distributed w/ mild steel included	Traditional w/ Mild Steel	Distributed w/o Mild Steel	Distributed w/ mild steel included
		Case B	Case C	Case D	Case B	Case C	Case D
11-Jun-20	40	-0.36	-0.58	-0.73	-10	-17	-21
18-Jun-20	47	-0.36	-0.59	-0.73	-10	-17	-21
29-Jul-20	88	-0.37	-0.60	-0.75	-10	-16	-21
1-Oct-20	152	-0.40	-0.66	-0.82	-23	-37	-46
26-Oct-21	542	-0.41	-0.67	-0.84	-24	-38	-48
7-Apr-22	705	-0.41	-0.67	-0.84	-24	-38	-48

Note:
1: Negative values indicate the camber was reduced when corresponding reinforcement layout was used.
2: Percent Change = (Case "X" - Case A)/Case A * 100%

Table 11 displays the difference in cambers between traditional strand patterns with no mild steel reinforcement (Case A) to each of the other longitudinal reinforcement variations using the Jayaseelan Time-step method. Long-term camber was reduced by 0.41 in. (24%) when mild steel (Case B) was used. Using a distributed strand pattern (Case C) reduced long-term camber by 0.67 in. (38%). Combining the use of a distributed strand pattern and mild steel reinforcement (Case D) reduced long term camber by 0.84 in. (48%). The data indicates that distributed strand patterns that include mild steel are the most effective at reducing long-term camber.

3.7 MEASUREMENT OF CAMBER

3.7.1 METHODOLOGY

Camber was physically measured using an engineering level and a Philadelphia rod, or a graduated tape measure. Elevation measurements were made most commonly at the bottom of the girder. This ensured consistency of measurement throughout beam fabrication, transportation, erection, and bridge construction. Elevation measurements were made at varying stages over the bridge's construction. Camber was computed from the elevation measurements for each individual bridge beam, and the average camber was calculated at each span. Measurements were taken at the following intervals during the construction of the bridge:

- June 11, 2020: During placement of girders on final location
- June 18, 2020: Immediately after placement of girders on final location
- July 29, 2020: 1 week before deck casting began
- October 20, 2020: 2 weeks after deck placement
- October 26, 2021: About 1 year into service
- April 7, 2022: About 1 year, six months into service

Elevations for each girder were measured at both ends and midspan. The average elevation of each end was found and compared to the elevation at midspan to find camber. All camber measurements were taken from under the bridge, except for measurements taken on July 29, 2020, in which cambers were measured from on top of the bridge days before deck casting. Since elevations could not be taken at the center of

bearing of the girders, a correction factor of 1.06 was applied to account for the measurements being taken approximately 1 ft. 6in. away from center of bearing.

Strain data from the structural monitoring program was also used to measure camber in the Mark 27, Span 9 and Mark 42, Span 14 girders. Curvature was derived using measured strain from the VBWs and moment area method was performed to find upward deflection. Results from this analysis only showed to provide an estimate of camber, as strain measurements were not perfectly linear down the cross section of the girder.

3.7.2 RESULTS

Tabulated data points for camber measurements are displayed in Table 12. The camber results are the average of all 4 girders in the span at the time of measurement. All measurements were taken from below the bridge except for measurements taken on July 29, 2020, in which measurements were taken on top of the girders. It is worth noting that Span 8 is inaccessible from underneath the bridge, so the only measurements for this span were taken on July 29, 2020. Figure 29 displays the average measured camber for each reinforcement layout at varying dates compared to all the girders' overall average camber.

Figure 30 and Figure 31 compares the results of measured camber from strain readings and measured camber using a Philadelphia rod and engineering level of Mark 27, Span 9 and Mark 42, Span 14 girders.

Table 12: Average Camber Measurements of Each Span Over Time

	Longitudinal Reinforcement Case	Cambers Measured June 11, 2020	Cambers Measured June 18, 2020	Cambers Measured July 29, 2020	Cambers Measured October 1, 2020	Cambers Measured October 27, 2021	Cambers Measured April 7, 2022
		Camber (in)	Camber (in)	Camber (in)	Camber (in)	Camber (in)	Camber (in)
Span 1	Case C	2.55	2.72	2.54	1.31	0.76	0.47
Span 2	Case C	2.69	2.76	2.64	0.66	0.62	0.78
Span 3	Case A	3.55	3.50	3.66	1.77	1.79	1.85
Span 4	Case A	4.21	4.19	4.13	2.10	2.19	2.27
Span 5	Case C	3.18	3.42	3.12	0.93	1.02	1.10
Span 6	Case D	2.77	2.87	2.77	0.66	0.65	0.66
Span 7	Case D	2.82	2.77	2.78	0.79	0.86	0.87
Span 8	Case B	(a)	(a)	2.69	(a)	(a)	(a)
Span 9	Case B	3.29	3.25	3.36	1.19	1.10	1.23
Span 10	Case A	3.46	3.23	3.42	1.28	1.38	1.47
Span 11	Case C	3.21	3.06	3.18	0.98	1.23	1.11
Span 12	Case A	4.11	4.02	3.95	2.01	2.15	2.19
Span 13	Case A	4.14	3.94	4.05	2.15	2.19	2.26
Span 14	Case C	(b)	2.85	2.93	0.75	0.91	0.98
Span 15	Case C	(b)	3.02	3.27	1.00	1.11	0.98
Average Camber	All Cases	3.33	3.26	3.23	1.25	1.28	1.30

Note:
1: Reported cambers are the average of all four girders in a span.
2: Camber measurements were taken from the bottom of the bridge except for measurements taken on July 29, 2020, in which cambers were measured from the top of the bridge.
3: Camber measurements taken from the bottom of the bridge are multiplied by a correction factor of 1.06 to account for the direct center of bearing not being accessible.
4: Span 8 is inaccessible from under the bridge. Readings were only taken on July 29, 2020, from the top of the bridge prior to deck casting.
5: Girders for spans 14 & 15 had not been placed at the time of measurements on June 11, 2020.

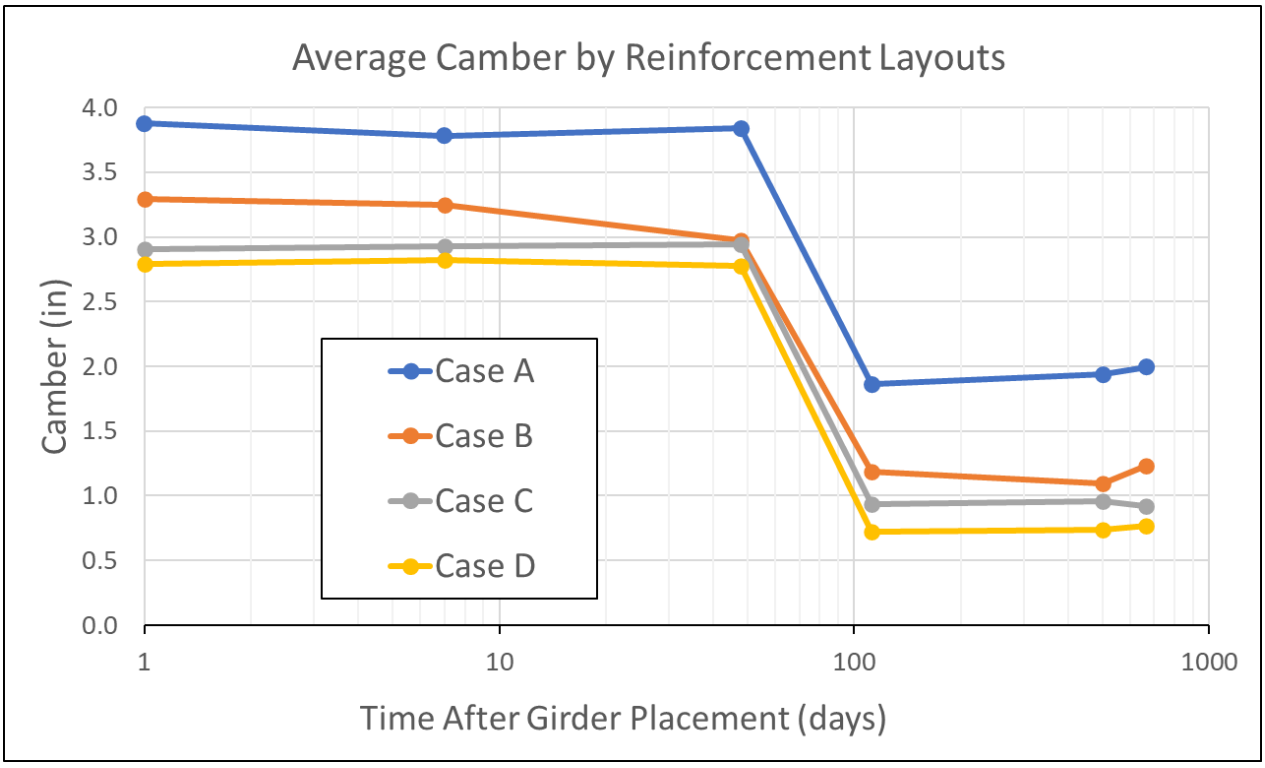

Figure 29: Average measured camber by reinforcement layouts. Note that girders were placed approximately 40 days after detensioning.

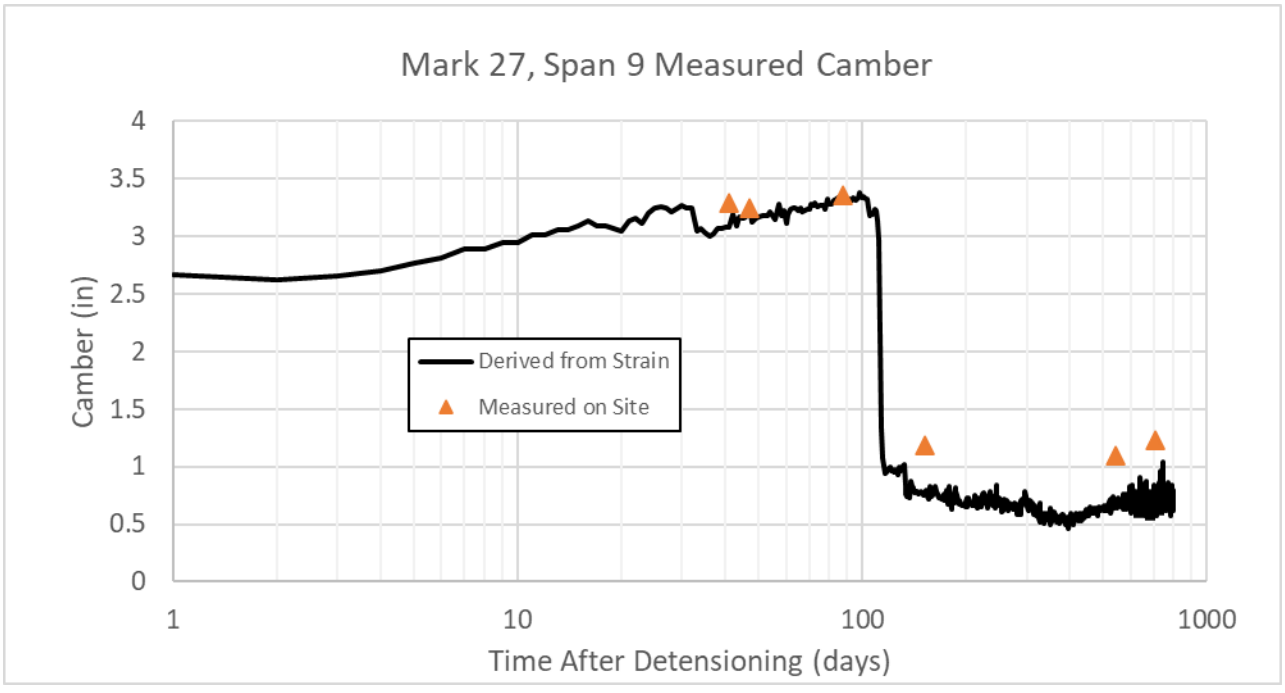

Figure 30: Mark 27, Span 9 measured camber from strain and on site.

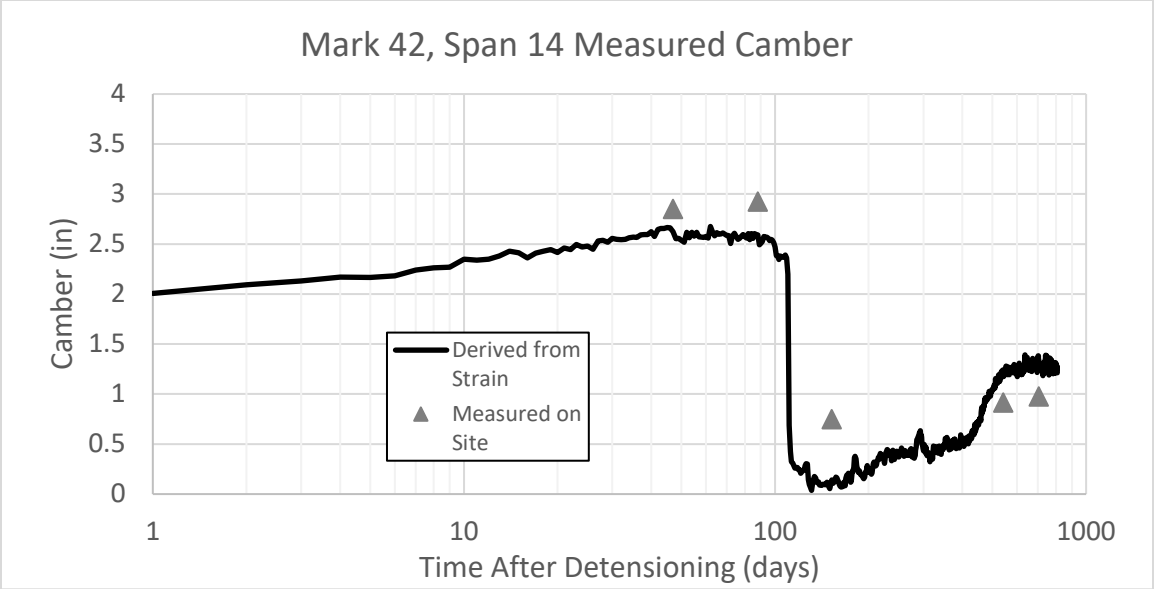

Figure 31: Mark 42, Span 14 measured camber from strain and on site.

3.7.3 DISCUSSION

Measurements taken before deck casting show that Case D girders experienced the least amount of camber. This shows that combining the use of a distributed strand pattern and mild steel likely improved constructability of the deck in these spans, as haunch and deck thickness was likely more consistent along the length of these spans due to them being more level during deck construction. Deck casting occurred for all spans in August of 2020. Measurements taken afterward in October show an average decrease in camber of 2.02 in. (range of 1.23 in. to 2.27 in.). Comparing the decrease in camber immediately after deck casting, on average, girders falling under Case A, B, C, and D reinforcement layouts experienced a downward deflection of 1.98 in., 1.79 in., 2.01 in., and 2.05 in, respectively. The data shows that the deflection caused by the dead load of the deck immediately after casting was not significantly different between the reinforcement layouts.

Camber measured using strain data was comparable to measurements taken in the field. Measurements from strain in Span 9 underpredicted camber by as much as 0.42 in. (43%) and overpredicted camber by as much as 0.010 in. (0.30%) when compared to cambers measured in the field. For Span 14, cambers measured with strain readings underpredicted camber by as much as 0.61 in. (137%) and overpredicted camber by as much as 0.31 in. (27%). Results from this show that the strain readings do not provide a completely accurate measurement of camber, but they can be a valuable tool in estimating long-term camber in bridges.

Table 13: Effects of distributed strand patterns and mild steel on camber.

		Change in Camber (in) From Case A			Percent Change		
Date	Days After Girder Placement	Traditional w/ Mild Steel	Distributed w/o Mild Steel	Distributed, w/ mild steel included	Traditional w/ Mild Steel	Distributed w/o Mild Steel	Distributed w/ mild steel included
		Case B	Case C	Case D	Case B	Case C	Case D
11-Jun-20	1	-0.58	-0.97	-1.08	-15	-25	-28
18-Jun-20	7	-0.53	-0.85	-0.96	-14	-22	-25
29-Jul-20	48	-0.87	-0.90	-1.07	-23	-23	-28
1-Oct-20	112	-0.67	-0.92	-1.14	-36	-50	-61
26-Oct-21	502	-0.84	-0.98	-1.20	-43	-51	-62
7-Apr-22	665	-0.76	-1.1	-1.2	-38	-54	-62

Note:
1: Negative values indicate the camber was reduced when corresponding reinforcement layout was used.
2: Percent Change = (Case "X" - Case A)/Case A * 100%

Table 13 displays the difference in cambers between traditional strand patterns with no mild steel reinforcement (Case A) to each of the other longitudinal reinforcement variations. Long-term camber was reduced by 0.76 in. (38%) when mild steel (Case B) was used. Using a distributed strand pattern (Case C) reduced long-term camber by 1.1 in. (54%). Combining the use of a distributed strand pattern and mild steel reinforcement (Case D) reduced long term camber by 1.2 in. (62%). The data shows that girders containing distributed strand patterns (Case C & D) experienced the least amount of camber during all stages of bridge construction and service. Case D girders experienced significantly less camber prior to deck casting when compared to Case C girders, but no appreciable difference between both cases was observed after the bridge had been in service for over a year.

3.8 COMPARISON OF ESTIMATED CAMBER TO MEASURED CAMBER

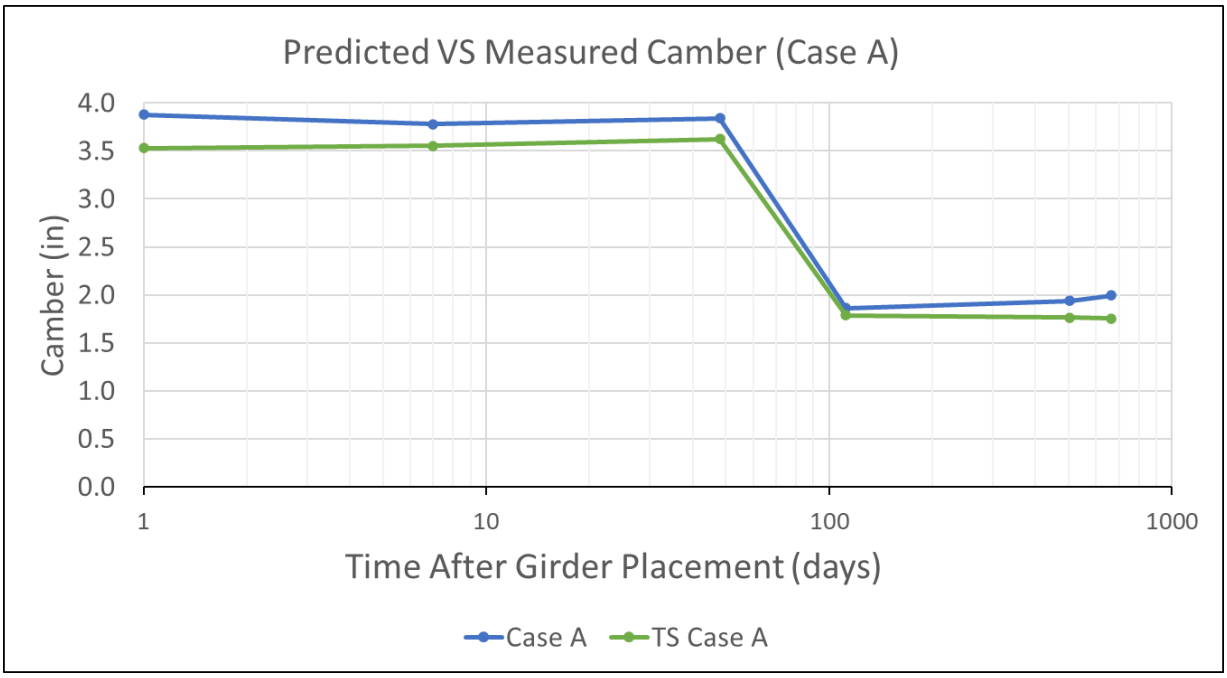

Figure 32: Predicted and measured camber for Case A.

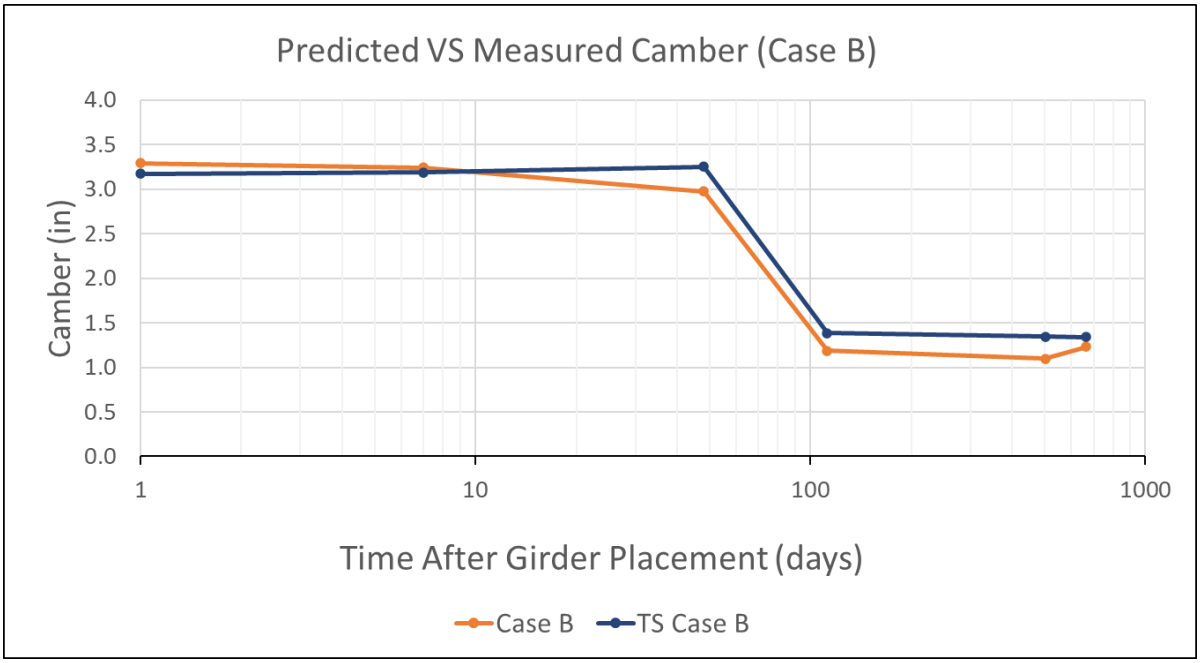

Figure 33: Predicted and measured camber for Case B.

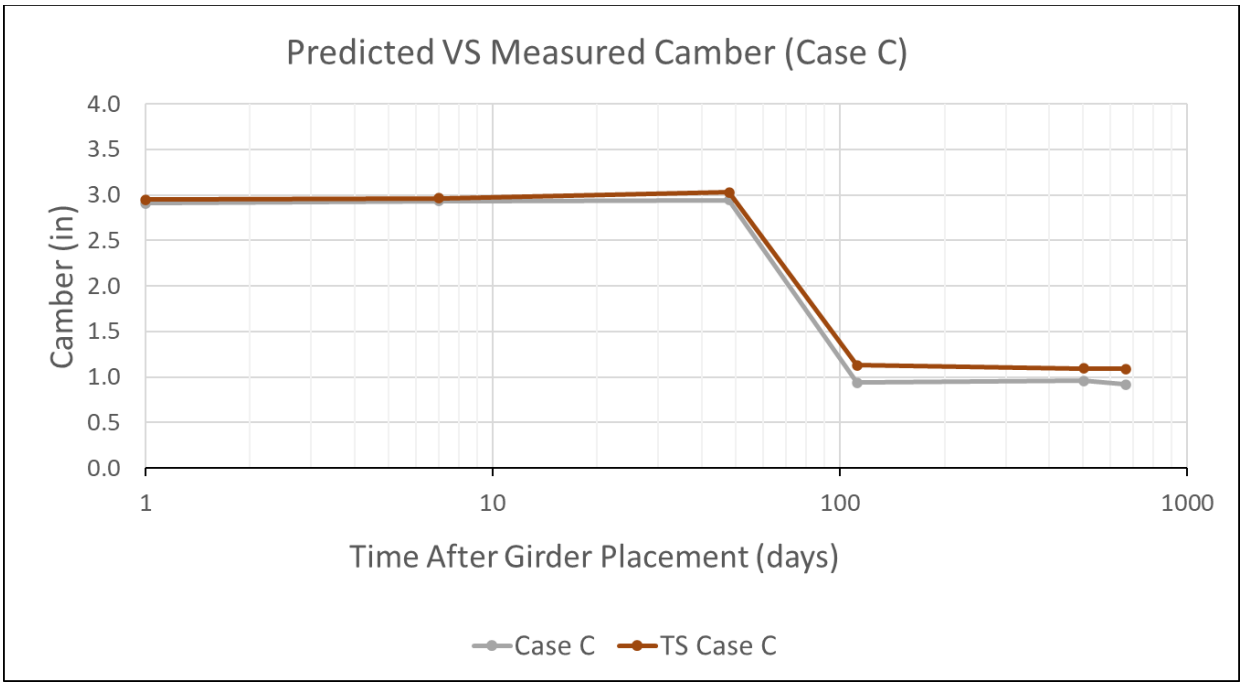

Figure 34: Predicted and measured camber for Case C.

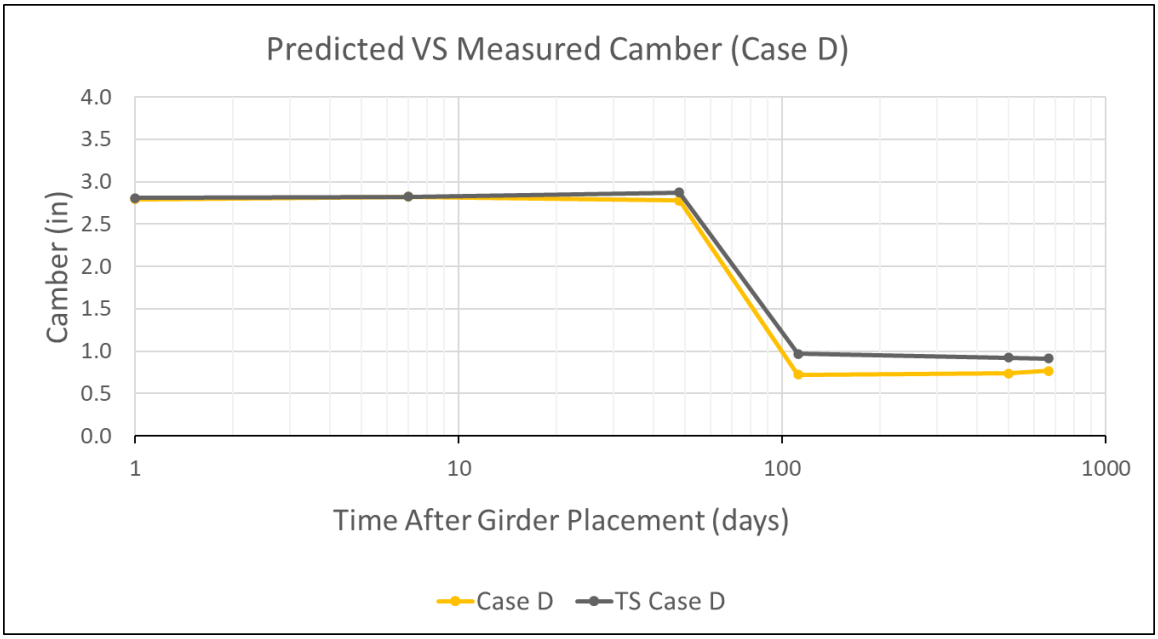

Figure 35: Predicted and measured camber for Case D.

Figure 32, Figure 33, Figure 34, and Figure 35 display predicted cambers using the Jayaseelan Time-step method and measured camber for each of the four longitudinal

reinforcement cases. Comparing the results for Case A, the Jayaseelan time step method underpredicted camber by an average of 0.21 in. between all measurements (-4.2 to -13% difference). Comparing the results for Case B, the Jayaseelan time step method overpredicted camber by an average of 0.11 in. between all measurements (-3.8 to 19% difference). Comparing the results for Case C, the Jayaseelan time step method overpredicted camber by an average of 0.11 in. between all measurements (1.2 to 17% difference). Comparing the results for Case D, the Jayaseelan time step method overpredicted camber by an average of 0.11 in. between all measurements (-0.14 to 25% difference). The data shows that the Jayaseelan Time-step method can appropriately predict camber and is a valuable tool in analyzing behavior of prestressed concrete girders.

3.9 CONCLUSIONS

3.9.1 Prestress Loss Conclusions

- The AASHTO Refined method found that Case B girders experienced 6.1% less prestress loss than Case A at 500 days.
- The AASHTO Refined method found that Case C girders experienced 4.9% less prestress loss than Case A at 500 days.
- The AASHTO Refined method found that Case D girders experienced 6.7% less prestress loss than Case A at 500 days.
- Comparing strain data to AASHTO refined, the AASHTO Refined overpredicted losses at 110 days for Span 9 by 1.3% and underpredicted losses at 110 days for Span 14 by 8.7%. For losses at 500 days, AASHTO Refined overpredicted losses by 13% for Span 9 and overpredicted losses for Span 14 by 1.6%.
- Comparing strain data to AASHTO Approximate, the AASHTO Approximate method overpredicted losses at 500 days in Span 9 by 29% and overpredicted losses in Span 14 by 16%.
- Comparing strain data to the PCI Design Handbook method, the PCI Design handbook method overpredicted losses at 110 days in Span 9 by 47% and overpredicted losses in Span 14 by 35%. PCI overpredicted losses at 500 days in Span 9 by 32% and overpredicted Span 14 by 19%.
- Comparing strain data to the Modified PCI method, overpredicted losses at 110 days in Span 9 by 45% and overpredicted losses in Span 14 by 35%. This method also overpredicted losses at 500 days in Span 9 by 32% and overpredicted losses in Span 14 by 21%.

- Comparing strain data to Jayaseelan time step, overpredicted losses at 110 days in Span 9 by 4.5% and underpredicted losses in Span 14 by 14%. Jayaseelan time-step underpredicted losses at 500 days in Span 9 by 0.3% and underpredicted losses in Span 14 by 14%.
- The comparison of prestress loss prediction methods to losses derived from strain measurements show that the AASHTO Refined method and Jayaseelan Time-step method provide the best reference to accurately predicting prestress losses.
- Analysis between predicted and measured elastic shortening loss show that current equations significantly overpredict early age concrete elastic modulus by up to 30%, leading to a underprediction of elastic shortening loss.

3.9.2 Camber Conclusions

- The inclusion of mild steel reinforcement in the bottom flange (Case B) moderately reduced the long-term camber by approximately 0.76 in. (38%) from Case A.
- The distributed strand pattern (Case C) significantly reduced the long-term camber by approximately 1.1 in. (54%) from the Case A.
- Combining mild steel reinforcement in the bottom flange and using a distributed strand pattern (Case D) reduced the long-term camber by approximately 1.2 in. (62%) from Case A.
- The Jayaseelan Time-Step method typically underestimated camber for Case A girders by an average of 0.21 in. (Between -4.2 to -13% at all time increments).

- The Jayaseelan Time-Step method typically overestimated camber for Case B girders by 0.11 in. (Between -3.8 to 19% at all time increments).
- The Jayaseelan Time-Step method typically overestimated camber for Case C girders by 0.11 in. (Between 1.2 to 17% at all time increments).
- The Jayaseelan Time-Step method typically overestimated camber for Case D girders by 0.11 in. (Between -0.14 to 25% at all time increments).
- The Jayaseelan Time-step method provides a reasonable prediction of camber in prestressed concrete girders.
- Camber was not able to be appropriately measured with strain readings. However, it can be a valuable tool in assessing performance of a bridge and should be utilized in future structural monitoring programs.

3.9.3 Recommendations

- Implementing mild steel reinforcing into the bottom flanges of prestressed concrete girders or using a distributed strand pattern in the design of pretensioned girder bridges is recommended. This will significantly decrease camber and slightly decrease prestress losses without significantly increasing fabrication cost or time. Combining both mild reinforcing and a distributed strand pattern further reduced camber and prestress losses and is recommended if viable.
    - Including 2.4 in^2 of mild reinforcement can significantly reduce camber by up to 38% and reduces prestress losses by about 6%.
    - Limiting prestress moment by using a distributed strand pattern can limit camber by up to 54% and reduce prestress losses by up to 5%.

    - Combining both mild reinforcement and distributed strand patterns can limit camber by up to 62% and reduce prestress losses by up to 7%.
- The AASHTO Refined method and Jayaseelan Time-step method provide accurate predictions of prestress losses. They are both recommended for use in design and the Jayaseelan Time-step method provides accurate prediction of camber for these types of girders.

CHAPTER IV

4 DETERMINATION OF DISTRIBUTION FACTORS THROUGH STATIC LOAD TESTING

4.1 INTRODUCTION

This chapter discusses the methods and results of static load testing performed on the SH4 bridge. This work aimed to measure the bridge girders' live load distribution factors using deflection measurements and strain readings. Distribution factors are typically approximated using AASHTO prescribed methods. The Lever Rule is a classic approximate method that has been used for many decades. It was originally codified in the AASHTO Standard Bridge Specifications prior to AASHTO LRFD Bridge specifications. The procedure was retained in the LRFD specification for calculating distribution factors of external girders even though it is widely believed to be conservative. Overestimation of the distribution factors with this method can lead to more prestressing reinforcement being needed, which can be inefficient and leads to larger camber and losses. Through load testing, distribution factors can be directly measured by comparing relative deflection of each girder. Pairing this testing with finite element modelling allows further understanding of the distribution of live loads and allows the effects of secondary structural components such as parapets and diaphragms to be analyzed.

4.2 BACKGROUND

4.2.1 The Lever Rule

The lever rule is found in chapter 4 of the 2020 edition of AASHTO LRFD. Provisions on computing distribution factors with the lever rule can be found in section 4.6.2.2.1. This method assumes a hinge on top of the girders in a span. Truck loading is placed on the span and reactions of the girders are calculated, deriving the distribution factor.

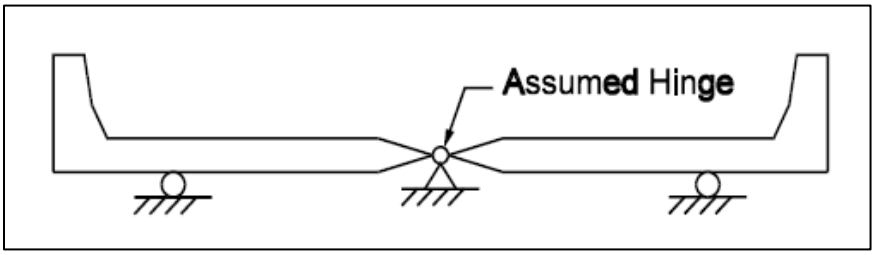

Figure 36: Lever rule example from section C4.6.2.2.1-1 of 2020 AASHTO LRFD.

4.2.2 The Rigid Method

Provisions for the rigid method are found in section 4.6.2.2.2 of 2020 AASHTO LRFD [4]. This method is used when rigid end diaphragms are used in the bridge's design. It assumes that the diaphragms are perfectly rigid and that the whole cross-section rotates as a rigid cross-section. End diaphragms are present on the SH 4 bridge, meaning that the bridge can be analyzed using this method.

$$R = \frac{N_L}{N_b} + \frac{X_{ext}\sum_{N_b} e}{\sum x^2} \qquad \text{(C4.6.2.2.2d-1)}$$

where:

R = reaction on exterior beam in terms of lanes
N_L = number of loaded lanes under consideration
e = eccentricity of a design truck or a design lane load from the center of gravity of the pattern of girders (ft)
x = horizontal distance from the center of gravity of the pattern of girders to each girder (ft)
X_{ext} = horizontal distance from the center of gravity of the pattern of girders to the exterior girder (ft)
N_b = number of beams or girders

Figure 37: Rigid method equation

4.2.3 AASHTO Methods

AASHTO provides empirically derived methods for determining distribution factors. These computations include multipresence factors in their formulae, except for when the lever rule is used. Results from this analysis are excluded in most discussions of this section, as this method uses the previously discussed lever rule and is limited to only determining distribution factors of girders that have an applied lane load.

Table 4.6.2.2.2d-1—Live Load Distribution Factor for Moment in Exterior Longitudinal Beams

Type of Superstructure	Applicable Cross-Section from Table 4.6.2.2.1-1	One Design Lane Loaded	Two or More Design Lanes Loaded	Range of Applicability
Wood Deck on Wood or Steel Beams	a, 1	Lever Rule	Lever Rule	N/A
Concrete Deck on Wood Beams	1	Lever Rule	Lever Rule	N/A
Concrete Deck or Filled Grid, Partially Filled Grid, or Unfilled Grid Deck Composite with Reinforced Concrete Slab on Steel or Concrete Beams; Concrete T-Beams, T- and Double T-Sections	a, e, k and also i, j if sufficiently connected to act as a unit	Lever Rule	$g = e\,g_{interior}$ $e = 0.77 + \frac{d_e}{9.1}$	$-1.0 \le d_e \le 5.5$
			use lesser of the values obtained from the equation above with $N_b = 3$ or the lever rule	$N_b = 3$

Figure 38: Table provided by AASHTO for determining distribution factors.

4.3 LOAD TEST METHODOLOGY

Static load tests were performed on Span 9 and Span 14 by placing loaded trucks on the bridge spans, in specific arrangements and in a specific manner, and by measuring beam deflections at midspan and recording strains during the load testing. Moving load tests were also performed but these tests are not a subject of this thesis research.

Two highway maintenance trucks were loaded with gravel and used to perform the load testing. A photograph of the trucks appears in Figure 48 and Figure 49. Schematics showing axle spacings is shown in Figure 44 and Figure 46. The two trucks had different gross vehicle weights (GVW) and the individual axle weights were not provided. Truck 1 had a GVW of 45,000 lbs. and Truck 2 had a GVW of 50,000 lbs. Only a total of two trucks were used during load testing. Both trucks were identical in geometry. Each truck had 3 axles, 1 in the front and two paired in the rear. The front tires had a 6 ft. center-to-center wheel spacing. The center-to-center axle spacing from the front axle to the first

rear axle was 14 ft. The distance from the first rear axle to the second rear axle was 4.5 ft. Since truck axle weights were not provided, it was assumed that 20% of the total truck load was applied to the front axle of the trucks, while the remaining 80% was split evenly between the two rear axles. The assumed distribution of forces is shown in Table 14 and Figure 39. The static load test consisted of placing the trucks filled with aggregate onto the bridge at different locations in two separate configurations, shown in Figure 45 and Figure 47. Deflections caused by the trucks were recorded.

Table 14: Assumed Truck Axle Weights

	Truck 1	Truck 2
Total Weight (kip)	45.0	50.3
Front Axle weight (kip)	9.0	10.1
1st Rear Axle Weight (kip)	18.0	20.1
2nd Rear Axle Weight (kip)	18.0	20.1

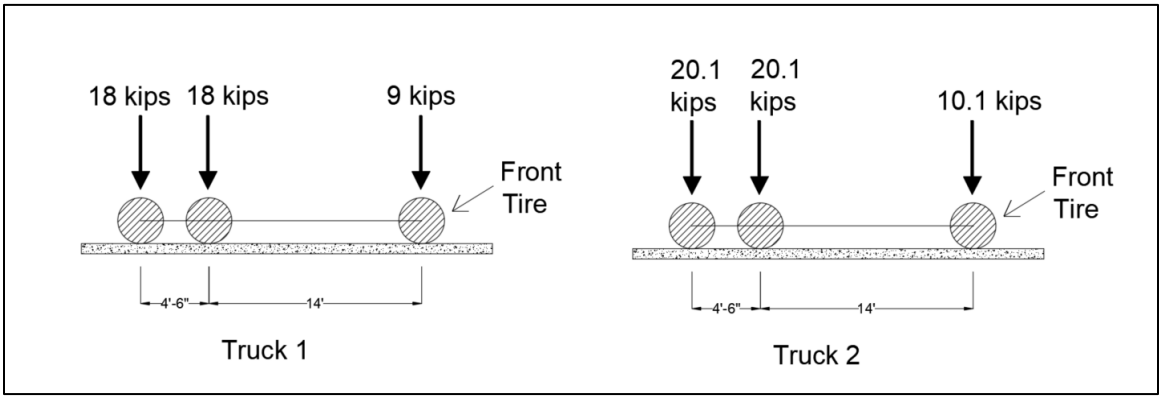

Figure 39: Assumed axle weights of each truck.

Instrumentation for the load test consisted of:

- One (1) LVDT placed at the midspan of each girder to measure deflection (total of 4 LVDTs per span).
- One (1) triaxial accelerometer placed on the Westernmost exterior girder bottom flange to measure acceleration at each span.
- One (1) triaxial accelerometer placed on the Westernmost interior girder bottom flange to measure acceleration of each span.
- One (1) triaxial accelerometer was placed on the bottom side of the deck at the span's midspan and mid-length between the exterior and interior girders.

The sample rate for accelerometers and LVDT's was set to 200 Hz. Details and photographs of the instrumentation plan are shown in Figure 40, Figure 41, Figure 42, and Figure 43. Although accelerometers were used in this testing, results and analysis are not shown in this thesis.

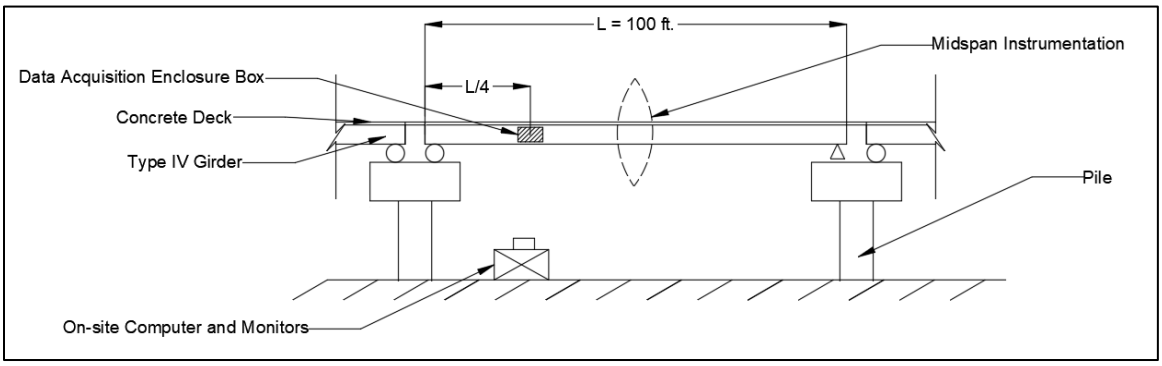

Figure 40: Instrumentation location for load testing plan.

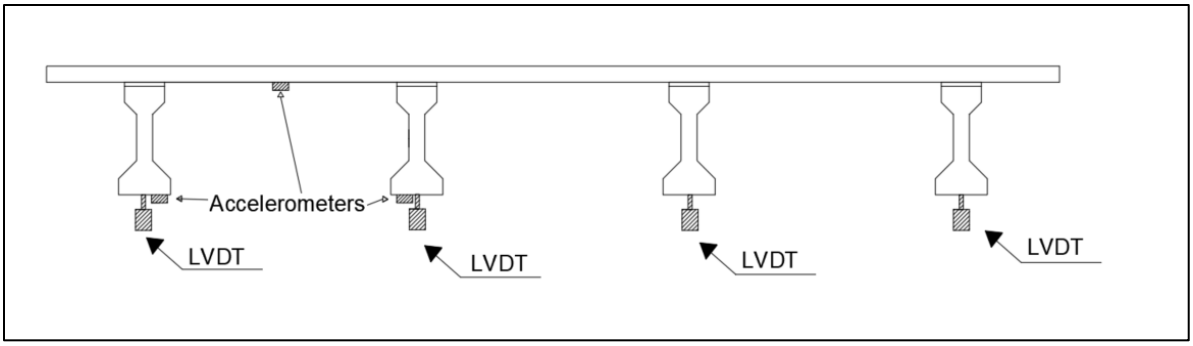

Figure 41: LVDT and accelerometer locations.

Figure 42: Instruments at midspan for SH 4 load test. Viewed are an LVDT and accelerometer.

Figure 43: Testing setup for SH 4 load test.

4.3.1 Static Load Testing

The static load testing plan for Span 9 and Span 14 consisted of two identical scenarios. For the first scenario, noted as Configuration 1, one truck was placed at an offset of 2 ft. from the nearest tire from the edge of the parapet on the Westernmost part of the span. The second scenario, noted as Configuration 3, includes a second truck spaced 10 ft. away from the parapet on the span's Westernmost part. The first truck is still present in this scenario. The significance of configuration 3 is that it imitates the lever rules method of determining the distribution factor for bridge girders. Details on truck placement for both scenarios are shown in Figure 44 and Figure 46. For each scenario, the front tires of the rear axle were placed at 16 ft. 8 in. increments along the length of each span for a total of 5 tests per scenario. Details on truck placements for configuration 1 and configuration 3 are shown in Figure 45 and Figure 47, respectively. For each increment,

the trucks were kept parked for a total of 3 minutes to allow appropriate time for instrumentation to take measurements.

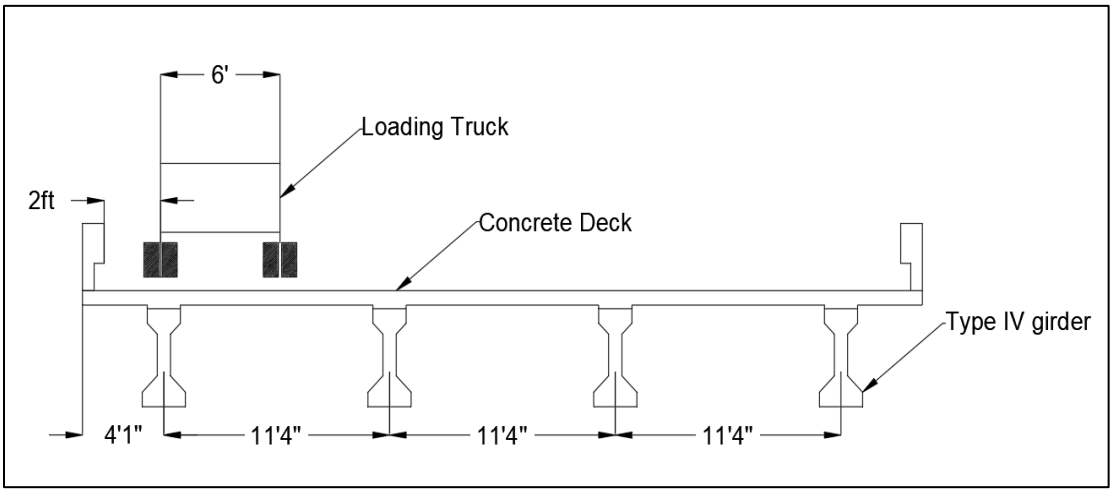

Figure 44: Truck configuration 1 view looking North.

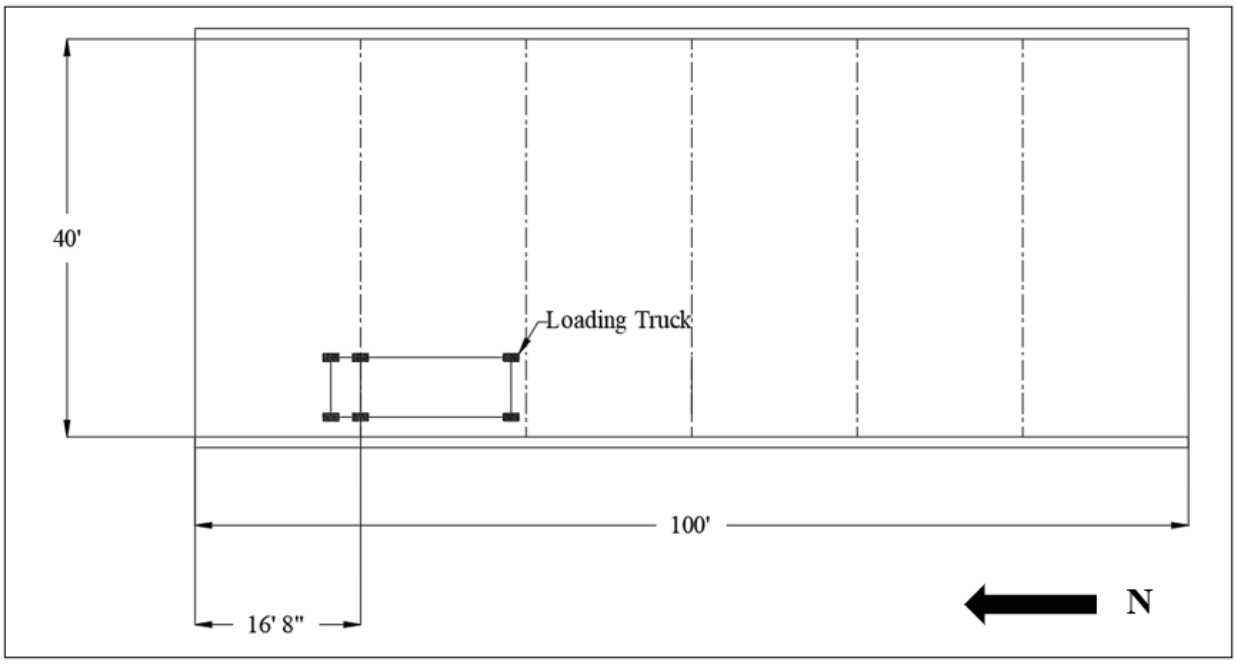

Figure 45: Truck configuration 1 plan view.

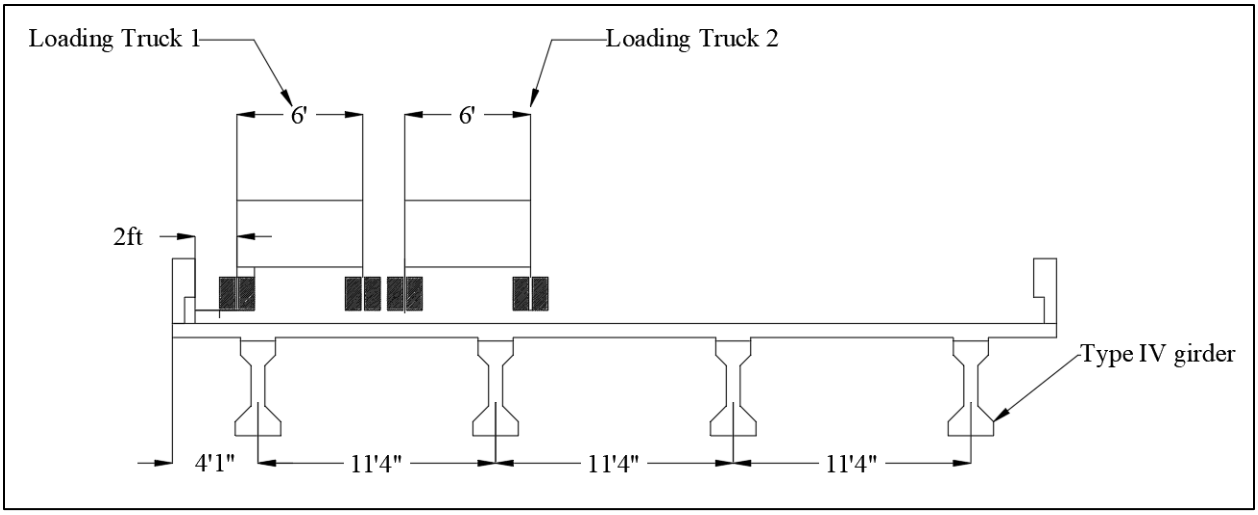

Figure 46: Truck configuration 3 view looking North.

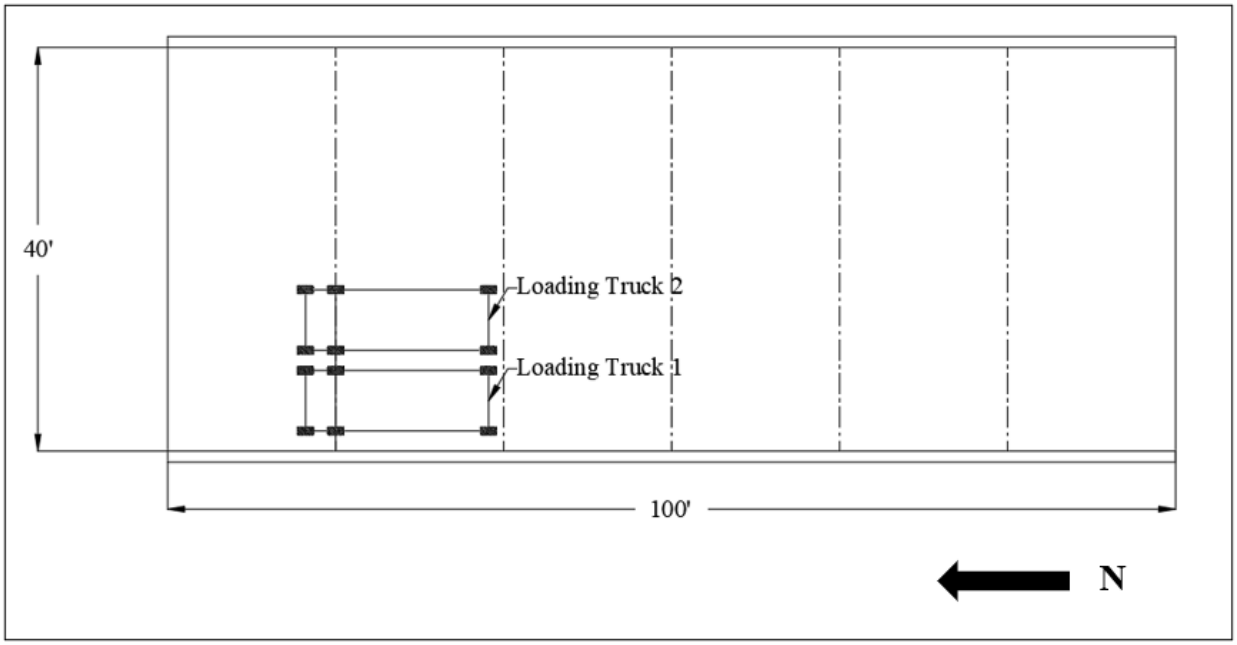

Figure 47: Truck configuration 3 plan view.

Figure 48: Truck configuration 1 for static load testing.

Figure 49: Truck configuration 3 for static load testing.

The distribution factor was also calculated in the Western girders using the embedded vibrating wire gauges. These instruments are only in the exterior Western girder of Span

9 and Span 14. The strain data during load testing was compared to strain data from before load testing to get the strain imposed by the truck loading. The curvature can be computed from the change in strain along the depth of the girder. Curvature can be multiplied by the modulus of the girder concrete and the moment of inertia of the exterior girder to find the internal moment of the girder. Modulus was taken as 5853 ksi, which is the estimated modulus at 28-days for each of the girders. Moment of inertia for the two external girders was calculated with transformed properties that included the girder and reinforcement, made composite with the deck and parapet. The values were found to be 1,096,410 in^4 and 1,029,610 in^4 for Mark 27, Span 9 and Mark 42, Span 14 girders, respectively. The found moment from curvature can then be related to the total applied moment from the truck configuration to determine the distribution factor of the external girder.

4.4 STATIC LOAD TESTING RESULTS

Raw deflection data collected from LVDTs from load testing is shown in Figure 50, Figure 51, Figure 52, and Figure 53. Note that an error was made during testing on Span 14, configuration 1, in which one of the truck rear tire placements at 33.3 ft was accidentally skipped. The test was reperformed later, but that station's data is not present in Figure 52.

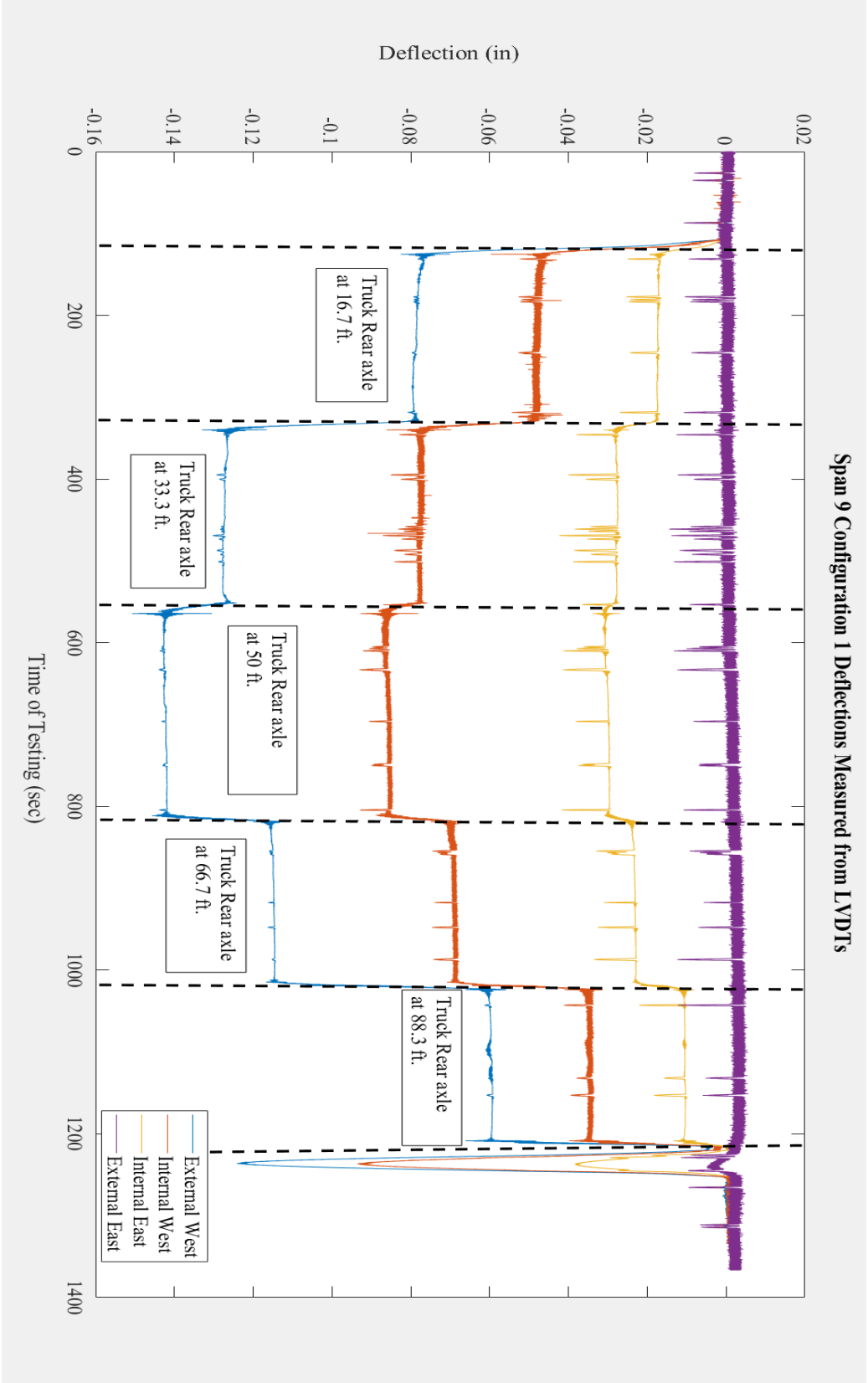

Figure 50: Span 9 Configuration 1 measured Midspan deflections.

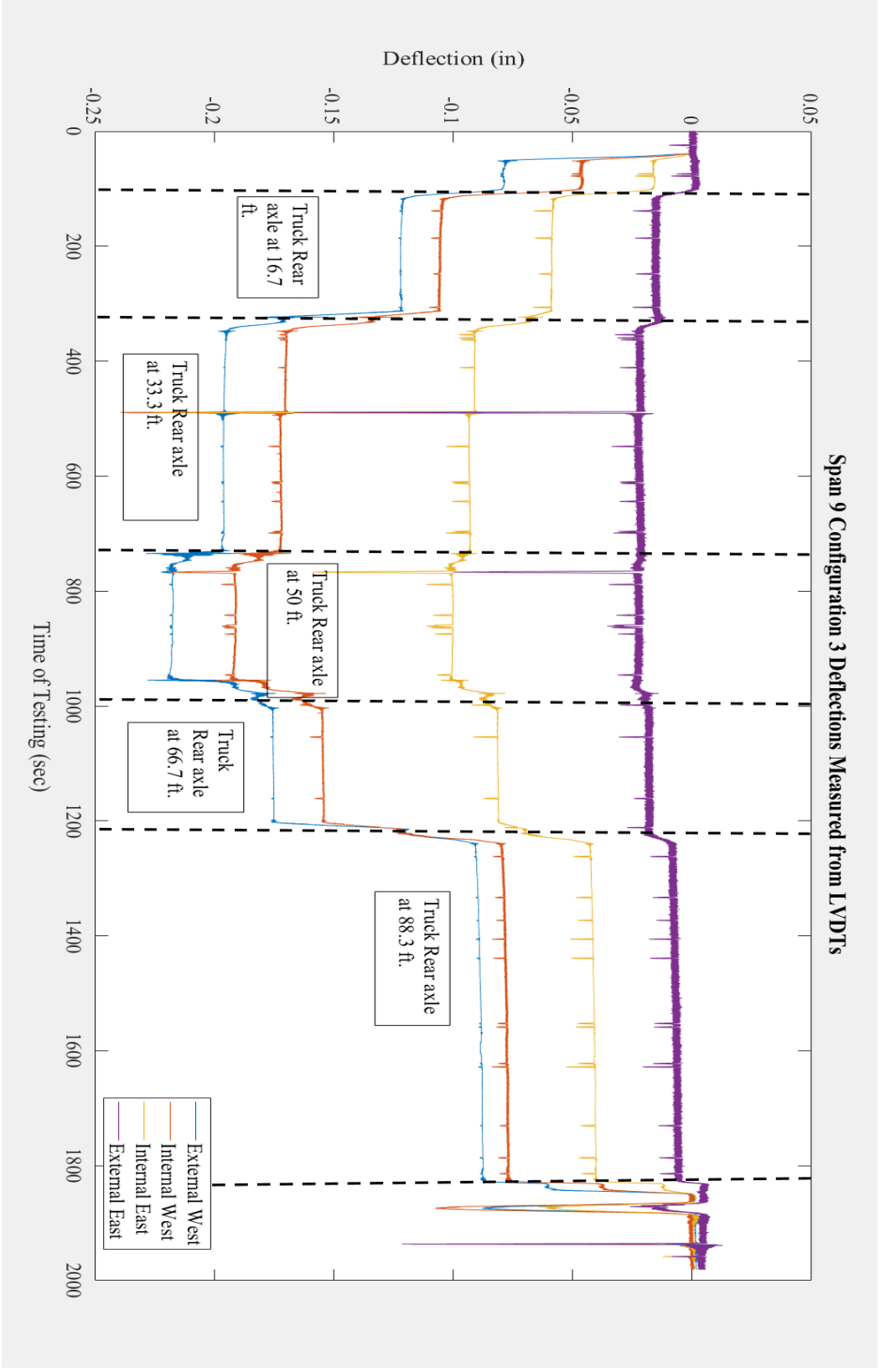

Figure 51: Span 9 Configuration 3 measured midspan deflections.

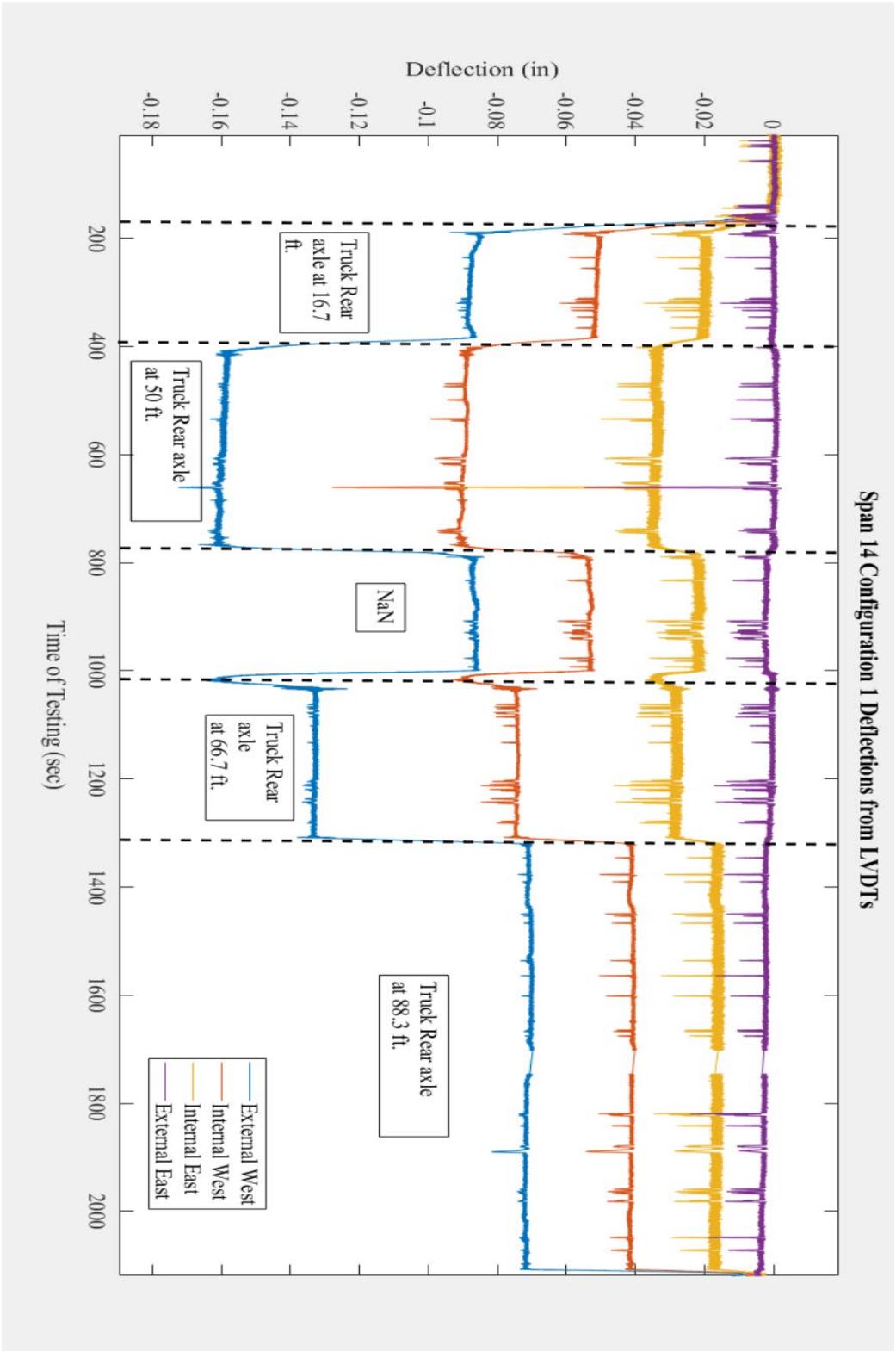

Figure 52: Span 14 Configuration 1 measured midspan deflections.

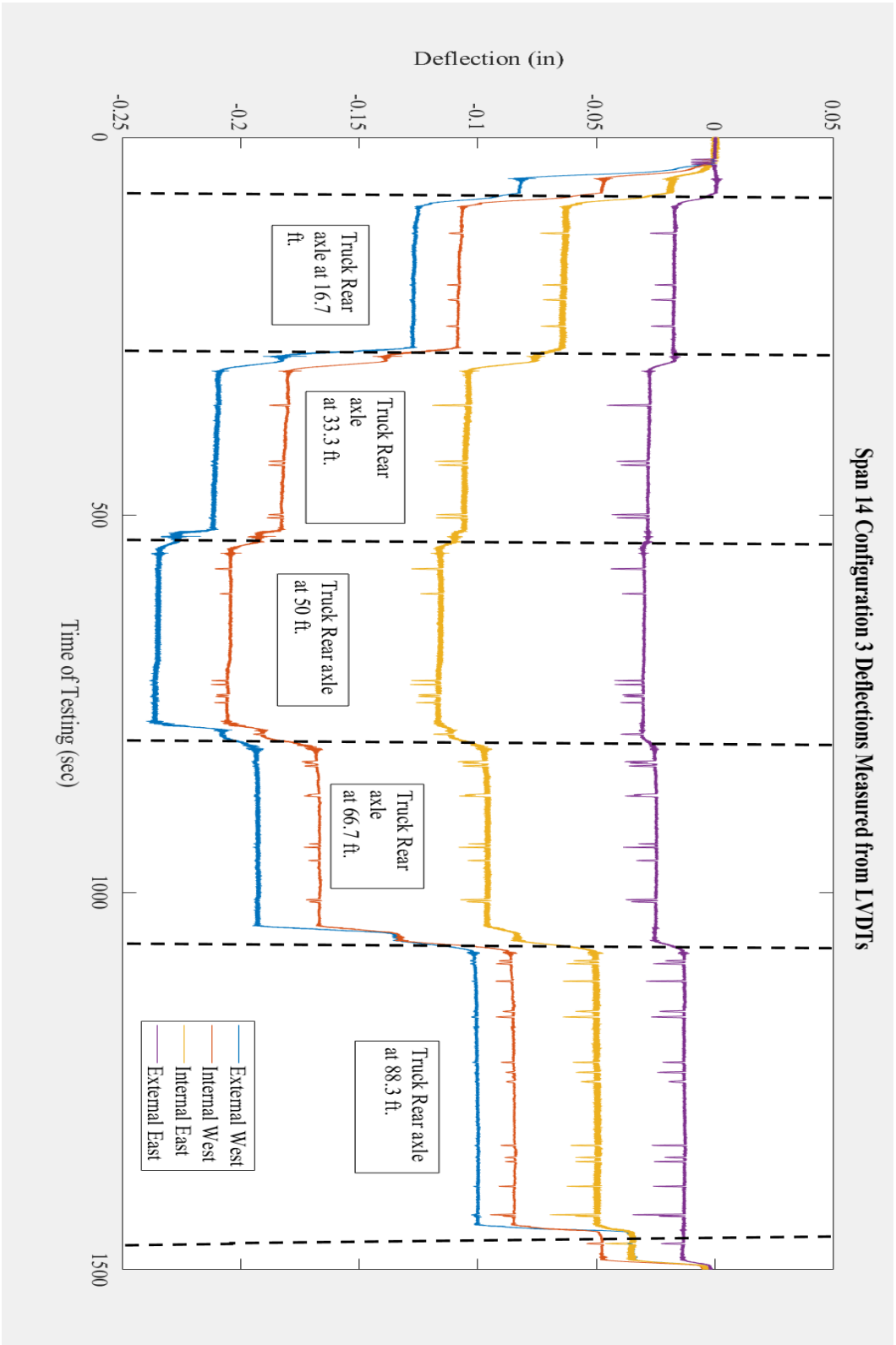

Figure 53: Span 14 Configuration 3 measured midspan deflections.

The following tables and graphs report deflections and distribution factors from the static load test. Deflection values were taken from LVDTs present during the tests and distribution factors were calculated from the relative deflections at each station. Tabulated finite element results are provided for easy comparison. Discussion on how finite element results were obtained are described in the next section. The distribution factors calculated using the lever rule, rigid method, and FEA are at the bottom of the tables for comparison.

Table 15: Span 9 Configuration 1 tabulated results.

Span 9 (Configuration 1 (Truck 1)) Deflections (in) and Distribution Factors (DF)								
	Deflections (in.)				Distribution Factors			
Girders	**External West**	**Internal West**	**Internal East**	**External East**	**External West**	**Internal West**	**Internal East**	**External East**
Truck location	1	2	3	4	1	2	3	4
16.7	0.08	0.05	0.02	0.00	0.54	0.33	0.12	0.00
33.3	0.13	0.08	0.03	0.00	0.55	0.33	0.12	0.00
50	0.14	0.09	0.03	0.00	0.55	0.33	0.12	0.00
66.7	0.12	0.07	0.02	0.00	0.56	0.34	0.11	-0.01
83.3	0.06	0.04	0.01	0.00	0.58	0.34	0.11	-0.03
Note: 1: All DFs displayed at the bottom of the table are calculated at midspan. 2: Multi presence factors are excluded from results.			**Measured at Midspan**		**0.55**	**0.33**	**0.12**	**0.00**
			Rigid Method		**0.65**	**0.38**	**0.12**	**-0.15**
			Lever Rule		**0.82**	**0.18**	**0.00**	**0.00**
			FEA		**0.54**	**0.31**	**0.14**	**0.01**

Table 16: Span 9, configuration 1 FEA results.

Configuration 1 (Truck 1)) Deflections (in) and Distribution Factors (DF) from Finite Element Analysis								
	Deflections (in.)				Distribution Factors			
Girders	External West	Internal West	Internal East	External East	External West	Internal West	Internal East	External East
Truck location	1	2	3	4	1	2	3	4
16.7	0.10	0.06	0.02	0.00	0.54	0.32	0.13	0.01
33.3	0.18	0.10	0.04	0.00	0.54	0.32	0.13	0.01
50	**0.21**	**0.12**	**0.05**	**0.01**	**0.54**	**0.32**	**0.13**	**0.01**
66.7	0.18	0.10	0.04	0.00	0.54	0.32	0.13	0.01
83.3	0.09	0.05	0.02	0.00	0.54	0.32	0.13	0.01

Table 17: Span 9 Configuration 3 tabulated results.

Span 9 Configuration 3 (Truck 1 + Truck 2) Deflections (in) and Distribution Factors (DF)								
	Deflections (in.)				Distribution Factors			
Girders	External West	Internal West	Internal East	External East	External West	Internal West	Internal East	External East
Truck location	1	2	3	4	1	2	3	4
16.7	0.12	0.11	0.06	0.02	0.81	0.70	0.39	0.10
33.3	0.20	0.17	0.09	0.02	0.81	0.71	0.38	0.10
50	0.22	0.19	0.10	0.02	0.82	0.72	0.38	0.09
66.7	0.18	0.15	0.08	0.02	0.82	0.72	0.38	0.08
83.3	0.09	0.08	0.04	0.01	0.83	0.73	0.38	0.07
Note: 1: All DFs displayed at the bottom of the table are calculated at midspan. 2: Multi presence factors are excluded from results.			**Measured at Midspan**		**0.82**	**0.72**	**0.38**	**0.09**
			Rigid Method		**1.03**	**0.68**	**0.30**	**-0.01**
			Lever Rule		**0.93**	**0.57**	**0.50**	**0.00**
			FEA		**0.89**	**0.67**	**0.34**	**0.10**

Table 18: Span 9, configuration 3 FEA results.

Span 9 Configuration 3 (Truck 1 + Truck 2) Deflections (in) and Distribution Factors (DF) from Finite Element Analysis								
	Deflections (in.)				Distribution Factors			
Girders	External West	Internal West	Internal East	External East	External West	Internal West	Internal East	External East
Truck location	1	2	3	4	1	2	3	4
16.7	0.17	0.14	0.07	0.02	0.43	0.35	0.16	0.06
33.3	0.33	0.26	0.12	0.04	0.44	0.35	0.16	0.05
50	**0.39**	**0.31**	**0.14**	**0.04**	**0.44**	**0.35**	**0.16**	**0.05**
66.7	0.32	0.26	0.12	0.04	0.44	0.35	0.16	0.05
83.3	0.16	0.13	0.06	0.02	0.43	0.35	0.16	0.06

Table 19: Span 14 Configuration 1 tabulated results.

Span 14 Configuration 1 (Truck 1) Deflections (in) and Distribution Factors (DF)								
	Deflections (in.)				Distribution Factors			
Girders	External West	Internal West	Internal East	External East	External West	Internal West	Internal East	External East
Truck location	1	2	3	4	1	2	3	4
16.7	0.09	0.05	0.02	0.00	0.55	0.32	0.12	0.01
33.3	0.12	0.07	0.03	0.00	0.55	0.32	0.13	0.00
50	0.16	0.09	0.04	0.00	0.56	0.32	0.12	0.00
66.7	0.13	0.08	0.03	0.00	0.56	0.32	0.12	0.00
83.3	0.07	0.04	0.02	0.00	0.54	0.31	0.13	0.02
Note: 1: All DFs displayed at the bottom of the table are calculated at midspan. 2: Multi presence factors are excluded from results.			**Measured at Midspan**		**0.56**	**0.32**	**0.12**	**0.00**
			Rigid Method		**0.65**	**0.38**	**0.12**	**-0.15**
			Lever Rule		**0.82**	**0.18**	**0.00**	**0.00**
			FEA		**0.491**	**0.297**	**0.154**	**0.058**

Table 20: Span 14, configuration 1 FEA results.

Span 14 (Configuration 1 (Truck 1)) Deflections (in) and Distribution Factors (DF) from Finite Element Analysis								
	Deflections (in.)				Distribution Factors			
Girders	External West	Internal West	Internal East	External East	External West	Internal West	Internal East	External East
Truck location	1	2	3	4	1	2	3	4
16.7	0.06	0.04	0.02	0.01	0.44	0.29	0.18	0.09
33.3	0.12	0.07	0.04	0.02	0.47	0.30	0.16	0.07
50	**0.14**	**0.09**	**0.05**	**0.02**	**0.49**	**0.30**	**0.15**	**0.06**
66.7	0.12	0.07	0.04	0.01	0.50	0.30	0.15	0.05
83.3	0.07	0.04	0.02	0.01	0.50	0.30	0.15	0.05

Table 21: Span 14 Configuration 3 tabulated results.

Span 14 Configuration 3 (Truck 1 + Truck 2) Deflections (in) and Distribution Factors (DF)								
	Deflections (in.)				Distribution Factors			
Girders	**External West**	**Internal West**	**Internal East**	**External East**	**External West**	**Internal West**	**Internal East**	**External East**
Truck location	1	2	3	4	1	2	3	4
16.7	0.13	0.11	0.06	0.02	0.80	0.68	0.40	0.11
33.3	0.21	0.18	0.11	0.03	0.80	0.69	0.40	0.11
50	0.24	0.21	0.12	0.03	0.80	0.70	0.40	0.10
66.7	0.19	0.17	0.10	0.03	0.80	0.69	0.40	0.10
83.3	0.10	0.09	0.05	0.01	0.81	0.69	0.40	0.10
Note: 1: All DFs displayed at the bottom of the table are calculated at midspan. 2: Multi presence factors are excluded from results.			**Measured at Midspan**		**0.80**	**0.70**	**0.40**	**0.10**
			Rigid Method		**1.03**	**0.68**	**0.30**	**-0.01**
			Lever Rule		**0.93**	**0.57**	**0.50**	**0.00**
			FEA		**0.79**	**0.64**	**0.38**	**0.19**

Table 22: Span 14, configuration 3 FEA results.

Span 14 Configuration 3 (Truck 1 + Truck 2) Deflections (in) and Distribution Factors (DF) from Finite Element Analysis								
	Deflections (in.)				Distribution Factors			
Girders	External West	Internal West	Internal East	External East	External West	Internal West	Internal East	External East
Truck location	1	2	3	4	1	2	3	4
16.7	0.11	0.09	0.06	0.04	0.36	0.31	0.21	0.13
33.3	0.22	0.18	0.11	0.06	0.38	0.32	0.20	0.11
50	**0.27**	**0.22**	**0.13**	**0.06**	**0.40**	**0.32**	**0.19**	**0.09**
66.7	0.22	0.18	0.11	0.05	0.40	0.32	0.19	0.09
83.3	0.11	0.09	0.05	0.02	0.40	0.32	0.19	0.09

4.5 FINITE ELEMENT MODELLING

Three-dimensional finite element models were developed to simulate the behavior of the bridge during the load testing. Two models were built, one representing Span 9 and the other representing Span 14. Both models are identical in geometry, loadings, and input values, except for shear and longitudinal reinforcement layouts. The girders, deck, diaphragms, and parapets were modeled as 3-dimensional solids. All reinforcement in the deck, diaphragms, and girders are included in each of the models. The prestressing strands and rebar were modeled to reduce computation time as 2-dimensional wire elements. The strands and rebars were made composite with the deck using the "Embedded Region" constraint. A photograph of the reinforcing in the model is shown in Figure 59.

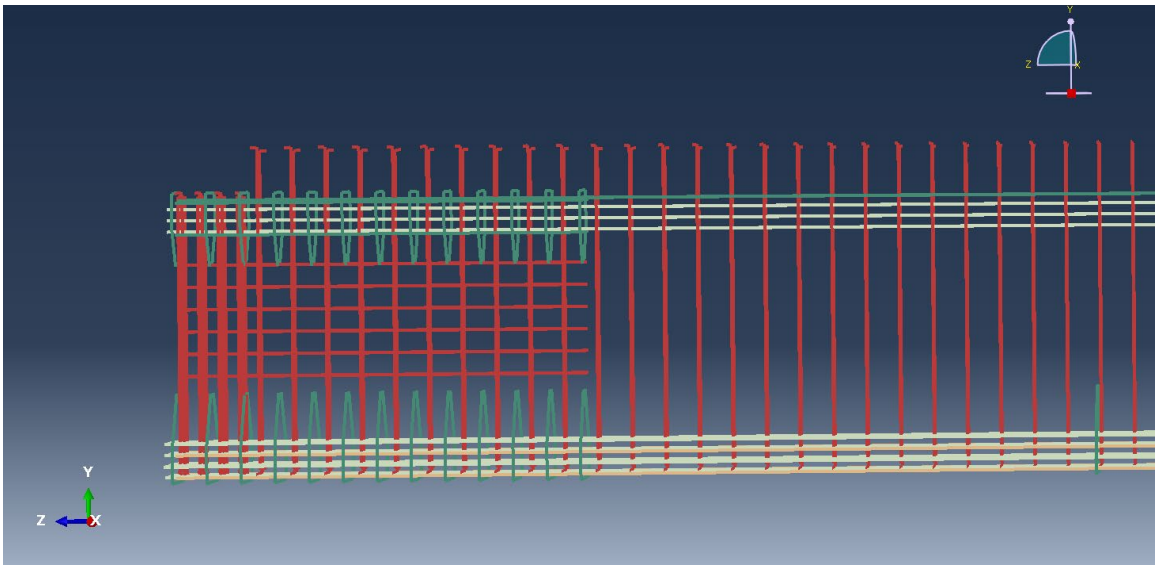

Figure 54: End region reinforcing in FEA model of Span 9.

The modulus of elasticity for the girders was set to 5853 ksi. The modulus of elasticity for the deck, diaphragms and parapets was set to 4684 ksi. The modulus of elasticity of the prestressing strands was set to 28500 ksi and the modulus for reinforcing steel was set to 29000 ksi. The meshing was set to 5.5 in. for the deck and 6 in. for all other components, show in Figure 55. The deck, parapets, and diaphragms were attached to the girders using a “Tie” constraint to simulate composite action between these components. Prestressing was applied to the model by imposing strain on the strands before the first step in the analysis. Since Abaqus cannot simulate the bridge's construction steps, the prestressing force in the model is not entirely accurate. To negate this inaccuracy, deflection and strain values were taken from the model with no truck loading applied and then compared to deflection and strain values taken after truck loading was applied to find deflection and strain caused by truck loading on the structure.

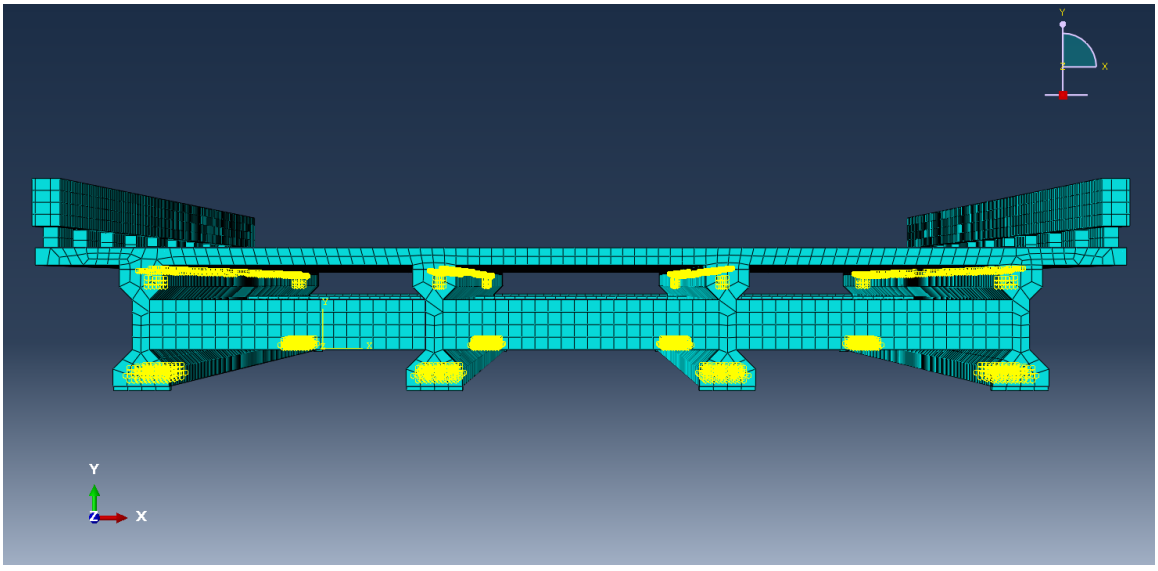

Figure 55: Photograph of the Abaqus model.

Bearing pads were set as 7 in. long and 26 in. wide. The center of each bearing pad was placed 7.5 inches away from the end face of each girder. Bearing pads were constrained to make the span act similar to a simply supported beam.

All static load tests were recreated in the finite element models. The models were run once without truck loading and once with truck loading. The deflection and change in strain caused by truck loading were found using superposition. Deflection and strain were found by subtracting the test results without truck loading from the test results that included truck loading. Distribution factors were computed similarly to the static load test, where the deflection of one girder is divided by the sum of deflections of all girders to get the distribution factor. Photographs of the model before and after being run are shown in Figure 56 and Figure 57, respectively.

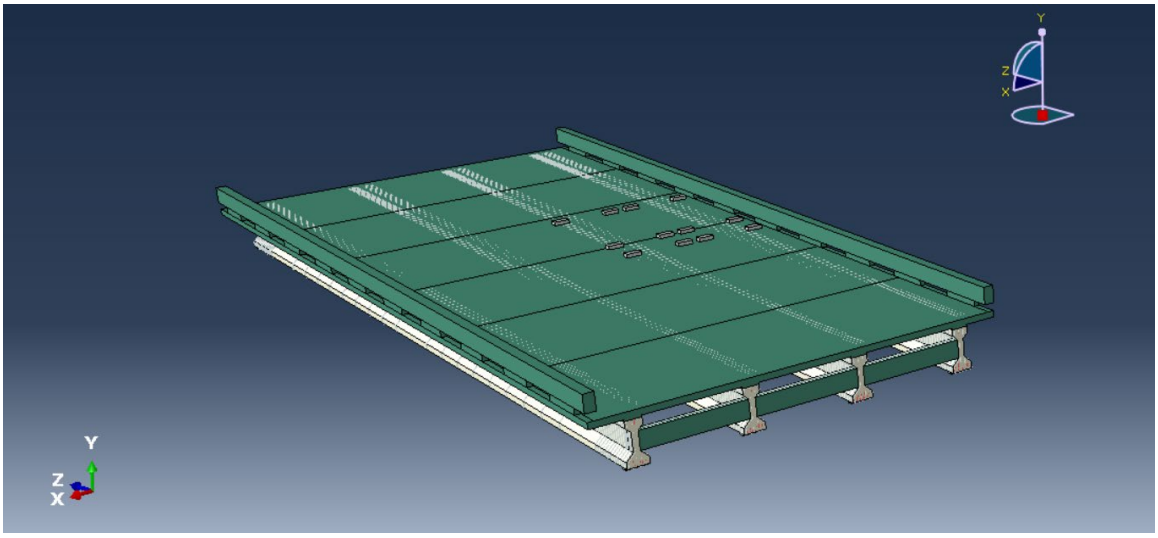

Figure 56: Abaqus model of Span 9 before the model was run. In view are truck wheel loads set to configuration 3 at midspan.

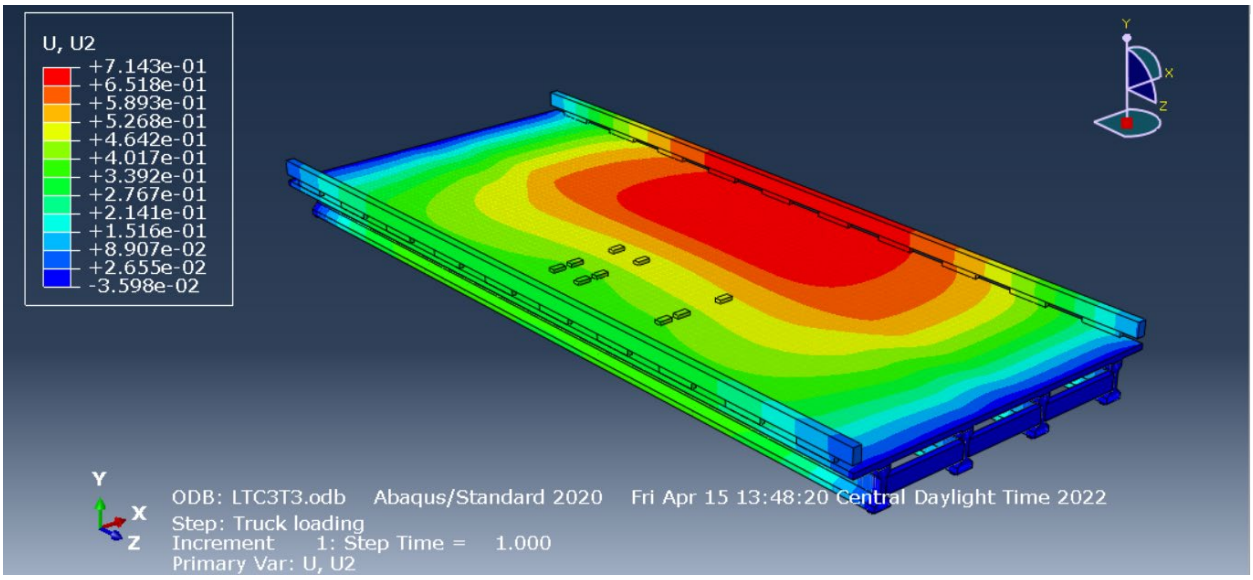

Figure 57: Span 9 configuration 3 deflection results. The dark red color displays upward deflection caused by camber. The lighter colors display that upward deflection was limited by truck loading.

4.6 DISCUSSION

Deflection and strain measurements were used to determine distribution factors for the girders of the spans. Distribution factors for each girder can be derived using deflection measurements and are calculated by dividing the deflection of a girder by the sum of all the deflections of all the girders and multiplied by the number of lanes loaded. This is shown in the following equation, modified from eq. 1 in Dong et al. (2020) [11]:

$$DF = \frac{\Delta_{girder}}{\sum \Delta_{girders}} * N_L$$

The results of the tests were compared to AASHTO prescribed methods, specifically the lever rule and rigid method.

4.6.1 Comparison of AASHTO Methods and Load Test Results

Table 23 displays the calculated results of the varying AASHTO methods for exterior and interior girders in both single lane and two lane loaded scenarios. Results varied between all methods in all scenarios with the AASHTO LRFD table method consistently providing the most conservative results. Note that multiple presence factors were not considered in these computations except for in the AASHTO LRFD case for an exterior girder, single lane loaded scenario, in which the lever rule was used and multiplied by a factor of 1.2.

Table 23: Comparison of AASHTO methods for determining distribution factors of exterior and interior girders.

Girder Location	Number of Lanes Loaded	Lever Rule	Rigid Method	AASHTO LRFD
Ext	1	0.82	0.65	0.99
Ext	2	0.93	1.03	0.89
Int	1	0.18	0.38	0.55
Int	2	0.57	0.68	0.81

Note:
1. Lever rule and rigid method results do not include multiple presence factors in this analysis.
2. The AASHTO LRFD method requires use of the lever rule to calculate distribution factors of a single lane loaded exterior girder. A multiple presence factor of 1.2 was used in calculation for this case. All other cases in this method consider multiple presence in their equations.

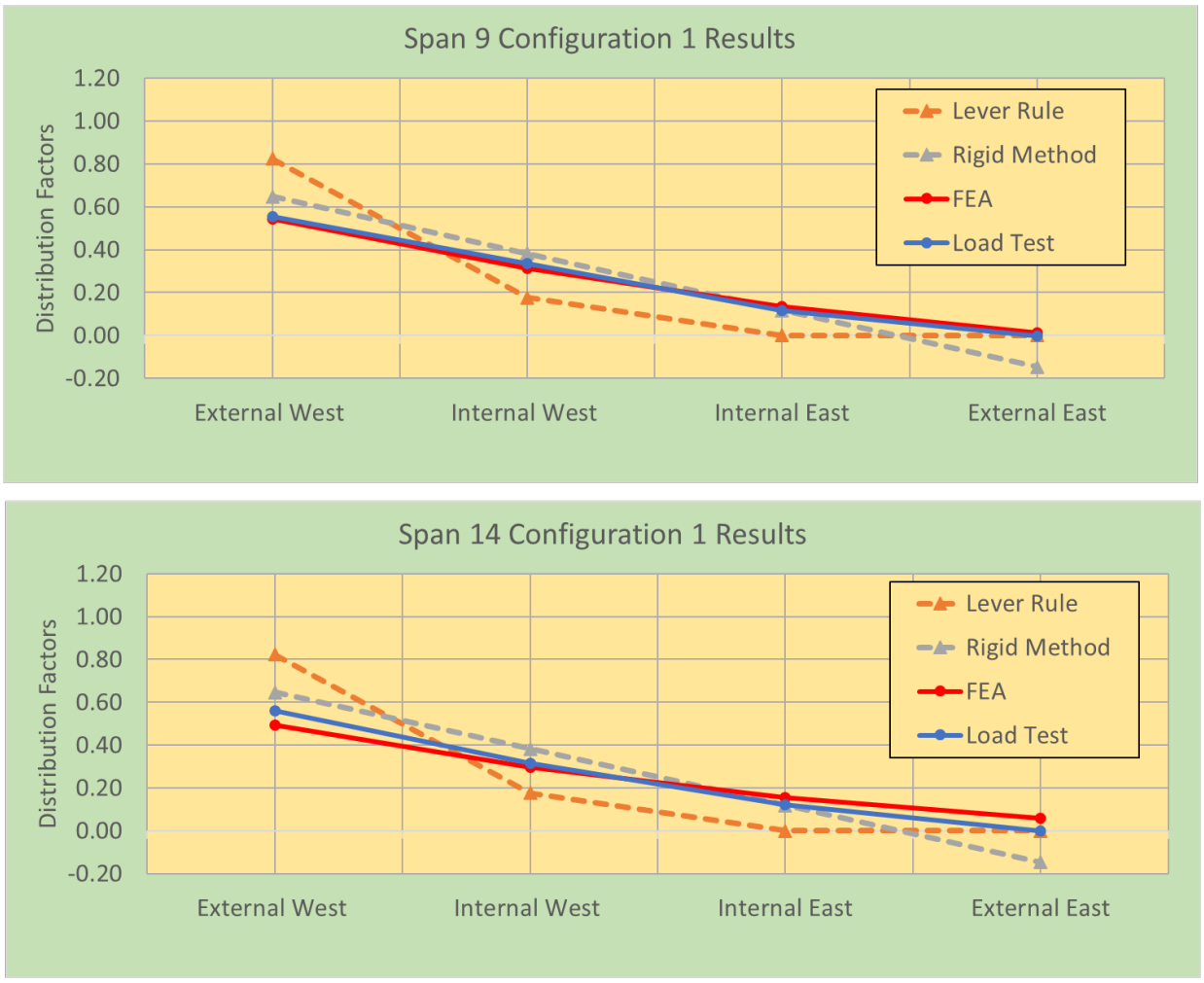

Figure 58: Truck configuration 1 at midspan results.

Figure 58 displays midspan distribution factors for configuration 1 from the load test, FEA, the lever rule, and the rigid method. Note that multiple presence factors are not included in these results. Comparing the load test results for Span 9, the lever rule overpredicts the distribution factor of the external West girder by about 0.27 (39%) and underpredicts the distribution factor of the internal West girder by 0.16 (62%). The rigid method overpredicts the distribution factor of the external West girder by about 0.094 (16%) and overpredicts the distribution factor of the internal West girder by 0.047 (13%). The finite element analysis underpredicts the distribution factor of the external West

girder by about 0.011 (1.9%) and underpredicts the distribution factor of the internal West girder by 0.023 (7.1%).

Comparing the load test results for Span 14, the lever rule overpredicts the distribution factor of the external West girder by about 0.26 (38%) and underpredicts the distribution factor of the internal West girder by 0.14 (57%). The rigid method overpredicts the distribution factor of the external West girder by about 0.086 (14%) and overpredicts the distribution factor of the internal West girder by 0.066 (19%). The finite element analysis underpredicts the distribution factor of the external West girder by about 0.070 (13%) and underpredicts the distribution factor of the internal West girder by 0.019 (6.2%).

Figure 59: Truck configuration 3 at midspan results

Figure 59 displays midspan distribution factors for configuration 3 from the load test, FEA, the lever rule, and the rigid method. Comparing the load test results for Span 9, the lever rule overpredicts the distribution factor of the external West girder by about 0.11 (13%) and underpredicts the distribution factor of the internal West girder by 0.15 (23%). The rigid method overpredicts the distribution factor of the external West girder by about 0.21 (23%) and underpredicts the distribution factor of the internal West girder by 0.038 (5.4%). The finite element analysis overpredicts the distribution factor of the external

West girder by about 0.077 (9.0%) and underpredicts the distribution factor of the internal West girder by 0.051 (7.3%).

Comparing the load test results for Span 14, the lever rule overpredicts the distribution factor of the external West girder by about 0.13 (15%) and underpredicts the distribution factor of the internal West girder by 0.13 (20%). The rigid method overpredicts the distribution factor of the external West girder by about 0.23 (25%) and underpredicts the distribution factor of the internal West girder by 0.02 (2.9%). The finite element analysis underpredicts the distribution factor of the external West girder by about 0.013 (1.6%) and underpredicts the distribution factor of the internal West girder by 0.058 (8.6%).

From this analysis, it is shown that the lever rule and rigid method are conservative in the calculation of the distribution factor for external girders. In contrast, the finite element approach showed to accurately measure distribution factors. The overestimation of the distribution factors of the external girder likely means more reinforcement was used in this span then was necessary.

4.6.2 Comparison of Load Test and FEA Results

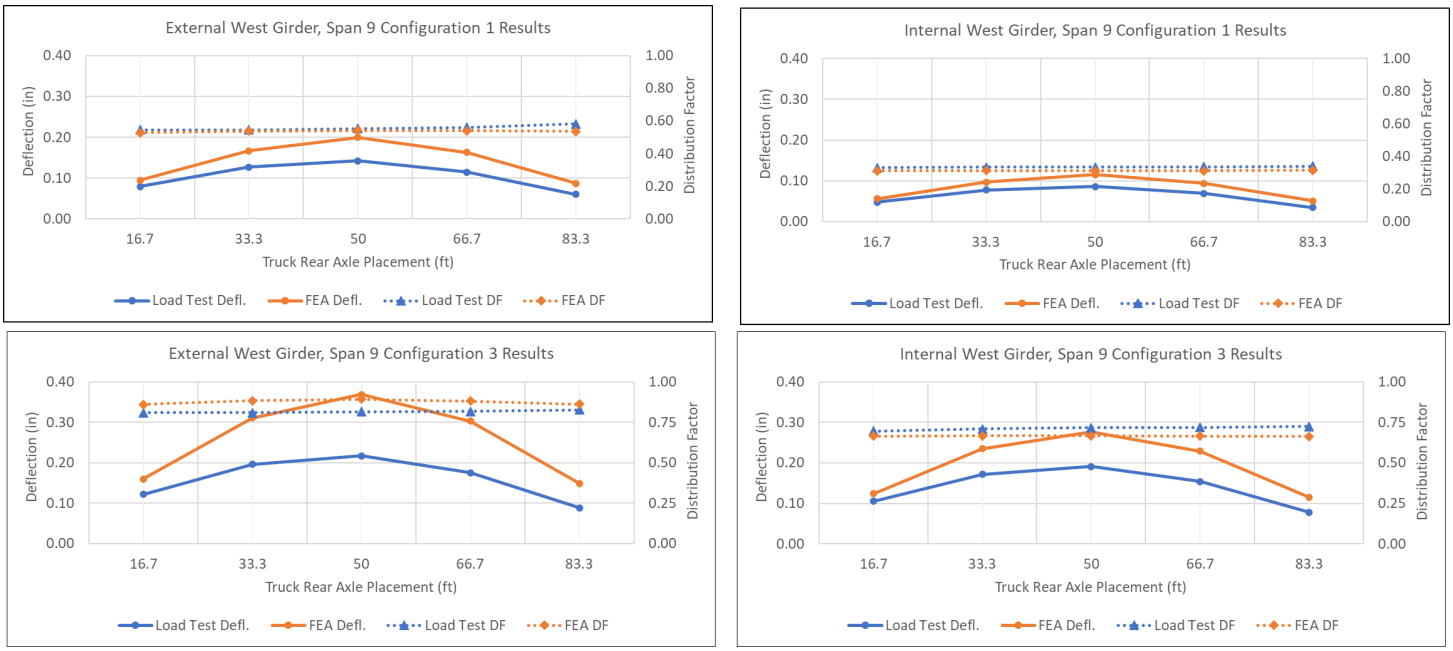

Figure 60: Span 9 Western Girders Load Test and FEA Results

Figure 60 displays deflections and distribution factors for the Westernmost girders of Span 9 at each truck station. It is observed that the finite element model consistently overpredicts deflection by as little as 0.01 in. and as much as 0.17 in. This is likely due to the bridge deck being continuous through this span and not being accounted for in this model, leading to higher midspan deflection. Distribution factors found using the FEA model followed similar behavior to that observed during the load test. For the external West girder, the DF of the midspan station from the load test was 0.55 and 0.82 for truck configurations 1 and 3, respectively. FEA found a distribution factor of 0.54 and 0.89, which is a 1.8% and 8.2% percent difference between measured and FEA results for C1 and 3 respectively. For the internal West girder, the DF of the midspan station from the load test was 0.33 and 0.72 for truck configurations 1 and 3, respectively. FEA found a

distribution factor of 0.32 and 0.67, a 3.1% and 7.2% percent difference between measured and FEA results for C1 and C3, respectively.

Figure 61: Span 14 Western Girders Load Test and FEA results.

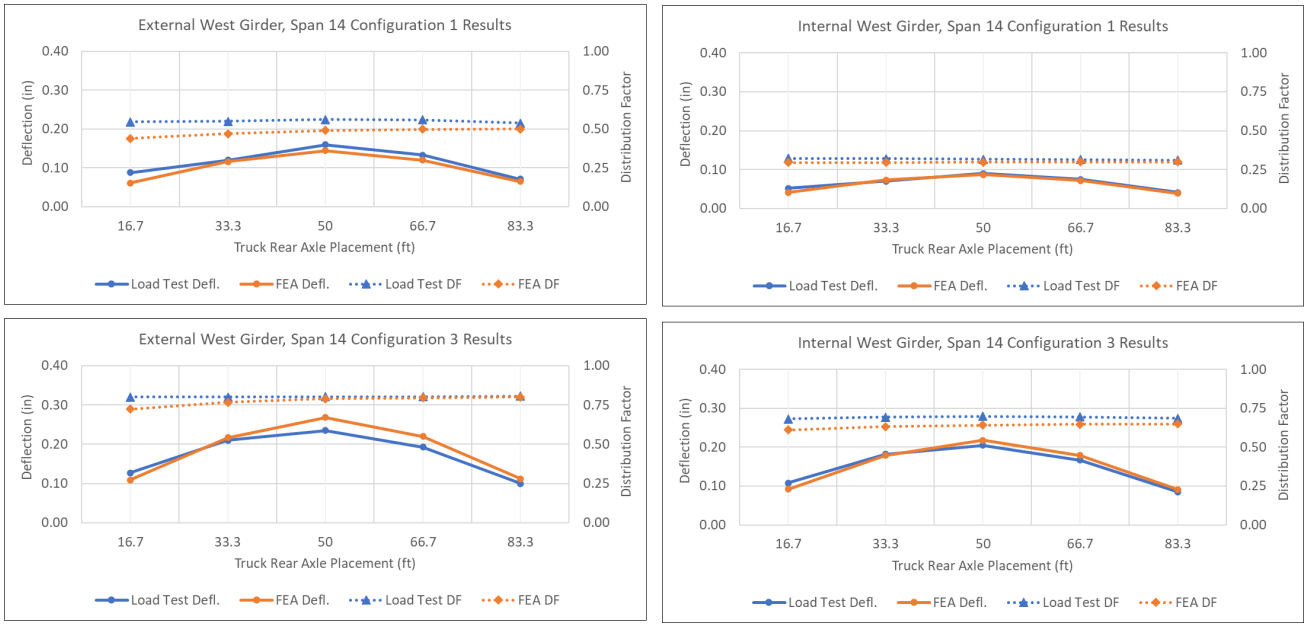

Figure 61 displays deflections and distribution factors for the Westernmost girders of Span 14 at each truck station. It is observed that the deflections found with the finite element model are relatively consistent with deflection measured to the load test. FEA underpredicted deflections by as low as 0.018 in and as much as 0.033 in. The FEA model is consistent with deflection results for Span 14, as opposed to span 9. This is likely because an expansion joint was included on one of the ends of the deck of Span 14, allowing more flexibility of the deck. Distribution factors found using the FEA model vary more when compared to the results from Span 9. For the external West girder, the DF of the midspan station from the load test was 0.56 and 0.80 for truck configurations 1 and 3, respectively. FEA found a distribution factor of 0.49 and 0.79, which is a 13% and 1.2% percent difference between measured and FEA results for C1 and C3, respectively.

For the internal West girder, the DF of the midspan station from the load test was 0.32 and 0.70 for truck configurations 1 and 3, respectively. FEA found a distribution factor of 0.30 and 0.64, which is a 6.5% and 9% percent difference for C1 and C3, respectively.

These results show that FEA can consistently and accurately measure the relative deflection of the girders, therefore measuring distribution factors accurately. FEA was not able to measure deflection accurately in for Span 9. This is likely attributed to a combination of the deck fixity of Span 9 not being properly accounted for and concrete modulus likely being underpredicted in this span.

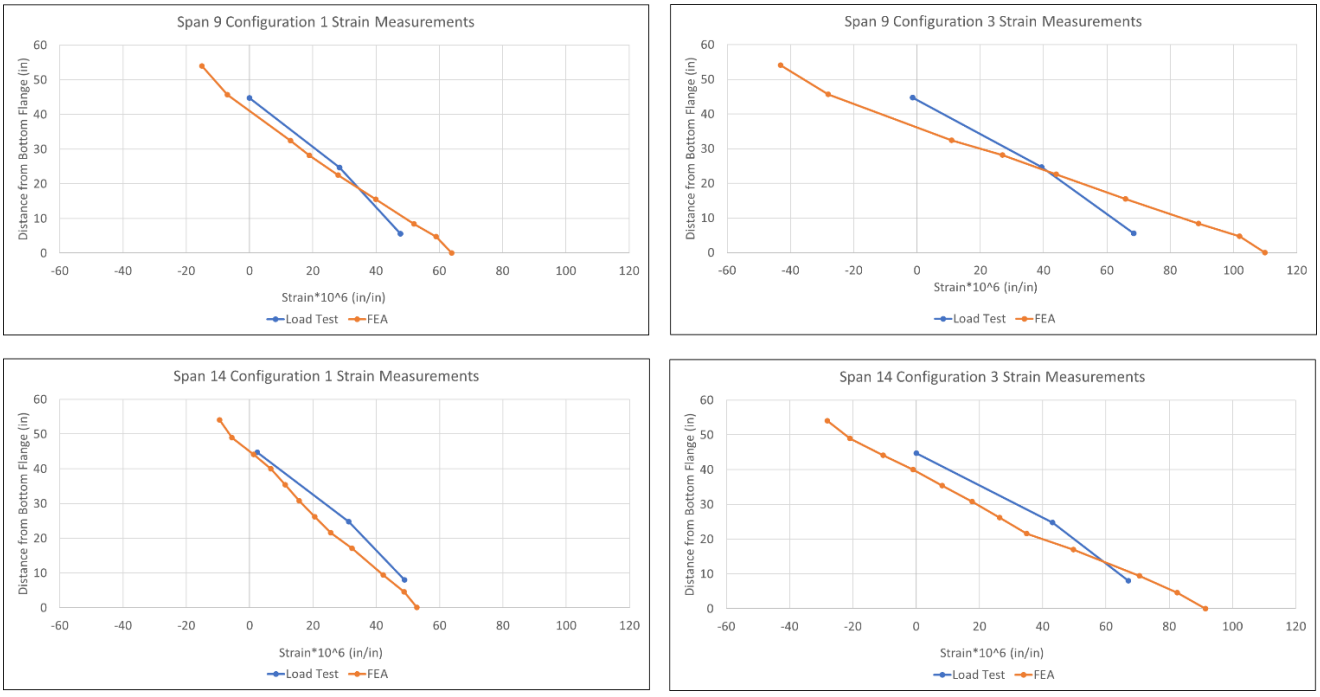

Figure 62: Strain measurements of external West girders from load test and FEA for trucks placed at midspan.

The measured strain of the Westernmost Girders from truck axles at the bridge's midspan from both instrumentation and the FEA model is shown in Figure 62. Vibrating wire

gauges are only located in three locations along the depth of each girder. Strain measurements from the finite element model can be obtained for all nodes on the girder at midspan. Both sets of strain measurements are not perfectly linear along the depths of the beam. Interpolating the FEA results to the depth at which the vibrating wire gauges were placed shows a maximum underprediction of FEA results of 29.9 microstrains and a maximum overprediction of 22.8 microstrains between all tests.

Since strain measurements are not perfectly linear, curvature imposed by truck loading at midspan can only be approximated. The curvature of Span 9 derived using sensor data found 1.11 * 10-6 (1/in) and 1.60 * 10-6 (1/in) for truck configurations 1 and 3, respectively. Curvature of Span 9 from FEA found 1.45 * 10-6 (1/in) and 2.85 * 10-6 (1/in) for truck configurations 1 and 3, respectively. This is a 26% and 56% difference between sensor and FEA results.

The curvature of Span 14 derived using sensor data found 1.04 * 10-6 (1/in) and 1.50 * 10-6 (1/in) for truck configurations 1 and 3, respectively. Curvature of Span 14 from FEA found 1.08 * 10-6 (1/in) and 2.11 * 10-6 (1/in) for truck configurations 1 and 3, respectively. This is a 3.2% and 34% difference between sensor and FEA results.

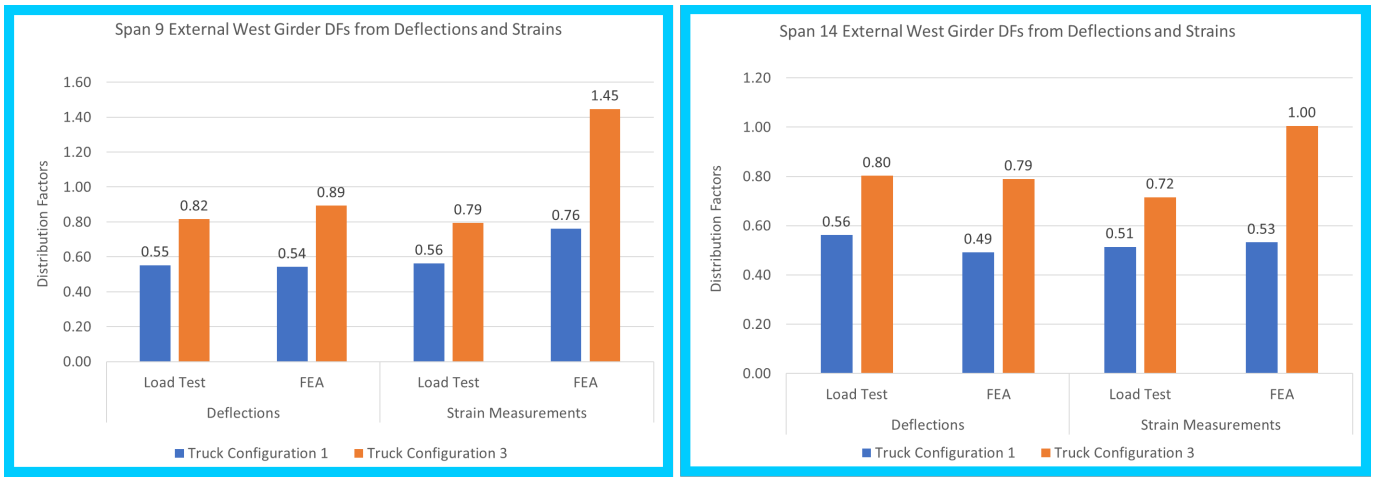

Figure 63: Comparison of distribution factors found using relative deflection and curvatures in the External West Girders.

Figure 63 displays distribution factors at midspan for the exterior Western girder of spans 9 and 14 calculated using relative deflection and curvature derived from strain measurements. Comparing the results of Span 9, deflections measured by LVDTs during the load test found a distribution factor of 0.55 and 0.82 for truck configurations 1 and 3 (C1 and C3), respectively. Using midspan strain readings from VWGs found a distribution factor of 0.56 and 0.79 for C1 and C3, respectively. This is a 1.8% and 8.1% percent difference for C1 and C3, respectively.

Comparing the results of the FEA, distribution factors based on the relative deflection of all girders in Span 9 displayed a distribution factor of 0.54 and 0.89 for C1 and C3, respectively. Using strain measurements found a distribution factor of 0.76 and 1.45 for C1 and C3, respectively. This is a percent difference of 34% and 48% for C1 and C3, respectively.

Comparing the results of Span 14, deflections measured by LVDTs during the load test found a distribution factor of 0.56 and 0.80 for truck configurations 1 and 3 (C1 and C3), respectively. Using midspan strain readings from VWGs found a distribution factor of 0.51 and 0.72 for C1 and C3, respectively. This is a percent difference of 9.3% and 11% for C1 and C3, respectively.

Comparing the results of the FEA, distribution factors based on the relative deflection of all girders in Span 14 displayed a distribution factor of 0.49 and 0.79 for C1 and C3, respectively. Using strain measurements found a distribution factor of 0.53 and 1.0 for C1 and C3, respectively. This is a percent difference of 7.8% and 23% for C1 and C3, respectively.

The data shows that physically measured strain readings can be used to compute the distribution factor, given that the concrete modulus and weight distribution of the trucks are accurately calculated. Results show that finite element can accurately determine distribution factors based on relative deflection, but not necessarily using derived curvature. Even though strains measured using deflection are similar to strains measured using instrumentation, the slope of the strain diagrams are not similar. This means that curvature can differ significantly between results, leading to an inaccurate calculation of the distribution factor when comparing the distribution of imposed truck moment at midspan. This is almost exclusively observed in the finite element results for Span 9.

4.6.3 Effects of Parapets and Diaphragms

Figure 64 and Figure 65 display results found using Finite Element software. For these tests, results from the original model are compared to results in which the parapet, diaphragms, or both are taken off the model and distribution factors are found.

FEA = Results using the original finite element model, includes parapets and diaphragms in the analysis

FEA P0 = Results using a modified finite element model, includes diaphragms, but parapets were taken out of the analysis

FEA D0 = Results using a modified finite element model, includes parapets, but diaphragms were taken out of the analysis

FEA P0D0 = Results using a modified finite elements model, diaphragms and parapets were taken out of the analysis

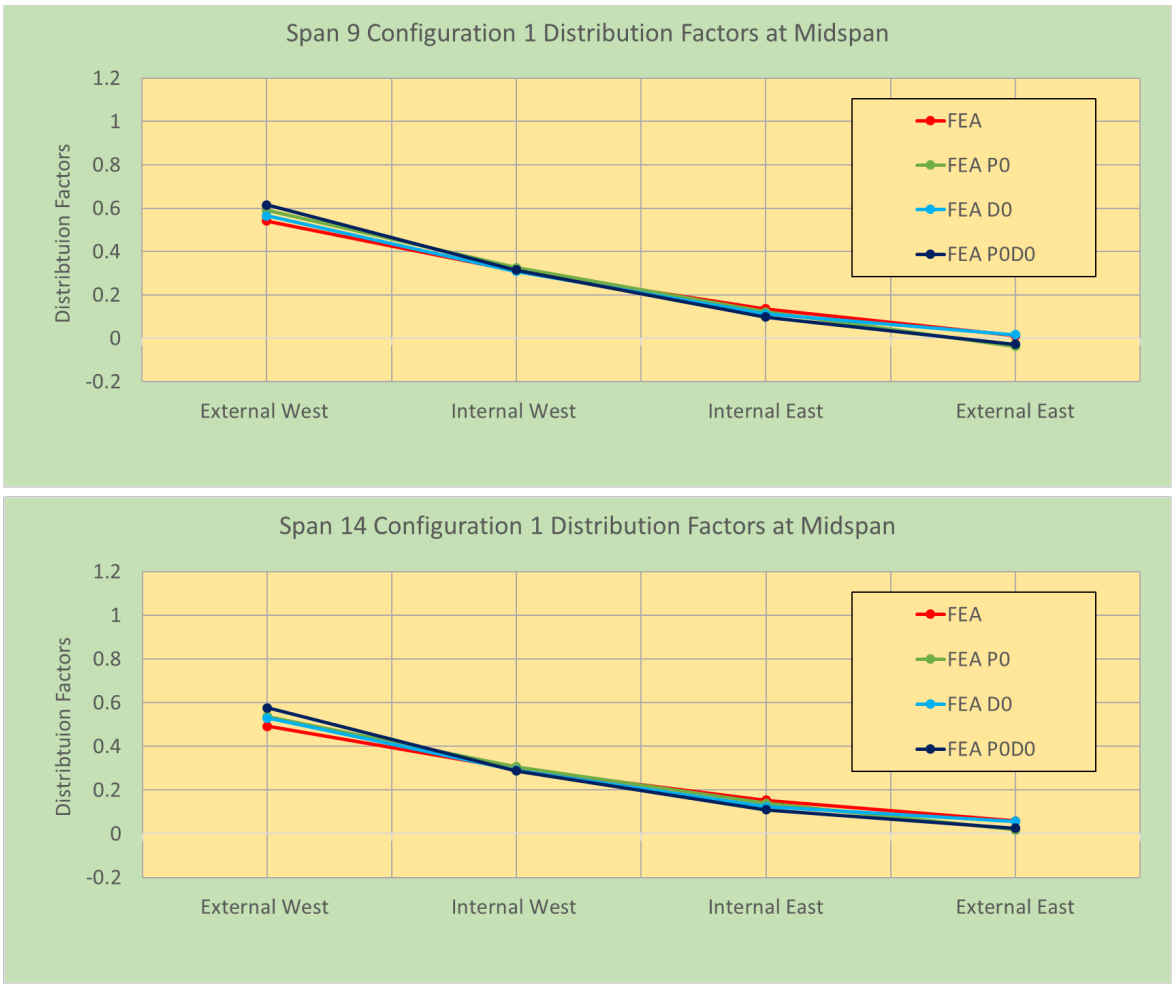

Figure 64: Configuration 1 finite element results.

Figure 64 displays the distribution factors at midspan for configuration 1 using finite element analysis in which secondary structural elements of the span were removed from the model. Comparing the results of the original finite element model of Span 9, removing the parapet increased the DF of the external West girder by 0.048 (8.6%) and increased the DF of the internal West girder by 0.014 (4.5%). Removing the diaphragm increased the DF of the external West girder by 0.022 (4.0%) and decreased the DF of the internal West girder by 0.003 (1.0%). Removing both the parapet and diaphragm

increased DF of the external West girder by 0.073 (13%) and increased DF of the internal West girder by 0.004 (1.2%).

Comparing the results of the original model of Span 14, removing the parapet increased the DF of the external West girder by 0.045 (8.8%) and increased the DF of the internal West girder by 0.009 (3.0%). Removing the diaphragm increased the DF of the external West girder by 0.037 (7.3%) and decreased the DF of the internal West girder by 0.006 (2.1% change). Removing both the parapet and diaphragm increased DF of the external West girder by 0.085 (16%) and decreased DF of the internal West girder by 0.009 (3.1%).

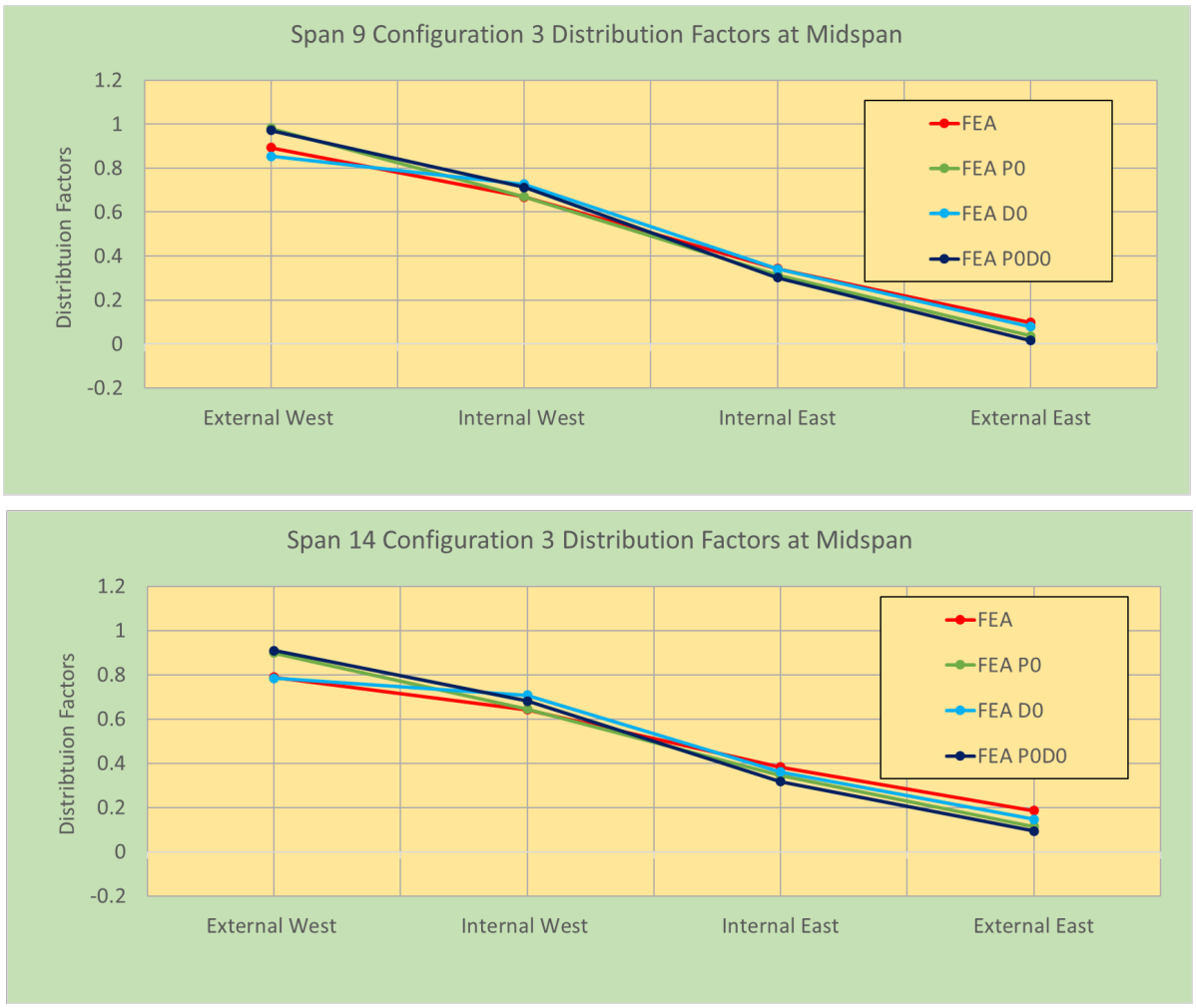

Figure 65: Configuration 3 finite element results.

Figure 65 displays the distribution factors at midspan for configuration 3 using finite element analysis in which key characteristics of the span were removed from the model. Comparing the results of the original finite element model of Span 9, removing the parapet increased the DF of the external West girder by 0.088 (9.4%) and increased the DF of the internal West girder by 0.002 (0.26%). Removing the diaphragm decreased the DF of the external West girder by 0.038 (4.4%) and increased the DF of the internal West girder by 0.058 (8.4%). Removing both the parapet and diaphragm increased DF of the

external West girder by 0.079 (8.5%) and increased DF of the internal West girder by 0.045 (6.5%).

Comparing the results of the original model of Span 14, removing the parapet increased the DF of the external West girder by 0.11 (13% change) and increased the DF of the internal West girder by 0.003 (0.47% change). Removing the diaphragm decreased the DF of the external West girder by 0.005 (0.58% change) and increased the DF of the internal West girder by 0.066 (9.8% change). Removing both the parapet and diaphragm increased DF of the external West girder by 0.12 (14% change) and increased DF of the internal West girder by 0.039 (5.9% change).

The results show that removing the parapets in analysis increases the distribution factor of the external girders, while removing the diaphragms slightly increases the distribution factor of the internal girders. This work shows that including the parapets are effective in distributing live load away from exterior girders and that diaphragms do not contribute significantly to load distribution.

4.7 CONCLUSIONS

4.7.1 Distribution Factor Conclusions

- AASHTO prescribed methods overestimate the distribution factors for bridge girders.
    - The lever rule overpredicted distribution factors of external girders by up to 39%.
    - The rigid method overpredicts distribution factors of external girders by up to 25%.
    - This overestimation of DF's is likely the cause for excessive camber and overdesigning of bridges.
- Finite element analysis accurately measures distribution factors for bridge girders but is not always accurate at measuring direct deflections. Distribution factors for external girders were underpredicted by as much as 13% and overpredicted by as much as 9% when compared to the load test results. Deflections were overpredicted by up to 57% using this method, showing that there are variables that were not properly accounted for in the model of Span 9.
- Finite element typically underestimated strains by up to 29.9 microstrains in the girder cross-section when compared to measured strains. Curvature derived from strain measurements was typically overestimated in FEA by up to 56% compared to embedded strain gauge data.
- Distribution factors were accurately measured using curvature derived from embedded VWGs, but not from FEA strain measurements from Span 9. This is

likely due to the continuity of the deck across this Span not being accounted for properly in the model.

- Looking into the effects of parapets in diaphragms in FEA, it was shown that:
    - Removing parapets from the model increased the distribution factors of the exterior girder by up to 13%.
    - Removing the diaphragms did not significantly change the distribution factor of the exterior girder and led to an increase by up to 7.3%.
    - When both the parapet and diaphragms were removed, the distribution factor of the external girder increased by up to 16%.
    - The finite element results suggest that the parapets contribute significantly to distribution of loads, while diaphragms minimally distribute loads. No current methods include the effects of parapets in distributing live load, but several methods consider the effects of diaphragms.

4.7.2 Recommendations

- AASHTO methods consistently overpredicted DF's. The rigid method is suggested for analysis as it more closely matched the results of the load test. It is also recommended that multiple presence factors should not be included in analysis for single lane loaded scenarios.
- The results of the finite element analysis show that parapets contribute significantly to load distribution between exterior and interior girders, even though they are not considered in the lever rule or rigid method. From this, it is recommended that future research should investigate the effects of parapets and include this in future methods for determining distribution factors.

CHAPTER V

5 SUMMARY AND CONCLUSIONS

5.1 SUMMARY

This research was performed to provide greater knowledge of concrete bridge construction. Instrument-based structural monitoring was vital in understanding the behavior of the concrete girders. The monitoring program offered insights into how heat of hydration of cement and construction practices affects concrete bridge girders and provided an indirect measurement of prestress losses. This research involved implementing a structural monitoring program, measuring camber, comparing prestress loss prediction models, and static load testing of the SH4 bridge. Through all this, a better understanding of the effects of mild steel reinforcement and distributed strand patterns on camber and prestress loss was formed. Static load testing showed that current practices for determining distribution factors are conservative.

5.2 CONCLUSIONS

5.2.1 Prestress Loss Conclusions

- The AASHTO Refined method found that Case B girders experienced 6.1% less prestress loss than Case A at 500 days.
- The AASHTO Refined method found that Case C girders experienced 4.9% less prestress loss than Case A at 500 days.
- The AASHTO Refined method found that Case D girders experienced 6.7% less prestress loss than Case A at 500 days.
- Comparing strain data to AASHTO refined, the AASHTO Refined overpredicted losses at 110 days for Span 9 by 1.3% and underpredicted losses at 110 days for Span 14 by 8.7%. For losses at 500 days, AASHTO Refined overpredicted losses by 13% for Span 9 and overpredicted losses for Span 14 by 1.6%.
- Comparing strain data to AASHTO Approximate, the AASHTO Approximate method overpredicted losses at 500 days in Span 9 by 29% and overpredicted losses in Span 14 by 16%.
- Comparing strain data to the PCI Design Handbook method, the PCI Design handbook method overpredicted losses at 110 days in Span 9 by 47% and overpredicted losses in Span 14 by 35%. PCI overpredicted losses at 500 days in Span 9 by 32% and overpredicted Span 14 by 19%.
- Comparing strain data to the Modified PCI method, overpredicted losses at 110 days in Span 9 by 45% and overpredicted losses in Span 14 by 35%. This method

also overpredicted losses at 500 days in Span 9 by 32% and overpredicted losses in Span 14 by 21%.

- Comparing strain data to Jayaseelan time step, overpredicted losses at 110 days in Span 9 by 4.5% and underpredicted losses in Span 14 by 14%. Jayaseelan time-step underpredicted losses at 500 days in Span 9 by 0.3% and underpredicted losses in Span 14 by 14%.
- The comparison of prestress loss prediction methods to losses derived from strain measurements show that the AASHTO Refined method and Jayaseelan Time-step method provide the best reference to accurately predicting prestress losses.
- Analysis between predicted and measured elastic shortening loss show that current equations significantly overpredict early age concrete elastic modulus by up to 30%, leading to a underprediction of elastic shortening loss.

5.2.2 Camber Conclusions

- The inclusion of mild steel reinforcement in the bottom flange (Case B) moderately reduced the long-term camber by approximately 0.76 in. (38%) from Case A.
- The distributed strand pattern (Case C) significantly reduced the long-term camber by approximately 1.1 in. (54%) from the Case A.
- Combining mild steel reinforcement in the bottom flange and using a distributed strand pattern (Case D) reduced the long-term camber by approximately 1.2 in. (62%) from Case A.

- The Jayaseelan Time-Step method typically underestimated camber for Case A girders by an average of 0.21 in. (Between -4.2 to -13% at all time increments).
- The Jayaseelan Time-Step method typically overestimated camber for Case B girders by 0.11 in. (Between -3.8 to 19% at all time increments).
- The Jayaseelan Time-Step method typically overestimated camber for Case C girders by 0.11 in. (Between 1.2 to 17% at all time increments).
- The Jayaseelan Time-Step method typically overestimated camber for Case D girders by 0.11 in. (Between -0.14 to 25% at all time increments).
- The Jayaseelan Time-step method provides a reasonable prediction of camber in prestressed concrete girders.
- Camber was not able to be appropriately measured with strain readings. However, it can be a valuable tool in assessing performance of a bridge and should be utilized in future structural monitoring programs.

5.2.3 Distribution Factor Conclusions

- AASHTO prescribed methods overestimate the distribution factors for bridge girders.
    - The lever rule overpredicted distribution factors of external girders by up to 39%.
    - The rigid method overpredicts distribution factors of external girders by up to 25%.
    - This overestimation of DF's is likely the cause for excessive camber and overdesigning of bridges.

- Finite element analysis accurately measures distribution factors for bridge girders but is not always accurate at measuring direct deflections. Distribution factors for external girders were underpredicted by as much as 13% and overpredicted by as much as 13% when compared to the load test results. Deflections were overpredicted by up to 9% using this method, showing that there are variables that were not properly accounted for in the model of Span 9.
- Finite element typically underestimated strains by up to 29.9 microstrains in the girder cross-section when compared to measured strains. Curvature derived from strain measurements was typically overestimated in FEA by up to 56% compared to embedded strain gauge data.
- Distribution factors were accurately measured using curvature derived from embedded VWGs, but not from FEA strain measurements from Span 9. This is likely due to the continuity of the deck across this Span not being accounted for properly in the model.
- Looking into the effects of parapets in diaphragms in FEA, it was shown that:
    - Removing parapets from the model increased the distribution factors of the exterior girder by up to 13%.
    - Removing the diaphragms did not significantly change the distribution factor of the exterior girder and led to an increase by up to 7.3%.
    - When both the parapet and diaphragms were removed, the distribution factor of the external girder increased by up to 16%.
    - The finite element results suggest that the parapets contribute significantly to distribution of loads, while diaphragms minimally distribute loads. No

current methods include the effects of parapets in distributing live load, but several methods consider the effects of diaphragms.

5.2.4 Recommendations

- Implementing mild steel reinforcing into the bottom flanges of prestressed concrete girders or using a distributed strand pattern in the design of pretensioned girder bridges is recommended. This will significantly decrease camber and slightly decrease prestress losses without significantly increasing fabrication cost or time. Combining both mild reinforcing and a distributed strand pattern further reduced camber and prestress losses and is recommended if viable.
    - Including 2.4 in^2 of mild reinforcement can significantly reduce camber by up to 38% and reduces prestress losses by about 6%.
    - Limiting prestress moment by using a distributed strand pattern can limit camber by up to 54% and reduce prestress losses by up to 5%.
    - Combining both mild reinforcement and distributed strand patterns can limit camber by up to 62% and reduce prestress losses by up to 7%.
- The AASHTO Refined method and Jayaseelan Time-step method provide accurate predictions of prestress losses. They are both recommended for use in design and the Jayaseelan Time-step method provides accurate prediction of camber for these types of girders.
- AASHTO methods consistently overpredicted DF's. The rigid method is suggested for analysis as it more closely matched the results of the load test. It is

also recommended that multiple presence factors should not be included in analysis for single lane loaded scenarios.

- The results of the finite element analysis show that parapets contribute significantly to load distribution between exterior and interior girders, even though they are not considered in the lever rule or rigid method. From this, it is recommended that future research should investigate the effects of parapets and include this in future methods for determining distribution factors.

REFERENCES

[1] ACI (American Concrete Institute). (1992). Prediction of creep, shrinkage, and temperature effects in concrete structures. ACI 209R-92

[2] ACI (American Concrete Institute). (2010). Report on high-strength concrete (ACI 363R-10).

[3] Almohammedi, A., Murray, C. D., Dang, C. N., & Hale, W. M. (2021). Investigation of measured prestress losses compared with design prestress losses in AASHTO Types II, III, IV, and VI bridge girders. PCI Journal, 66(3).

[4] American Association of State Highway and Transportation Officials. (2020). *AASHTO LRFD bridge construction specifications* (9th ed.). American Association of State Highway and Transportation Officials.

[5] Baran, E., Shield, C. K., & French, C. E. (2005). A comparison of methods for experimentally determining prestress losses in pretensioned prestressed concrete girders. *Special Publication, 231*, 161-180.

[6] Barr, P. J., Eberhard, M. O., & Stanton, J. F. (2001). Live-load distribution factors in prestressed concrete girder bridges. *Journal of Bridge Engineering, 6*(5), 298-306.

[7] Brinckerhoff, P. (2005). A context for common historic bridge types. *Engineering and Industrial Heritage, NCHRP Project*, 25-25.

[8] Conner, S., & Huo, X. S. (2006). Influence of parapets and aspect ratio on live-load distribution. *Journal of Bridge Engineering, 11*(2), 188-196.

[9] Cousins, T. E., & Gomez, J. (2005). Investigation of long-term prestress losses in pretensioned high performance concrete girders (No. FHWA/VTRC 05-CR20). Virginia Transportation Research Council.

[10] Cousins, T. E., Stallings, J. M., & Simmons, M. B. (1994). Reduced strand spacing in pretensioned, prestressed members. *Structural Journal, 91*(3), 277-286.

[11] Dong, C., Bas, S., Debees, M., Alver, N., & Catbas, F. N. (2020). Bridge load testing for identifying live load distribution, load rating, serviceability and dynamic response. *Frontiers in Built Environment, 6*, 46.

[12] French, C. E., & O'Neill, C. (2012). Validation of prestressed concrete I-beam deflection and camber estimates. *MnDOT (Minnesota Department of Transportation) final report, 16*.

[13] Hale, W. M., & Russell, B. W. (2006). Effect of allowable compressive stress at release on prestress losses and on the performance of precast, prestressed concrete bridge girders. *PCI Journal, 51*(2). g

[14] Hassanain, M. A., & Loov, R. E. (1999). Design of prestressed girder bridges using high performance concrete-an optimization approach. *PCI Journal, 44*(2).

[15] Jayaseelan, H., & Russell, B. W. (2019). Reducing cambers and prestress losses by including fully tensioned top prestressing strands and mild reinforcing steel. *PCI Journal, 51*(2).

[16] Kelly, D. J., Bradberry, T. E., & Breen, J. E. (1987). *Time dependent deflections of pretensioned beams*.

[17] Kizilarslan, E., Okumus, P., & Oliva, M. G. (2020). Debonding strands as an anchorage zone crack control method for pretensioned concrete bulb-tee girders. *PCI Journal, 65*(5).

[18] Lin, C., & VanHorn, D. (1968). The effect of midspan diaphragms on load distribution in a prestressed concrete box-beam bridge-philadelphia bridge, June 1968.

[19] Mante, D. M., Barnes, R. W., Isbiliroglu, L., Hofrichter, A., & Schindler, A. K. (2019). Effective Strategies for Improving Camber Predictions in Precast, Prestressed Concrete Bridge Girders. *Transportation Research Record, 2673(3)*, 342-354. https://doi.org/10.1177/0361198119833965

[20] Martin, L. D., Perry, C. J., & Precast/Prestressed Concrete Institute. (2004). *PCI design handbook*: precast and prestressed concrete (6th ed.). Precast/Prestressed Concrete Institute.

[21] Naaman, A. E., Siriaksorn, A., Hill, A. W., Rao, A. P., Rajagopalan, K., & Tam, A. (1979). Serviceability based design of partially prestressed beams. *PCI Journal, 24*(2), 64-89.

[22] Roberts-Wollmann, C. L., Arrellaga, J. A., Breen, J. E., & Kreger, M. E. (1996). Field measurements of prestress losses in external tendons. *Structural Journal, 93*(5), 595-601.

[23] Russell, B. W. (2018). *Using Fully Bonded Top Strands in Pretensioned Concrete Bridge Girders. ASPIRE Summer*, *2018*, 26-28.

[24] Stallings, J. M., Barnes, R. W., & Eskildsen, S. (2003). Camber and prestress losses in Alabama HPC bridge girders. *PCI Journal, 48*(5), 90-104.

[25] Storm, T., Rizkalla, S. H., & Zia, P. (2013). Effects of Production Practices on Camber of Prestressed Concrete Bridge Girders. *PCI Journal, 58*, 96-111.

[26] Tadros, M., Al-Omaishi, N., Seguirant, S., & Gallt, J. (2003). NCHRP Report 496: Prestress losses in pretensioned high-strength concrete bridge girders. *Transportation Research Board, Washington DC, 63.*

[27] Tadros, M. K., Fawzy, F. F., & Hanna, K. E. (2011). Precast, prestressed girder camber variability. *PCI Journal, 56*, 135-154.

[28] Tadros, M. K., Ghali, A., & Meyer, A. W. (1985). Prestressed loss and deflection of precast concrete members. *PCI Journal, 30*(1), 114-141.

[29] Tawadrous, R., Morcous, G., & Maguire, M. (2019). Performance Evaluation of a New Precast Concrete Bridge Deck System. *Journal of Bridge Engineering, 24*(6), 04019051. https://doi.org/doi:10.1061/(ASCE)BE.1943-5592.0001422

[30] Zia, P., Preston, H. K., Scott, N. L., & Workman, E. B. (1979). Estimating prestress losses. *Concrete International, 1*(6), 32-38.

6 APPENDICIES

6.1 APPENDIX A: CONCRETE MATERIAL PROPERTIES

Table 24: ODOT Specifications for Class AA and Class P mixture proportions.

	ODOT Requirements for Class P Concrete (Girders)	ODOT Requirements for Class AA Concrete (Deck Placement)
Minimum Cement Content (PCY)	564	564
Total Air Content (%)	5.0±1.5	6.5±1.5
Water to Cementitious Materials Ratio (w/cm)	0.25-0.44	0.25-0.44
Slump (in.)	3.0±1.0	2.0±1.0
Minimum Compressive Strength at Prestress Release (psi)	7000	n.a.
Minimum Compressive Strength at 28 days (psi)	10,000	4,000
Note: Class P concrete is used for prestressed concrete bridge girders Class AA concrete is required for concrete decks		

Table 25: Fresh concrete properties, Beam Mark 27, Span 9.

Beam Mark 27, Span 9	
Spread (ASTM C1611) (in):	**20.6**
Air Content (ASTM C231) (%):	**5.0**
Air Temperature (°F):	**92.8**
Unit Weight (ASTM C138) (lb/ft3):	**135**

Table 26: Hardened concrete properties, Beam Mark 27, Span 9.

Beam Mark 27, Span 9						
Concrete Compressive Strength (ASTM C39, psi)						
Day	**3**	**14**	**28**	**90**	**184**	**365**
Cylinder 1	8,930	9,300	10,840	12,300	10,800	13,300
Cylinder 2	8,580	10,150	10,780	10,700	10,700	13,100
Mean	8,760	9,730	10,810	11,500	10,750	13,200
Stdev	250	600	40	1,130	70	140
Splitting Cylinder Tensile Strength (ASTM C496, ksi)						
Day	**3**	**14**	**28**	**90**	**184**	**365**
Cylinder 1	0.57	-	0.74	0.69	0.85	0.63
Cylinder 2	0.60	-	0.69	0.81	0.78	0.64
Mean	0.59	-	0.72	0.75	0.82	0.64
Stdev	0.02	-	0.04	0.08	0.05	0.01
Concrete Elastic Modulus (ASTM C469, ksi)						
Day	**3**	**14**	**28**	**90**	**184**	**365**
Cylinder 1	3,600	-	3,710	4,880	-	-
Cylinder 2	4,590	-	4,570	5,060	-	-
Mean	4,090	-	4,140	4,970	-	-
Stdev	700	-	610	130	-	-

Table 27: Fresh concrete properties, Beam Mark 42, Span 14.

Beam Mark 42, Span 14	
Spread (ASTM C1611) (in):	20.6
Air Content (ASTM C231) (%):	3.6
Conc. Temp. (°F):	72
Air Temperature (°F):	92.8
Unit Weight (ASTM C138) (lb/ft3):	143.4

Table 28: Hardened concrete properties, Beam Mark 42, Span 14.

Beam Mark 42, Span 14						
Concrete Compressive Strength (ASTM C39, psi)						
Day	**3**	**14**	**28**	**90**	**184**	**365**
Cylinder 1	8,660	9,630	10,090	11,700	11,800	12,600
Cylinder 2	9,270	10,080	10,890	12,100	12,000	12,600
Mean	8,970	9,860	10,490	11,900	11,900	12,600
Stdev	430	320	570	280	140	0
Splitting Cylinder Tensile Strength (ASTM C496, ksi)						
Day	**3**	**14**	**28**	**90**	**184**	**365**
Cylinder 1	0.56	-	0.71	0.74	0.68	0.63
Cylinder 2	0.66	-	0.60	0.63	0.72	0.63
Mean	0.61	-	0.66	0.69	0.70	0.63
Stdev	0.07	-	0.08	0.08	0.03	0.00
Concrete Elastic Modulus (ASTM C469, ksi)						
Day	**3**	**14**	**28**	**90**	**184**	**365**
Cylinder 1	1,580	-	5,020	3,710	-	-
Cylinder 2	4,570	-	4,670	4,080	-	-
Mean	4,570	-	4,850	3,890	-	-
Stdev	2,120	-	250	260	-	-

Table 29: Fresh properties of concrete deck, Span 9.

Span 9 Deck			
Job Site Truck #	**Slump (ASTM C143) (in)**	**Unit Weight (ASTM C138) (lb/ft3):**	**Air Content (ASTM C231) (%):**
1	6	141	6.5
4	2	136	7.5
8	4	142	7.6
11	7	139	7.2
Mean	5	139	7.2
Stdev	2	2.53	0.50

Table 30: Hardened properties of concrete deck, Span 9.

Span 9 Deck						
Concrete Compressive Strength (ASTM C39, psi)						
Day	**3**	**14**	**28**	**90**	**184**	**365**
Cylinder 1	4,840	5,270	5,700	6,980	8,100	8,640
Cylinder 2	4,650	5,161	6,973	7,040	7,800	6,600
Mean	4,750	5,220	6,340	7,010	7,950	7,620
Stdev	130	80	900	40	210	1,440
Splitting Cylinder Tensile Strength (ASTM C496, ksi)						
Day	**3**	**14**	**28**	**90**	**184**	**365**
Cylinder 1	0.48	0.47	0.59	0.49	0.44	0.60
Cylinder 2	0.40	0.51	0.35	0.51	0.44	0.60
Mean	0.44	0.49	0.47	0.50	0.44	0.60
Stdev	0.06	0.03	0.17	0.01	0	0
Concrete Elastic Modulus (ASTM C469, ksi)						
Day	**3**	**14**	**28**	**90**	**184**	**365**
Cylinder 1	3,480	-	-	-	-	-
Cylinder 2	1,130	-	-	-	-	-
Mean	2,310	-	-	-	-	-
Stdev	1,660	-	-	-	-	-

Table 31: Fresh properties of concrete deck, Span 14.

Span 14 Deck			
Job Site Truck #	**Slump (ASTM C143) (in)**	**Unit Weight (ASTM C138) (lb/ft3):**	**Air Content (ASTM C231) (%):**
1	3	181	7.5
4	5.5	142	6.5
8	7	136	6.3
11	7.75	141	6.6
Mean	5.8	150	6.7
Stdev	2.1	20.8	0.53

Table 32: Hardened properties of concrete deck, Span 14.

Span 14 Deck						
Concrete Compressive Strength (ASTM C39, psi)						
Day	**3**	**14**	**28**	**90**	**184**	**365**
Cylinder 1	4,450	5,630	5,150	6,160	6,700	6,190
Cylinder 2	3,540	5,010	5,260	6,140	6,280	6,380
Mean	4,000	5,320	5,210	6,150	6,490	6,290
Stdev	640	440	80	10	300	130
Splitting Cylinder Tensile Strength (ASTM C496, ksi)						
Day	**3**	**14**	**28**	**90**	**184**	**365**
Cylinder 1	0.35	0.25	0.25	0.63	0.49	0.54
Cylinder 2	0.46	0.25	0.4	0.44	0.49	0.59
Mean	0.41	0.25	0.33	0.54	0.49	0.57
Stdev	0.08	0	0.11	0.13	0	0.04
Concrete Elastic Modulus (ASTM C469, ksi)						
Day	**3**	**14**	**28**	**90**	**184**	**365**
Cylinder 1	3,820	-	-	-	-	-
Cylinder 2	3,750	-	-	-	-	-
Mean	3,750	-	-	-	-	-
Stdev	60	-	-	-	-	-

6.2 APPENDIX B: CALCULATION OF PRESTRESS LOSSES

6.2.1 Appendix B1: AASHTO Approximate Method

$\Delta f_{pT} = \Delta f_{pES} + \Delta f_{pLT}$ (AASHTO 2020 5.9.3.1-1)

Where:

Δf_{pT} = Total loss (ksi)

Elastic shortening loss:

$\Delta f_{pES} = \frac{E_p}{E_{ct}} f_{cgp}$ (AASHTO 2020 5.9.3.2.3a-1)

Where:

E_p = Modulus of Elasticity of the prestressing strands.

E_{ct} = Compressive Modulus of Elasticity of the concrete at transfer.

$f_{cgp} = \frac{P_{pt}}{A_g} + \frac{P_{pt} e_c^2}{I_g} - \frac{M_g e_c}{I_g}$

f_{cgp} = Concrete stress at the center of gravity of prestressing tendons due to the prestressing force immediately after transfer and the self-weight of the member at the section of maximum moment. For the approximate method, the gross section properties were used. Details on how to calculate f_{cgp} using transformed section properties are discussed in the AASHTO Refined section.

P_{pt} = Total prestressing force after transfer.

A_g = Gross cross-sectional area.

e_c = Eccentricity of prestresssing strands at midspan.

I_g = Gross moment of interia.

The modulus of elasticity of concrete, E_{ci}, was estimated using the equation given in AASHTO 2020 LRFD Specifications and Commentary.

$E_c = 120{,}000K_1 w_c^2 f'^{0.33}_c$ (AASHTO 2020 5.4.2.4-1)

Where:

K_1 = Correction factor for the source of aggregate, taken as 1.0. Can be modified if testing of the source aggregate is performed.

w_c = Unit Weight of concrete, taken as 0.15 kcf.

f'_c = Compressive strength of concrete for use in design, specified at 10 ksi.

The long-term prestress losses due to creep of concrete, shrinkage of concrete, and relaxation of prestressing strands are estimated using the following formula:

$\Delta f_{pLT} = 10.0 \frac{f_{pi} A_{ps}}{A_g} \gamma_h \gamma_{st} + 12.0 \gamma_h \gamma_{st} + \Delta f_{pR}$ (AASHTO 2020 5.9.3.3-1)

Where:

$\gamma_h = 1.7 - 0.01H$ (AASHTO 2020 5.9.3.3-2)

$\gamma_{st} = \frac{5}{1 + f'_{ci}}$ (AASHTO 2020 5.9.3.3-3)

γ_h = Correction factor for relative humidity of ambient air.

γ_{st} = Correction factor for specified concrete strength at all times of prestress transfer to the concrete member.

f_{pi} = Stress in prestressing steel immediately prior to transfer (202.5 ksi).

H = Average annual ambient relative humidity, taken 65% for Oklahoma.

Δf_{pR} = An estimate of relaxation loss, taken as 2.4 ksi for low relaxation strand.

6.2.2 Appendix B2: AASHTO Refined Method

Elastic shortening:

$\Delta f_{pES} = \frac{E_p}{E_{ci}} f_{cgp}$ (AASHTO 2020 5.9.3.2.3a-1)

Where:

E_p = modulus of elasticity of prestressing steel (ksi).

E_{ci} =modulus of elasticity of concrete at transfer (ksi).

$f_{cgp} = \frac{P_{pi}}{A_{ti}} + \frac{P_{pi} e_{ti}^2}{I_{ti}} - \frac{M_g e_{ti}}{I_{ti}}$

f_{cgp} = Sum of concrete stresses at the center of gravity of prestressing strands due to prestressing force at transfer and the self-weight of the member. f_{cgp} was modified to use transformed section properties.

P_{pi} = Total prestressing force before transfer.

A_{ti} = Area of transformed section at transfer.

e_{ti} = Eccentricity of strands with respect to the transformed section at transfer.

I_{ti} = Moment of inertia of transformed section at transfer.

M_g = Unfactored bending moment due to self-weight.

Calculations of long-term losses are provided in equation 5.9.3.4.1-1.

$$\Delta f_{pLT} = \left(\Delta f_{pSR} + \Delta f_{pCR} + \Delta f_{pR1}\right)_{id} +$$

$$\left(\Delta f_{pSD} + \Delta f_{pCD} + \Delta f_{pR2} - \Delta f_{pSS}\right)_{df}$$ (AASHTO 2020 5.9.3.4.1-1)

Where:

Δf_{pLT} = Change in prestressing steel stress due to time-dependent loss.

Δf_{pSR} = Prestress loss due to shrinkage of girder concrete between transfer and deck placement (ksi).

Δf_{pCR} = Prestress loss due to creep of the girder concrete between transfer and deck placement (ksi).

Δf_{pR1} = Prestress loss due to relaxation of prestressing strands between transfer and deck placement (ksi).

Δf_{pSD} = Prestress loss due to shrinkage of girder concrete between time of deck placement and final time (ksi).

Δf_{pCD} = Prestress loss due to creep of girder concrete between time of deck placement and final time (ksi).

Δf_{pR2} = Prestress loss due to relaxation of prestressing strands in the composite section between time of deck placement and final time (ksi).

Δf_{pSS} = Prestress gain due to shrinkage of deck in composite section between time of deck placement and final time (ksi).

$\left(\Delta f_{pSR} + \Delta f_{pCR} + \Delta f_{pR1}\right)_{id}$ = Sum of time-dependent prestress losses between transfer and deck placement (ksi).

$\left(\Delta f_{pSD} + \Delta f_{pCD} + \Delta f_{pR2} - \Delta f_{pSS}\right)_{df}$ = Sum of time-dependent prestress losses after deck placement (ksi).

The following section goes over the calculation of prestress losses before placement of the deck.

Shrinkage of girder concrete:

$\Delta f_{pSR} = \varepsilon_{bid} E_P K_{id}$ (AASHTO 2020 5.9.3.4.2a-1)

Where:

$\varepsilon_{bid} = k_s k_{hs} k_f k_{td} 0.48 * 10^{-3}$ (AASHTO 2020 5.4.2.3.3-1)

$$K_{id} = \frac{1}{1+\frac{E_P A_{ps}}{E_{ci} A_g}\left(1+\frac{A_g e_{ps}^2}{I_g}\right)[1+0.7\psi_b(t_f,t_i)]}$$ (AASHTO 2020 5.9.3.4.2a-2)

$$\psi_b(t_f,t_i) = 1.9 k_s k_{hc} k_f k_{td} t_i^{-0.118}$$ (AASHTO 2020 5.4.2.3.2-1)

ε_{bid} = Concrete shrinkage strain of girder between the time of transfer and deck placement per (AASHTO 2020 5.4.2.3.3-1) (in/in).

E_P = Modulus of elasticity of prestressing steel (ksi).

K_{id} = Transformed section coefficient that accounts for time-dependent interaction between concrete and bonded steel in the section being considered for the time period between transfer and deck placement.

e_{pg} = Eccentricity of prestressing force with respect to the centroid of girder (in.); positive in standard construction where it is below girder centroid.

$\psi_b(t_f,t_i)$ = Girder creep coefficient at final time due to loading introduced at transfer per (AASHTO 2020 5.4.2.3.2-1).

t_f = Final age (day).

t_i = Age of concrete at time of transfer (day).

Creep of girder concrete:

$$\Delta f_{pCR} = \frac{E_P}{E_{ci}} f_{cgp} \psi_b(t_d,t_i) K_{id}$$ (AASHTO 2020 5.9.3.4.2b-1)

Where:

$\psi_b(t_d, t_i)$ = Girder creep coefficient at time of deck placement due to loading introduced at transfer per (AASHTO 5.4.2.3.2-1).

t_d = Age at deck placement (day).

Relaxation of prestressing strands is computed as follows:

$\Delta f_{pR1} = \frac{f_{pt}}{K_L}\left(\frac{f_{pt}}{f_{py}} - 0.55\right)$ (AASHTO 2020 5.9.3.4.2c-1)

Where:

f_{pt}= Stress in prestressing strands immediately after transfer, taken as not less than $0.55f_{py}$

K_L= Factor accounting for the type of steel, taken as 30 for low relaxation strands

Alternatively, Δf_{pR1} can be simplified to 1.2 ksi if low relaxation strands are used.

The following covers calculation of prestress losses after placement of deck.

Shrinkage of girder concrete:

$\Delta f_{pSD} = \varepsilon_{bdf} E_P K_{df}$ (AASHTO 2020 5.9.3.4.2a-1)

Where:

$K_{df} = \frac{1}{1+\frac{E_P A_{ps}}{E_{ci} A_c}\left(1+\frac{A_c e_{pc}^2}{I_c}\right)[1+0.7\psi_b(t_f, t_i)]}$ (AASHTO 2020 5.9.3.4.2a-2)

ε_{bdf} = Shrinkage strain of girder between the time of deck placement and final time (in/in).

K_{df} = Transformed section coefficient that accounts for time-dependent interaction between concrete and bonded steel in the section being considered for the time period between deck placement and final time.

e_{pg} = Eccentricity of prestressing force with respect to centroid of girder (in.); positive in common construction where it is below girder centroid.

$\psi_b(t_f, t_i)$ = Girder creep coefficient at final time due to loading introduced at transfer per (AASHTO 2020 5.4.2.3.2-1).

t_f = final age (day).

t_i = Age of concrete at time of transfer (day).

Creep of girder concrete:

$\Delta f_{pCD} = \frac{E_p}{E_{ci}} f_{cgp}[\psi_b(t_f, t_i) - \psi_b(t_d, t_i)]K_{df} + \frac{E_p}{E_c}\Delta f_{cd}\psi_b(t_f, t_d)K_{df}$ (AASHTO 5.9.3.4.3b-1)

Where:

Δf_{cd} = change in concrete stress at centroid of prestressing strands due to long-term losses between transfer and deck placement, combined with deck weight and superimposed loads (ksi).

$\psi_b(t_f, t_d)$ = Girder creep coefficient at final time due to loading at deck placement per (AASHTO 2020 5.4.2.3.2-1).

Relaxation:

Relaxation of prestressing strands after the deck casting is equivalent to relaxation of prestressing strands before deck casting.

$\Delta f_{pR2} = \Delta f_{pR1}$ (AASHTO 2020 5.9.3.4.3c-1)

Shrinkage of deck concrete:

Shrinkage of deck concrete typically causes a prestress gain due to the disproportionate shrinkage of the deck relative to the girder.

$$\Delta f_{pSS} = \frac{E_P}{E_c} \Delta f_{cdf} K_{df} \left[1 + 0.7\psi_b\left(t_f, t_d\right)\right]$$

$\Delta f_{cdf} = \frac{\varepsilon_{ddf} A_d E_{c\,deck}}{\left[1+0.7\psi_d\left(t_f,t_d\right)\right]} \left(\frac{1}{A_c} - \frac{e_{pc} e_d}{I_c}\right)$ (AASHTO 2020 5.9.3.4.3d-2)

Δf_{cdf} = Change in concrete stress at centroid of prestressing strands due to shrinkage of deck concrete (ksi).

ε_{ddf} = Shrinkage strain of deck concrete between placement and final time as per (AASHTO 5.4.2.3.3-1) (in/in).

A_d = area of deck concrete (in^2).

$E_{c\,deck}$ = Modulus of elasticity of deck concrete (ksi).

$\psi_b(t_f, t_d)$ = Girder creep coefficient at final time due to loading at deck placement per (AASHTO 2020 5.4.2.3.2-1).

$\psi_b(t_f, t_d)$ = Creep coefficient of deck concrete at final time due to loading introduced shortly after deck placement per (AASHTO 2020 5.4.2.3.2-1).

e_d = Eccentricity of the deck with respect to the gross composite section, positive in typical construction where the deck is above the girder (in).

6.2.3 Appendix B3: PCI Design Handbook Methods

Modulus of elasticity was calculated using the equation 6-1 provided in ACI Committee 363R-10 [2]

$E_c = 40000\sqrt{f'_c} + 1 \times 10^6 psi$ (ACI 363R-10 6-1)

For:

$$3000\ psi < f'_c < 12{,}000\ psi$$

w = Unit weight of concrete in lb/ft^3, taken as 150.

The total losses can be computed using the following equation:

$TL = ES + CR + SH + RE$ (PCI 4.7.3.1)

Where:

TL = Total Losses.

ES = Elastic Shortening.

SH = Shrinkage of Concrete.

CR = Creep of Concrete.

The elastic shortening losses can be computed using this equation:

$$ES = \frac{K_{es}E_{ps}f_{cir}}{E_{ci}} \qquad \text{(PCI 4.7.3.2)}$$

Where:

$$f_{cir} = K_{cir}\left(\frac{P_i}{A_g} + \frac{P_i e^2}{I_g}\right) - \frac{M_g e}{I_g} \text{ (PCI 4.7.3.3)}$$

K_{cir} = 0.9 for pretensioned members.

K_{es} = 1.0 for pretensioned members.

E_{ps} = Modulus of Elasticity of the prestressing strands.

e = Eccentricity of the center of gravity of tendons with respect to the center of gravity of concrete at the cross-section considered.

M_g = Bending moment due to self-weight of the prestressed member.

I_g = Moment of inertia of gross concrete section of the cross-section considered.

The creep of the concrete can be computed using the following equation:

$$CR = K_{cr}(E_{ps}/E_c)(f_{cir} - f_{cds}) \qquad \text{(PCI 4.7.3.4)}$$

Where:

$$f_{cds} = \frac{M_{cds} \times e}{I_g} \text{ (PCI 4.7.3.5)}$$

M_{cds} = Moment due to all superimposed dead loads applied after prestressing.

K_{cr} = 2, for normal-weight concrete.

The prestress losses due to the shrinkage of concrete can be computed using the following equation:

$SH = 8.2 \times 10^{-6} \times K_{sh} E_{ps} (1 - 0.06 \frac{V}{S}) \times (100 - RH)$ (PCI 4.7.3.6)

Where:

K_{sh} = 1.0 for pretensioned members.

RH = Average ambient relative humidity taken as 65%.

Relaxation of prestressing strands is calculated with the following equation:

$RE = [K_{re} - J(SH + CR + ES)]C$ (PCI 4.7.3.7)

Where:

K_{re} = 5,000 for grade 270 low-relaxation strands, found in table 4.7.3.1

J = 0.040 for grade 270 low-relaxation strands, found in table 4.7.3.1

C = 1, from table 4.7.3.2

6.2.4 Appendix B4: Jayaseelan Time-step Method

This method estimates concrete compressive strength, f'_c, at a specific concrete age using ACI 209R-92 [1] Eq. (2-1):

$(f'_c)_t = \frac{t}{\alpha + \beta t} (f'_c)_{28}$ (ACI 209R 2-1)

Where:

α = 0.7 for Type III cement.

β = 0.98 for steam cured concrete.

f'_c = Specified 28-day compressive strength of concrete.

This method uses AASHTO LRFD [4] specifications for determining the creep coefficient, $\psi(t, t_i)$, and shrinkage strain, ε_{sh}.

Creep:

$\psi(t, t_i) = 1.9 k_s k_{hc} k_f k_{td} t_i^{-0.118}$ (AASHTO 2020 5.4.2.3.2-1)

Where:

$k_s = 2.45 - 0.13(V/S) \geq 1.0$ (AASHTO 2020 5.4.2.3.2-2)

$k_{hc} = 1.56 - 0.008H$ (AASHTO 2020 5.4.2.3.2-3)

$k_f = \frac{5}{1+f'_{ci}}$ (AASHTO 2020 5.4.2.3.2-4)

$k_{td} = \frac{t}{61+4f'_{ci}+t}$ (AASHTO 5.4.2.3.2-5)

Note that the equation for k_{td} has been modified in the 2020 addition of AASHTO LRFD. For purposes of this paper, the original procedure was kept the same.

K_s = Factor for the effect of volume to surface ratio (V/S).

k_{hc} = Humidity factor for creep.

k_f = Adjustment factor for concrete compressive strength.

H = Relative humidity.

V/S = Volume to surface ratio.

f'_{ci} = Specified concrete compressive strength at release.

Shrinkage:

$\varepsilon_{sh} = k_s k_{hs} k_f k_{td} 0.48 * 10^{-3}$ (AASHTO 2020 5.4.2.3.3-1)

Where:

$k_{hs} = 2.00 - 0.014H$ (AASHTO 2020 5.4.2.3.3-2)

k_{hs} = Humidity factor for shrinkage.

Elastic shortening loss:

$$ES = \frac{E_{ps}}{E_{cr}} f_{cgp}$$

Where:

$$f_{cgp} = \left[P_{pi} - A_{ps}(SH + RE)\right] \times \left[\frac{1}{A_{tr}} + \frac{e_{tr}^2}{I_{tr}}\right] - \left[\frac{M_{SW} \times e_{tr}}{I_{tr}}\right]$$

E_{cr} = Modulus of elasticity of concrete at transfer or time of load application.

f_{cgp} = Stress in concrete at the center of gravity of prestressing tendons due to the prestressing force immediately after transfer and self-weight of the member at the section of maximum moment.

A_{tr} = Transformed cross-sectional area.

e_{tr} = Eccentricity of prestressing strands calculated using transformed cross-section properties.

I_{tr} = Transformed moment of inertia of the section.

M_{SW} = moment due to self-weight of the girder.

Creep:

$$CR(t) = CR(t-1) + \Delta\varepsilon_{cr}(t)E_{ps}$$

Where:

$$\Delta\varepsilon_{cr}(t) = \frac{1}{E_c(t)} f_{cgp}[\psi(t,1) - \psi(t-1,1)]$$

$\Delta\varepsilon_{cr}(t)$ = Incremental creep strain at time t.

Shrinkage loss:

$$SH(t) = E_{ps}\varepsilon_{sh}(t)K_{sht}$$

Where:

$$K_{sht} = \frac{\left(\frac{1}{A_{tr}} + \frac{e_{tr}^2}{I_{tr}}\right)}{\left(\frac{1}{A_g} + \frac{e_g^2}{I_g}\right)}$$

K_{sht} = Transformed cross-section coefficient that accounts for the time-dependent interaction between concrete and prestressing steel.

A_g = Gross cross-sectional area.

e_g = Eccentricity of the prestressing strands calculated using gross cross-section properties.

I_g = Gross moment of inertia of the cross-section.

Relaxation loss:

$$RE(t) = \left[\frac{f_{pt}}{K'_L}\frac{\log(24t+1)}{\log(24t_i+1)}\left(\frac{f_{pt}}{f_{py}} - 0.55\right)\right]\left[1 - \frac{3\big(SH(t)+CR(t)\big)}{f_{pt}}\right]$$

Where:

f_{pt} = Initial prestress in prestressing strands immediately after transfer.

f_{py} = Specified yield strength of prestressing steel.

K'_L = Factor accounting for the type of prestressing steel used, 45 for low relaxation strands.

Total loss:

$$TL = ES + CR(t) + SH(t) + RE(t)$$

Table 33: Prestress losses calculated at midspan using Jayaseelan Time-step method at significant events.

Prestress losses at midspan calculated with the Jayaseelan time-step method							
CASE	**Significant Event**	**Concrete age, days**	**ES, ksi**	**CR, ksi**	**SH, ksi**	**RE, ksi**	**Losses at midspan, ksi**
A	Placement	35	21.5	8.3	3.6	0.9	34.3
	Prior to Deck Casting	110	21.5	12.2	5.4	1.1	40.2
	After Deck Casting	111	21.5	7.5	5.3	1.3	35.6
	In service	500	21.5	8.93	6.5	1.6	38.53
B	Placement	35	19.7	7.6	3.5	1	31.8
	Prior to Deck Casting	110	19.7	11.1	5.3	1.2	37.3
	After Deck Casting	111	19.7	6.88	5.2	1.3	33.08
	In service	500	19.7	8.2	6.3	1.7	35.9
C	Placement	35	19.5	7.5	3.6	1	31.6
	Prior to Deck Casting	110	19.5	11.1	5.4	1.2	37.2
	After Deck Casting	111	19.5	6.7	5.4	1.3	32.9
	In service	500	19.5	8	6.5	1.7	35.7
D	Placement	35	19	7.3	3.5	1.1	30.9
	Prior to Deck Casting	110	19	10.8	5.3	1.3	36.4
	After Deck Casting	111	19	6.5	5.2	1.4	32.1
	In service	500	19	7.7	6.3	1.7	34.7
Note: CR = prestress loss due to creep; ES = prestress loss due to elastic shortening; RE = prestress loss due to relaxation; SH = prestress loss due to shrinkage. 1 ksi = 6.895 MPa.							

6.2.4.1 Appendix B4.1: Jayaseelan Time-step Method with “Case 0” Beam

The following tables and graphs include a “Case 0” that is a recreation of Case A, but excludes fully tensioned top strands. Camber and prestress losses were recomputed with this reinforcement layout.

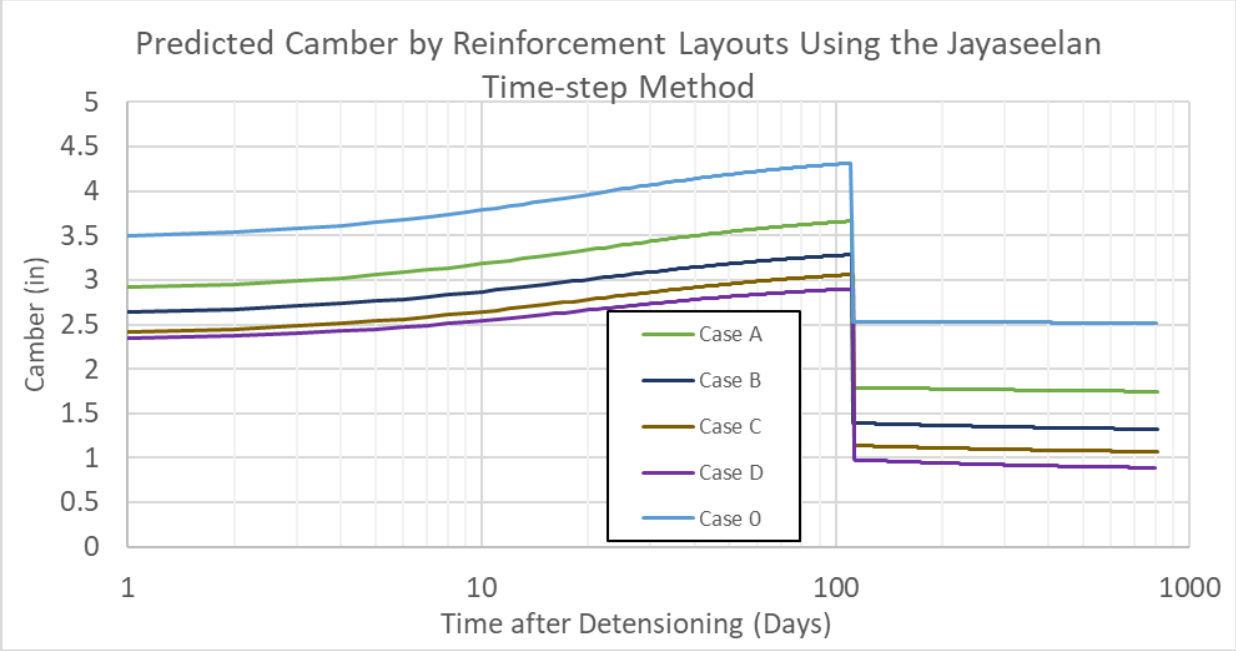

Figure 66: Predicted camber with Jayaseelan Time-step method that include a reinforcement "Case 0" that is a modified version of Case A that doesn’t include top strands.

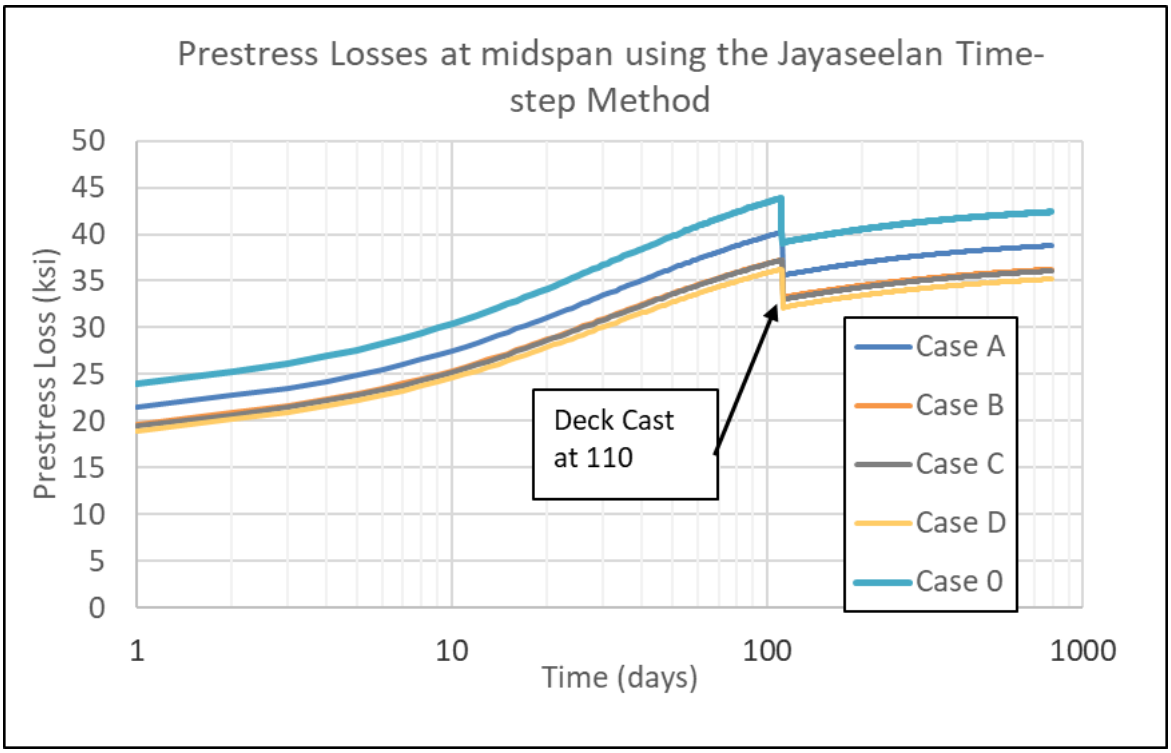

Figure 67: Prestress losses with Jayaseelan Time-step method that include a reinforcement "Case 0" that is a modified version of Case A that doesn't include top strands.

6.3 APPENDIX C: INTERNAL MOMENTS DERIVED FROM MEASURED STRAIN DURING LOAD TESTING AND IN FEA

Table 34: Span 9, Configuration 1 internal moment derived from strain readings.

Span 9 Raw Strain Data, Configuration 1						
Truck Location (ft)	Measurement Location	Sensor Location From Bottom Flange (in)	Unloaded Strain (10^{-6} in/in)	Loaded Strain (10^{-6} in/in)	Strain Caused by Truck Loading (10^{-6} in/in)	Derived Curvature (10^{-6} rad/in)	Internal Moment (kip-ft)
16.7	Strain at 32 in.	44.7	-449	-453	-4.19	0.129	69.1
		24.7	-512	-518	-6.79		
		5.5	-1226	-1225	0.88		
	Strain at midspan	44.7	-1493	-1496	-3.32	0.525	281.0
		24.7	-1296	-1285	11.49		
		5.5	-1355	-1338	17.27		
33.3	Strain at 32 in.	44.7	-449	-454	-5.34	0.114	61.2
		24.7	-512	-519	-7.10		
		5.5	-1226	-1227	-0.86		
	Strain at midspan	44.7	-1493	-1495	-2.04	0.989	529.0
		24.7	-1296	-1274	21.97		
		5.5	-1355	-1319	36.74		
50	Strain at 32 in.	44.7	-449	-455	-5.71	0.094	50.2
		24.7	-512	-519	-7.00		
		5.5	-1226	-1228	-2.04		
	Strain at midspan	44.7	-1493	-1493	-0.02	1.220	652.2
		24.7	-1296	-1268	28.38		
		5.5	-1355	-1308	47.78		
66.7	Strain at 32 in.	44.7	-449	-454	-5.51	0.067	35.8
		24.7	-512	-518	-6.59		
		5.5	-1226	-1229	-2.88		
	Strain at midspan	44.7	-1493	-1494	-1.95	0.823	440.2
		24.7	-1296	-1276	19.77		
		5.5	-1355	-1325	30.31		
83.3	Strain at 32 in.	44.7	-449	-454	-5.01	0.031	16.7
		24.7	-512	-518	-6.03		
		5.5	-1226	-1230	-3.79		
	Strain at midspan	44.7	-1493	-1496	-3.91	0.409	218.6
		24.7	-1296	-1287	9.07		
		5.5	-1355	-1343	12.11		

Table 35: Span 9, Configuration 1 internal moment derived from FEA strain measurements.

Span 9 FEA Strain Data, Configuration 1							
Truck Location (ft)	Measurement Location	Sensor Location From Bottom Flange (in)	Unloaded Strain (10^{-6} in/in)	Loaded Strain (10^{-6} in/in)	Strain Caused by Truck Loading (10^{-6} in/in)	Derived Curvature (10^{-6} rad/in)	Internal Moment (kip-ft)
16.7	Strain at 32 in.	45.6	-86	-87	-0.30	0.132	70.6
		22.5	-294	-298	-4.07		
		4.7	-924	-919	5.10		
	Strain at midspan	45.6	-140	-142	-2.72	0.559	299.0
		22.5	-187	-178	9.87		
		4.7	-236	-216	20.15		
33.3	Strain at 32 in.	45.6	-86	-86	0.12	0.056	30.0
		22.5	-294	-296	-2.54		
		4.7	-924	-922	2.42		
	Strain at midspan	45.6	-140	-146	-6.24	1.190	636.4
		22.5	-187	-167	20.58		
		4.7	-236	-194	42.43		
50	Strain at 32 in.	45.6	-86	-86	0.21	0.012	6.6
		22.5	-294	-295	-1.37		
		4.7	-924	-923	0.72		
	Strain at midspan	45.6	-140	-147	-7.90	1.637	875.5
		22.5	-187	-159	28.30		
		4.7	-236	-177	59.06		
66.7	Strain at 32 in.	45.6	-86	-86	0.16	-0.003	-1.4
		22.5	-294	-295	-0.60		
		4.7	-924	-924	0.05		
	Strain at midspan	45.6	-140	-146	-6.41	1.141	609.9
		22.5	-187	-168	19.33		
		4.7	-236	-196	40.24		
83.3	Strain at 32 in.	45.6	-86	-86	0.07	-0.003	-1.8
		22.5	-294	-294	-0.28		
		4.7	-924	-924	-0.07		
	Strain at midspan	45.6	-140	-142	-2.55	0.509	272.3
		22.5	-187	-179	8.87		
		4.7	-236	-218	18.28		

Table 36: Span 9, Configuration 3 internal moment derived from strain readings.

Span 9 Raw Strain Data, Configuration 3							
Truck Location (ft)	Measurement Location	Sensor Location From Bottom Flange (in)	Unloaded Strain (10^{-6} in/in)	Loaded Strain (10^{-6} in/in)	Strain Caused by Truck Loading (10^{-6} in/in)	Derived Curvature (10^{-6} rad/in)	Internal Moment (kip-ft)
16.7	Strain at 32 in.	44.7	-449	-455	-5.73	0.183	98.1
		24.7	-512	-520	-8.34		
		5.5	-1226	-1224	1.46		
	Strain at midspan	44.7	-1493	-1497	-4.11	0.823	440.2
		24.7	-1296	-1279	17.11		
		5.5	-1355	-1327	28.16		
33.3	Strain at 32 in.	44.7	-449	-456	-6.93	0.161	86.3
		24.7	-512	-521	-9.03		
		5.5	-1226	-1226	-0.60		
	Strain at midspan	44.7	-1493	-1496	-3.05	1.484	793.4
		24.7	-1296	-1265	31.53		
		5.5	-1355	-1300	55.11		
50	Strain at 32 in.	44.7	-449	-456	-7.38	0.132	70.6
		24.7	-512	-521	-9.08		
		5.5	-1226	-1228	-2.20		
	Strain at midspan	44.7	-1493	-1494	-1.32	1.784	953.8
		24.7	-1296	-1257	39.38		
		5.5	-1355	-1287	68.60		
66.7	Strain at 32 in.	44.7	-449	-456	-7.05	0.088	46.9
		24.7	-512	-520	-8.71		
		5.5	-1226	-1229	-3.61		
	Strain at midspan	44.7	-1493	-1496	-3.22	1.246	666.1
		24.7	-1296	-1268	27.92		
		5.5	-1355	-1310	45.60		
83.3	Strain at 32 in.	44.7	-449	-456	-6.63	0.032	17.0
		24.7	-512	-520	-8.20		
		5.5	-1226	-1231	-5.39		
	Strain at midspan	44.7	-1493	-1498	-5.22	0.609	325.9
		24.7	-1296	-1284	12.64		
		5.5	-1355	-1337	18.67		

Table 37: Span 9, Configuration 3 internal moment derived from FEA strain measurements.

Span 9 FEA Strain Data, Configuration 3						
Truck Location (ft)	Measurement Location	Sensor Location From Bottom Flange (in)	Unloaded Strain (10^{-6} in/in)	Loaded Strain (10^{-6} in/in)	Strain Caused by Truck Loading (10^{-6} in/in)	Derived Curvature (10^{-6} rad/in)	Internal Moment (kip-ft)
16.7	Strain at 32 in.	45.6	-86	-87	-0.62	0.184	98.5
		22.5	-294	-299	-4.94		
		4.7	-924	-917	6.91		
	Strain at midspan	45.6	-140	-148	-8.02		
		22.5	-187	-171	16.29	1.048	560.5
		4.7	-236	-201	34.85		
33.3	Strain at 32 in.	45.6	-86	-86	0.14	0.091	48.4
		22.5	-294	-297	-3.25		
		4.7	-924	-920	3.84		
	Strain at midspan	45.6	-140	-162	-22.94		
		22.5	-187	-155	32.91	2.408	1287.6
		4.7	-236	-161	75.53		
50	Strain at 32 in.	45.6	-86	-86	0.36	0.028	14.9
		22.5	-294	-296	-2.27		
		4.7	-924	-923	1.50		
	Strain at midspan	45.6	-140	-168	-28.46		
		22.5	-187	-143	44.47	3.180	1700.5
		4.7	-236	-134	101.60		
66.7	Strain at 32 in.	45.6	-86	-86	0.30	0.005	2.6
		22.5	-294	-295	-1.25		
		4.7	-924	-924	0.50		
	Strain at midspan	45.6	-140	-162	-22.33		
		22.5	-187	-156	31.14	2.305	1232.5
		4.7	-236	-164	71.94		
83.3	Strain at 32 in.	45.6	-86	-86	0.13	0.002	1.2
		22.5	-294	-294	-0.43		
		4.7	-924	-924	0.21		
	Strain at midspan	45.6	-140	-147	-7.23		
		22.5	-187	-173	14.76	0.952	509.1
		4.7	-236	-204	31.71		

Table 38: Table 37: Span 14, Configuration 1 internal moment derived from strain readings.

Span 14 Raw Strain Data, Configuration 1							
Truck Location (ft)	Measurement Location	Sensor Location From Bottom Flange (in)	Unloaded Strain (10^{-6} in/in)	Loaded Strain (10^{-6} in/in)	Strain Caused by Truck Loading (10^{-6} in/in)	Derived Curvature (10^{-6} rad/in)	Internal Moment (kip-ft)
16.7	Strain at 32 in.	44.7	-563	-565	-1.59	0.138	69.1
		24.7	-1016	-1019	-3.27		
		5.5	-1816	-1813	3.80		
	Strain at midspan	44.7	-1431	-1432	-0.81	0.501	251.7
		24.7	-1464	-1451	13.14		
		5.5	-1581	-1562	18.84		
33.3	Strain at 32 in.	44.7	-563	-565	-1.89	-0.003	-1.5
		24.7	-1016	-1019	-3.13		
		5.5	-1816	-1818	-2.01		
	Strain at midspan	44.7	-1431	-1434	-2.39	0.396	199.0
		24.7	-1464	-1455	9.41		
		5.5	-1581	-1567	13.15		
50	Strain at 32 in.	44.7	-563	-565	-1.40	0.062	31.3
		24.7	-1016	-1018	-2.67		
		5.5	-1816	-1815	1.04		
	Strain at midspan	44.7	-1431	-1429	2.41	1.188	596.7
		24.7	-1464	-1433	31.38		
		5.5	-1581	-1532	48.98		
66.7	Strain at 32 in.	44.7	-563	-565	-1.69	0.029	14.6
		24.7	-1016	-1018	-2.91		
		5.5	-1816	-1817	-0.55		
	Strain at midspan	44.7	-1431	-1431	-0.14	0.819	411.2
		24.7	-1464	-1444	20.50		
		5.5	-1581	-1549	31.96		
83.3	Strain at 32 in.	44.7	-563	-565	-1.75	-0.003	-1.7
		24.7	-1016	-1018	-2.98		
		5.5	-1816	-1818	-1.88		
	Strain at midspan	44.7	-1431	-1434	-2.29	0.386	193.8
		24.7	-1464	-1455	9.12		
		5.5	-1581	-1568	12.84		

Table 39: Table 37: Span 14, Configuration 1 internal moment derived from FEA strain measurements.

Span 14 FEA Strain Data, Configuration 1							
Truck Location (ft)	Measurement Location	Sensor Location From Bottom Flange (in)	Unloaded Strain (10^{-6} in/in)	Loaded Strain (10^{-6} in/in)	Strain Caused by Truck Loading (10^{-6} in/in)	Derived Curvature (10^{-6} rad/in)	Internal Moment (kip-ft)
16.7	Strain at 32 in.	47.3	-106	-106	-0.16	-0.031	-15.4
		22.7	-146	-144	1.28		
		6.9	-1490	-1491	-1.40		
	Strain at midspan	47.3	-122	-124	-1.31		
		22.7	-184	-178	6.59	0.332	166.8
		6.9	-226	-214	12.11		
33.3	Strain at 32 in.	47.3	-106	-106	-0.79	-0.174	-87.5
		22.7	-146	-147	-1.44		
		6.9	-1490	-1498	-7.83		
	Strain at midspan	47.3	-122	-125	-2.63		
		22.7	-184	-167	17.29	0.802	402.9
		6.9	-226	-197	29.78		
50	Strain at 32 in.	47.3	-106	-107	-0.97	-0.220	-110.7
		22.7	-146	-148	-2.59		
		6.9	-1490	-1500	-9.87		
	Strain at midspan	47.3	-122	-127	-4.25		
		22.7	-184	-159	25.65	1.226	615.8
		6.9	-226	-181	45.29		
66.7	Strain at 32 in.	47.3	-106	-106	-0.73	-0.189	-94.7
		22.7	-146	-148	-2.18		
		6.9	-1490	-1498	-8.35		
	Strain at midspan	47.3	-122	-124	-1.76		
		22.7	-184	-167	17.63	0.780	391.8
		6.9	-226	-197	29.76		
83.3	Strain at 32 in.	47.3	-106	-106	-0.41	-0.107	-53.6
		22.7	-146	-147	-1.20		
		6.9	-1490	-1494	-4.72		
	Strain at midspan	47.3	-122	-123	-0.56		
		22.7	-184	-176	7.86	0.337	169.2
		6.9	-226	-213	13.05		

Table 40: Span 14, Configuration 3 internal moment derived from strain readings.

Span 14 Raw Strain Data, Configuration 3						
Truck Location (ft)	Measurement Location	Sensor Location From Bottom Flange (in)	Unloaded Strain (10^{-6} in/in)	Loaded Strain (10^{-6} in/in)	Strain Caused by Truck Loading (10^{-6} in/in)	Derived Curvature (10^{-6} rad/in)	Internal Moment (kip-ft)
16.7	Strain at 32 in.	44.7	-563	-566	-2.84	0.167	83.7
		24.7	-1016	-1021	-5.48		
		5.5	-1816	-1813	3.69		
	Strain at midspan	44.7	-1431	-1434	-2.69	0.751	377.1
		24.7	-1464	-1445	19.17		
		5.5	-1581	-1554	26.75		
33.3	Strain at 32 in.	44.7	-563	-566	-2.49	0.124	62.2
		24.7	-1016	-1021	-5.13		
		5.5	-1816	-1814	2.37		
	Strain at midspan	44.7	-1431	-1433	-1.45	1.405	705.8
		24.7	-1464	-1428	35.83		
		5.5	-1581	-1527	53.65		
50	Strain at 32 in.	44.7	-563	-566	-2.49	0.124	62.2
		24.7	-1016	-1021	-5.13		
		5.5	-1816	-1814	2.37		
	Strain at midspan	44.7	-1431	-1431	0.05	1.713	860.0
		24.7	-1464	-1421	43.21		
		5.5	-1581	-1513	67.18		
66.7	Strain at 32 in.	44.7	-563	-566	-2.46	0.046	23.1
		24.7	-1016	-1020	-4.36		
		5.5	-1816	-1817	-0.66		
	Strain at midspan	44.7	-1431	-1433	-1.96	1.220	612.7
		24.7	-1464	-1435	29.07		
		5.5	-1581	-1535	45.86		
83.3	Strain at 32 in.	44.7	-563	-566	-2.42	0.002	1.2
		24.7	-1016	-1020	-4.10		
		5.5	-1816	-1819	-2.32		
	Strain at midspan	44.7	-1431	-1434	-3.08	0.582	292.4
		24.7	-1464	-1450	13.83		
		5.5	-1581	-1561	19.74		

Table 41: Span 14, Configuration 3 internal moment derived from FEA strain measurements.

Span 14 FEA Strain Data, Configuration 3							
Truck Location (ft)	Measurement Location	Sensor Location From Bottom Flange (in)	Unloaded Strain (10^{-6} in/in)	Loaded Strain (10^{-6} in/in)	Strain Caused by Truck Loading (10^{-6} in/in)	Derived Curvature (10^{-6} rad/in)	Internal Moment (kip-ft)
16.7	Strain at 32 in.	47.3	-106	-105	0.16	0.026	13.1
		22.7	-146	-142	3.22		
		6.9	-1490	-1488	1.21		
	Strain at midspan	47.3	-122	-125	-2.44	0.607	305.0
		22.7	-184	-172	12.79		
		6.9	-226	-204	22.10		
33.3	Strain at 32 in.	47.3	-106	-106	-0.66	-0.134	-67.1
		22.7	-146	-145	0.17		
		6.9	-1490	-1496	-6.06		
	Strain at midspan	47.3	-122	-132	-9.41	1.498	752.3
		22.7	-184	-157	27.65		
		6.9	-226	-175	51.11		
50	Strain at 32 in.	47.3	-106	-106	-0.66	-0.134	-67.1
		22.7	-146	-145	0.17		
		6.9	-1490	-1496	-6.06		
	Strain at midspan	47.3	-122	-139	-16.33	2.259	1134.6
		22.7	-184	-145	39.01		
		6.9	-226	-151	74.95		
66.7	Strain at 32 in.	47.3	-106	-106	-0.92	-0.191	-95.9
		22.7	-146	-148	-1.92		
		6.9	-1490	-1498	-8.63		
	Strain at midspan	47.3	-122	-130	-7.55	1.456	731.2
		22.7	-184	-156	28.18		
		6.9	-226	-175	51.27		
83.3	Strain at 32 in.	47.3	-106	-106	-0.46	-0.106	-53.2
		22.7	-146	-147	-1.05		
		6.9	-1490	-1494	-4.74		
	Strain at midspan	47.3	-122	-123	-1.04	0.608	305.3
		22.7	-184	-170	14.08		
		6.9	-226	-203	23.53		

VITA

Christopher Filip

Candidate for the Degree of

Master of Science

Thesis: CAMBER, PRESTRESS LOSS, AND DETERMINATION OF DISTRIBUTION FACTORS IN PRETENSIONED GIRDER BRIDGES

Major Field: Civil Engineering

Biographical:

Education:

Completed the requirements for the Master of Science in Civil Engineering at Oklahoma State University, Stillwater, Oklahoma, in December 2022.

Completed the requirements for the Bachelor of Science in Civil Engineering at Oklahoma State University, Stillwater, Oklahoma, in May 2020.